Computational Studies in the Few-Body Problem

A thesis presented in partial fulfilment of the requirements for the degree of

Doctor of Philosophy

in

Applied Mathematics

at Massey University, Albany,

New Zealand

Valerie Chopovda

November 27, 2019

Abstract

In this research we investigate the gravitational four-body problem which describes the motion in the system of four stars moving under their mutual gravitational forces. It involves studies of the dynamics of few-body systems and finding periodic orbits, and subsequently an analysis of their stability. One of the challenges of the problem is the necessity of using regularisation algorithms in order to avoid singularities when there is a possibility of collision or close encounter between stars.

One of the featured solutions of the problem is the collinear Schubart orbit discovered for systems of three [59] and four [70] bodies. This orbit has been shown to form families of collinear and planar orbits for three bodies by Hénon [32]. Sweatman discovered Schubart orbits in the collinear symmetric four-body problem [70, 71].

In this work we generate the families of Schubart orbits starting from the planar orbit obtained by Sweatman [73]. Utilising the symmetries of the four-body Schubart orbits, we solve the Caledonian symmetric four-body problem (CS4BP). Initially we consider the case of equal masses. This is later extended to the case of pairwise symmetric masses.

The family is parametrised by two parameters: the mass of the outer bodies and the distance between the two closest non-symmetric bodies. The collinear orbits are collisional, but there are no collisions when the orbits evolve to planar motion.

The planar family of pairwise symmetric masses is bounded by the line of the collinear Schubart orbits. Within its boundaries, there are four regions separated by two special types of orbits present in the family: the equal-mass orbits and the double choreography orbits. Two of the regions are symmetrical to the other two.

We perform a linear stability analysis of the discovered solutions both in and out of the plane. We also distinguish the influence of symmetrical and non-symmetrical perturbations on the orbits. An algorithm for the orbit search and orbital stability analysis is presented.

Acknowledgements

First and foremost, I am extremely grateful to my supervisors, Associate Professor Winston LeMay Sweatman and Emeritus Professor Robert McKibbin, for their guidance, support, endless ideas, inspiration and patience. This research would not have been possible without them.

Next, I thank the Institute of Natural and Mathematical Sciences for providing me with a doctoral scholarship and the opportunity to work and gain experience in both research and teaching. I also thank the New Zealand Mathematical Society (NZMS) and the Australia and New Zealand Industrial and Applied Mathematics Society (ANZIAM) for their support of my study trips.

I would like to thank my colleagues whom I met during my postgraduate and doctoral studies and who shared their knowledge with me: Alona Ben-Tal, Graeme Wake, Shaun Cooper, Carlo Laing, Mick Roberts, Gaven Martin. My special thanks to my fellow PhD students.

I wish to offer my sincere gratitude to my family, my beloved father and mother, who have always supported and encouraged my endeavours. My deepest thanks to my husband, Igor Khripunov, who has helped me through extremely difficult times over the course of my PhD; for that I am very grateful.

A paper based on the work presented in Chapter 6 of this thesis has been published as the following.

Chopovda, V., & Sweatman, W. L. (2018) *The family of planar periodic orbits generated by the equal-mass four-body Schubart interplay orbit.* Celestial Mechanics and Dynamical Astronomy, 130(5), 1-15.

Dedication

This thesis is dedicated to the two most important people in my life: to my beloved mother, Elena Chopovda, who was the most open-hearted, sincere and loving person I ever had in my life, and to my beloved son, Martin Khripunov, for whom I shall be the same.

Contents

Notation

* *Note: all variables are dimensionless. Details about the non-dimensionalisation can be found in Appendix A.*

capital letters

A	angular momentum of the system
B	planar monodromy matrix
D	vertical monodromy matrix
E	total energy of the system
G	gravitational constant
H	Hamiltonian
I	identity matrix
K	kinetic energy of the system
M	total mass of the system
N	number of bodies of the system
P, Q	regularised momenta and position coordinates
R	variational matrix for differential corrections
S	full monodromy matrix
T	period of an orbit
U	potential energy of the system

small letters

d_{ij}	distance between bodies i and j
e	eccentricity
k	stability index
m	mass
t	time
x, y, z	position components in real coordinate system
$\dot{x}$, $\dot{y}$, $\dot{z}$	velocity components in real coordinate system
u, v, w	momenta components in real coordinate system
p, q	interbody distance and momenta coordinates in real coordinate system

greek

Δ	stepsize
Γ	regularised Hamiltonian
ϵ, η	relative errors
λ, μ, ν, γ	eigenvalues of a monodromy matrix
τ	regularised time
θ	angle of rotation of the system, radians
ξ	perturbation

subscript

0	related to initial time $t = 0$
i	index of an i^{th} body
ij	index of a relative quantity between bodies i and j

superscript

j	j^{th} iteration in the iteration process

Chapter 1

Introduction

1.1 Project Description

The few-body problem is a well-known problem in Celestial Mechanics which exhibits rich and varied dynamics. It was first formulated precisely by Newton. When the objects involved are point masses, it may be stated as follows: "Given at any time the positions and velocities of three or more massive particles moving under their mutual gravitational forces, the masses also being known, calculate their positions and velocities for any time" [58].

Few-body systems occur when single and binary masses interact. For example, one of the brightest stars in the night sky, the star Castor in the constellation Gemini, is normally perceived as a single star; however it is a system of three binaries revolving about their common centre of mass [61]. Extending our knowledge of few-body systems advances our understanding of dynamics and applications in astronomy and engineering [74].

It is known that the simplest of the few-body problems, the two-body problem, is solvable analytically. Depending on the eccentricity of the orbit of one body around the other, the motion is either elliptical, parabolic or hyperbolic [58]. As was first shown by Poincare [54], it gets much more complicated when a third body is introduced to the system, even if the third body is infinitesimal compared to the other members of the system.

Since its formulation, there have been conducted extensive studies in the three-body problems, general and restricted. In the framework of the planar circular restricted three-body problem five stationary solutions have been found by Euler and Lagrange, also known as Lagrange points [16]. For the general problem interesting orbits have been found, for example, the planar Standish orbit [31, 76] and the rectilinear Schubart orbit [32, 59]. A spectacular figure-8 choreography orbit was discovered by Moore [48] and proved to exist by Montgomery and Chenciner [18].

The four-body problem is of interest in its own right: it arises physically as the encounter of two binary stars, or a system of two stars with accompanying planets. In fact, most of the stars in our Galaxy belong to binary systems [28, 39, 66]. The four-body problem also "serves as a stepping stone between the simpler three-body problem and the N-body problem with larger number of bodies", as stated by Sweatman [70].

Four-body problems may be found even in our own Solar System. One example could be the "Sun - Jupiter - Saturn - X" model, where X is an inner terrestrial planet, or an asteroid, or a satellite of an outer planet [58]. In outer space another interesting four-body system is the system HD 131399Ab in the Centaurus constellation that consists of a binary star and a giant star with an exoplanet. It was discovered using direct imaging by Wagner et al. [80].

Another example is the system of planet Jupiter with three of its Galilean moons - Io, Europa, and Ganymede. This system illustrates a near-periodic symmetric orbit: when Europa and Ganymede are in conjunction, Io is in opposition to them. Also, when Europa is in conjunction with Io or Ganymede, the inner one of the pair is near perijove, and the outer one is near apojove [13].

In this research we study the families of periodic four-body orbits that perform an interplay type of motion. These orbits arise from simple one-dimensional periodic orbits: the Schubart orbits, discovered and studied by Sweatman [70, 71, 73]; also [37, 51, 4, 5]. Such families are known and well-studied in the three-body case by Hénon [31, 32, 33, 34], Mikkola and Hietarinta [42, 43, 44, 35], and others. The aim of the present work is to extend the results to cases with four bodies.

We start our investigation by considering the Caledonian symmetric four-body problem [58, 66, 67, 73] for equal masses. This is a system with a rotational symmetry so that two of the masses are images of the other two masses about the centre of mass. It also has a past-future symmetry, so that the dynamical behaviour of the system after time $t = 0$ is a mirror image of its behaviour before time $t = 0$.

The appeal in considering a gravitational system with symmetries is partially due to its greater simplicity than a general N-body system. It can, however, provide insight and ideas. Some important orbits in the general problem are symmetric and can initially be found and studied more readily in a symmetric context [74].

1.2 Thesis Overview

This thesis is structured as follows. In Chapter 2, we review the literature on past research conducted in the three- and four- body problems. A description of the studies by Hénon [31, 32, 33, 34] and Sweatman [70, 71] is provided. These particular studies led to the current project and constantly served as an inspiration for overcoming difficulties that appeared during the study. We describe the regularisation theory and methods that are used for searching and integrating orbits in our research.

In Chapter 3, we introduce the Caledonian Symmetric Four-Body Problem (CS4BP) [66] which uses a reduced and simplified set of variables for the four-body system. This problem is useful as it suits the properties of the type of solutions we are searching for. The equal-mass four-body Schubart orbit [70] and the family of collinear Schubart orbits [71] have also been studied in a symmetrical framework.

The assumptions used for modelling the CS4BP are described. The Hamiltonian and equations of motion for four bodies with Levi-Civita regularisation are derived. In modelling the problem, we follow closely the approach by Sivasankaran, Steves and Sweatman [64, 63].

Chapter 4 introduces the general four-body problem and the equations describing it.

Solving this problem for our orbits tests their survival under general conditions with no symmetrical restrictions imposed. The Hamiltonian and ten integrals of the problem are described. We use the Heggie regularisation scheme which utilises the Kustaanheimo-Stiefel coordinate transformation [1, 27, 41, 45]. This scheme was originally introduced as an extension of the Levi-Civita coordinates in the case of a three-dimensional general system.

In Chapter 5, we outline our approach to search for the planar four-body interplay orbits. The algorithm is given in detail for the case of equal masses. We then describe how this algorithm can be generalised for pairwise symmetric solutions for unequal masses. The strategies for analysing the linear and non-linear stability of the orbits are described.

All of the algorithms mentioned in Chapter 5 have been implemented in the MATLAB environment, including the integrators for the symmetric system from Chapter 3 and general system from Chapter 4. Additionally, the collinear four-body program in terms of the coordinates used in Sweatman [70, 71] was coded in order to calculate the boundaries of the family. Some additional algorithms were generated, mostly for the purpose of comparing the accuracy of the chosen methods. These are mentioned throughout the current thesis.

Chapters 6 and 7 describe the discovered family of periodic orbits generated from the four-body collinear Schubart orbit. First, in Chapter 6, we describe the results achieved for the case of four equal masses and discuss their properties. The results, presented in this chapter, are published and appear in Chopovda and Sweatman [22].

We extend these results to the case of pairwise symmetric unequal masses in Chapter 7. Using the data from Sweatman [71], for collinear orbits, we construct boundaries for the planar family. We locate the equal-mass orbits within this region. The stability of the newly-discovered orbits is analysed. This is followed by a discussion of results and conclusions of the research.

The numerical studies involve the use of self-contained dimensionless N-body units [29]. In Appendix A we describe the non-dimensionalisation of the system. In principle, this could be reversed in order to assess the actual physical units and to get an idea of the scale for such systems.

Chapter 2

Literature Review

This chapter is dedicated to a review of the research on three- and four- body problems. This primarily concerns searches for families of periodic orbits and a stability analysis for these orbits, but it also relates to the study of Schubart-like orbits. Because of the abundance of literature dedicated to the three-body problem, we choose only those papers that are in some way related to the Schubart orbit and its family. The literature review on four-body problems is mostly focused on symmetric problems.

Since one of the difficulties in exploring the N-body problem is the singularities in the equations due to collisions and near-collision events of the bodies, it is necessary to discuss methods for avoiding these singularities. Another part of this review is dedicated to types of regularisation for the equations of motion during numerical simulations of three- and four-body problems.

There are, however, many books about the general theory of celestial mechanics and stellar dynamics that give a good introduction to the problem, methods that are used for studying the gravitational systems and studies that have been done in the past. Whittaker [81] provides a detailed summary of the theory of particle dynamics, with particular interest to Hamiltonian systems. The problem of three bodies with its possible reductions is given and the stability of periodic orbits in general. One of the chapters is dedicated to a detailed proof of the theorems by Bruns and Poincaré about the classical integrals of motion for the problem.

Siegel and Moser [62] explain the general theory and the establishment of the three-body problem. The analytical background of periodic solutions in the restricted three-body problem and their stability is given. They provide a derivation of Sundman's theorem about a series solution for the three-body problem with the exception of a triple collision. The solutions leading to a triple collision are discussed.

Stiefel and Scheifele [69] is one of the classical books in celestial mechanics that discusses the classical theory of Keplerian motion, and the theory and geometry of the K-S regularisation. The perturbation theory is formulated and discussed in terms of canonical analytical mechanics. The numerical methods for solving different problems of stellar dynamics are presented.

Szebehely [75] is another interesting book that covers the analytical and numerical explorations in the restricted three-body problem. It gives a detailed summary of the results by that time, both in the circular restricted three-body problem and modifications of the problem to the elliptic problem, the problem in 3D and Hill's problem. Principal aspects of the restricted problem are discussed, such as curves of zero velocity, libration points and stability in their neighbourhood.

Aarseth [1] provides algorithms for N-body numerical simulations and a description of the methods and transformations that are commonly used with few- and N-body problems. A summary of types of regularisations are presented with algorithmic descriptions for each of them. Part of the book explains the organisation and setup of the `CHAIN`-algorithm developed by Mikkola and Aarseth [41, 45], the code for which is freely available on the internet by the link `https://www.ast.cam.ac.uk/~sverre/web/pages/nbody.htm`. Aarseth also considers practical aspects of the N-body problem with respect to star clusters, galaxies and planetary systems.

Heggie and Hut [28] published a book "The Gravitational Million-Body Problem" that is aimed at understanding the dynamics of globular clusters. They discuss the importance of studying the million-body problem by considering the problem from the point of view of several disciplines: physics, astronomy, mathematics, and computer science. The book includes an investigation of the few-body problem with gravitational scattering, binary star systems and

formation of triple-star systems provided with numerical methods relevant for the problem. This is followed by explorations of the million-body system evolution including discussion of energy within a star cluster and the evolution of parameters such as total mass and a measure of the cluster radius.

Roy [58] discusses the possible types of motion in stellar systems from the simplest case of two bodies to many-body problems. The Caledonian Symmetric $2N$-body problem is introduced and discussed for the cases of $N = 1,\ 2,\ 3$. A significant part of the book is dedicated to the stability and evolution of the Solar System, in particular the Earth-Moon system and the systems of Saturn and Jupiter with satellites. Some of the artificial orbits and applied aspects of the orbital motion are discussed by considering the dynamics of a rocket, artificial satellites and also interplanetary trajectories.

2.1 The three-body problem

The three-body problem is one of the most extensively studied problems, both analytically and by numerical experiments, in stellar dynamics. In its general statement it is very complicated for a systematic analysis. For this reason there exist studies of the problem in a restricted form.

The restricted three-body problem is introduced with the assumption that the mass of one of the bodies is infinitesimal (or zero), so that its motion does not affect the other two bodies. The two remaining bodies execute elliptic or circular orbits about their common centre of mass. Depending on the type of orbits, the problem is called *the circular restricted three-body problem* or *the elliptic restricted three-body problem*, respectively. In fact, the circular restricted three-body problem is the case of elliptical orbits with eccentricity $e = 0$.

Within the restricted and general problems, one can define a more specified problem depending on the initial configuration of the bodies. For example, in the Sitnikov problem, the third body is defined to move under the influence of the first two bodies in a plane perpendicular to the orbital plane of the first two bodies. In the Pythagorean three-body

problem the bodies are arranged on the vertices of a $3-4-5$ right triangle and have a mass ratio $3:4:5$ [31, 76].

Also, depending on the initial conditions, there can be problems defined on a plane (*the planar three-body problem*) or within a line (*the rectilinear three-body problem*). Introduction of various types of simplifications and restrictions helps significantly in reducing the number of degrees of freedom in the considered three-body system, which still exhibits rich and varied dynamics.

One family of particularly interesting solutions has been discovered for the general planar problem of three equal bodies by Hadjidemetriou [25], Hénon [32] and Broucke [12] independently in the 1970s. According to Broucke [12], Hadjidemetriou was the first one to obtain the orbits, although he only explored some of the orbits. The whole family, from its very start, the Schubart orbit [59], was studied by Hénon [32]. The solutions are now known as the Broucke - Hénon - Hadjidemetriou family.

In his study, Hadjidemetriou [24, 25] started with the orbit from the circular restricted three-body problem and numerically continued it to the orbits for the general three-body problem by varying the mass m_3. In doing so, he pointed out that it is natural to search for general orbits starting from the well-known orbits rather than to search at random [24]. In a following study [25], he extended the family of orbits for the case of three equal masses by choosing the coordinate x_3 as a parameter. Hadjidemetriou then used the orbits discovered to test his method of finding the orbital stability, based on integration of the orbits for only half of their period.

Hénon published a series of four articles [31, 32, 33, 34] on the topic of families of periodic orbits in the planar general three-body problem. The overall idea was to show how periodic solutions for the three bodies form one-parameter families, for given masses, not only in restricted problems, but also in the general problem. This was done by providing examples for some known orbits like the Standish orbit [31], the Szebehely orbit [76, 31] and the Schubart orbit [59, 32, 34], with analyses of their stability.

Hénon considered the general three-body problem with restrictions applied to the initial conditions of the orbits. In his study, the origin of time and initial rotation angle of the system are fixed, with an argument that one obtains an infinity of periodic solutions by changing time and rotating the initial system around the centre of mass. The origin of time for the orbits was chosen to coincide with the minimum of the distance between two bodies (a central body with one outer bodies). The initial angle was fixed with all three bodies starting on the line $y = 0$ with velocity vectors perpendicular to this line. The families of orbits were generated by varying one of the integrals of motion: the angular momentum A of the system.

Hénon's study of the Schubart orbit is of particular interest. The periodic solution that Schubart discovered in 1956 [59] is a rectilinear orbit with two types of collisions: between bodies 1 and 2 at $t = 0$ and between bodies 2 and 3 at $t = T/2$, where T is the period of an orbit. The middle body 2 acts as an intermediary between the other two, preventing them from approaching each other at the centre. The topological proof of the existence of Schubart orbit was provided by Moeckel [47].

A family of periodic orbits was generated from the equal-mass Schubart orbit, again using angular momentum as a parameter. It was found that the angular momentum along the family first grows until it reaches a local maximum, then it decreases until a minimum is reached, after which angular momentum continues growing towards infinity.

Both extrema of angular momentum correspond to changes in stability of the orbits: the Schubart orbit itself is stable, and so are the orbits from the first region. The area between the two local extrema of angular momentum consists entirely of unstable orbits and, after angular momentum passes through the local minimum, the orbits become stable again. The family finishes with two bodies separated by an infinite radius from the third one.

In the last article of the series, Hénon explored the stability of the family of the collinear Schubart orbits. These were generated from the equal-mass Schubart orbit by fixing the total mass of the system. The considered cases covered all possible values of the three masses including the limiting cases when one or two masses vanish. The masses were parametrised by fixing the total mass of the system.

In order to better present the results, Hénon constructed an equilateral triangle of height 1 (the value of the total mass) with vertices labelled as 1, 2, 3. Within the triangle diagram, each point is characterised by its distances to the three sides. These distances represent the values of the masses. For example, the point located at the vertex 1 means that $m_1 = 1$, $m_2 = 0$, $m_3 = 0$.

The constructed triangle of three mass ratios allowed Hénon to see and distinguish domains of stability and instability for three-body Schubart orbits. This study found the possible mass ratios for three-body stable systems. It was shown that the domain of stability covers about 46% of the total area of the triangle.

In the meantime, Broucke [12, 13] found some new families of periodic orbits of three equal masses by exploring the general three-body problem with no regularisation applied; one of the families which was partially repeated by Hénon. Broucke studied the symmetry properties that orbits of general planar and restricted circular and elliptic three-body problems possess. Different strategies for the differential corrections method for obtaining periodic solutions in various coordinate systems (such as heliocentric, barycentric, etc.) were presented in [12].

Broucke [13] distinguished two types of periodic orbits: absolute periodic and relative periodic orbits. For the absolute periodic orbits the period of orbits coincide with the period of the system's rotation about the centre of mass, so the bodies come to exactly the same positions at the end of each period. In the relative periodic orbits, the positions and velocities of the bodies are relative to each period T during which the system has rotated by a fixed angle θ. Thus, the relative periodicity is with respect to the rotating frame of reference with angular velocity $\omega = \theta/T$, which would be absolutely periodic if the angle θ is a rational fraction of 2π.

Broucke also studied the stability properties for the elliptic and circular three-body problems [10, 14], that are, in principle, extendable to the stability analysis for the general three-body problem. He used variational equations for constructing a 4×4 fundamental matrix whose eigenvalues indicate the stability of the periodic solution. The eigenvalues of the Hamiltonian systems occur in reciprocal pairs λ, $1/\lambda$ [81]. So, the characteristic equation of

the fundamental matrix can be written as [10, 32, 81]

$$\lambda^4 + a_1\lambda^3 + a_2\lambda^2 + a_1\lambda + 1 = 0.$$

The coefficients $a_1,\ a_2 \in \mathbb{R}$ are called the stability coefficients. Rewriting the characteristic equation in the form

$$(\lambda^2 - k_1\lambda + 1)(\mu^2 - k_2\mu + 1) = 0,$$

where $\lambda,\ 1/\lambda,\ \mu,\ 1/\mu$ are the four eigenvalues of the fundamental matrix, gives the stability parameters $k_1 = \lambda + 1/\lambda,\ k_2 = \mu + 1/\mu$ described by Whittaker [81]. The orbit is stable if k_1 and k_2 are real, and are both less than 2 in absolute value [10, 32, 71, 81]. Also, since the determinant of the fundamental matrix is 1, for a stable orbit the eigenvalues are located on a unit circle.

Broucke distinguished seven regions of stability in the $(a_1,\ a_2)$ plane [10], depending on the form of the eigenvalues. Later, Broucke analysed the stability and properties of the eigenvalues on the boundaries between the stability regions [14]. Of the seven regions only one region is stable [32], that is the region I (Figure 2.1) with

$$-4 < a_1 < 4, \qquad 2|a_1| - 2 < a_2 < \frac{a_1^2}{4} + 2, \qquad k_1^2 < 4, \qquad k_2^2 < 4$$

The other six regions (regions from II to VII in Figure 2.1) are all unstable and differ from one another by the form of the eigenvalues. Region II is called the complex unstable region, which can only appear for systems with at least four degrees of freedom. Regions III - V are unstable and differ by the signs of stability parameters of the system. Broucke [10] calls Regions VI-VII semi-unstable, as one of the stability parameters is stable, but the other one is unstable.

In $1988-1991$, Mikkola and Hietarinta [42, 43, 44] investigated the one-dimensional three-body problem for the case of equal masses with positive or negative energy of the system. Depending on whether the sign of the total energy is positive or negative, the system possesses more kinetic or potential energy in magnitude, respectively (see Section 3.1 for details). The

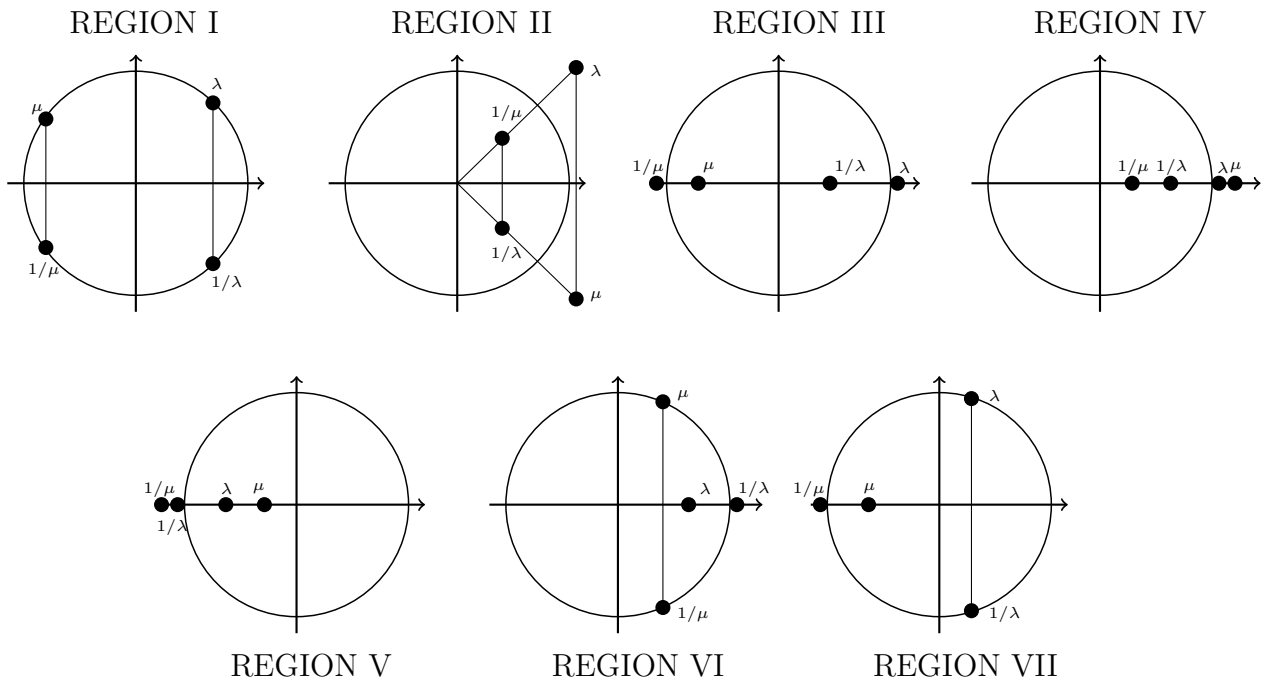

Figure 2.1: Seven stability regions, according to Broucke [10, 14].

stability of the Schubart orbit for cases of different masses is revisited [44], also with the study of the region of quasi-periodic orbits surrounding the Schubart orbit. Another article, published by Hietarinta and Mikkola [35] two years later, summarises the results of their work and extends the study of equal-mass configurations to unequal masses.

Hietarinta and Mikkola [35] made a rough classification for types of motion possible in three-body dynamics. In general, they distinguished the systems that *stay bound* and those that *break up*. Bounded systems include periodic orbits and sets of quasiperiodic orbits situated around periodic ones. In particular, they consider the Schubart region that consists of a set of quasiperiodic orbits that surrounds the Schubart orbit and the Schubart orbit itself. These orbits exist only for systems with negative energy. For positive energies at least one particle has to escape and leave the other two as a binary; alternatively all three particles can separate completely, which is impossible for negative energies.

The break-up systems are divided into two groups by the "dwell time", or the time during which all three particles stay close together, both in forward and backward integration of the system. If a dwell time is nearly zero, the system is called "fast scattering". Chaotic scattering, or long interplay, also resonant scattering, systems have arbitrarily long interplay time.

The regions of all types of motion were discovered using a Poincaré section constructed from the quantities R and θ. Both are derived from the variables of the system: R is a half of the relative distance between one pair of bodies, and θ is introduced as the relation between relative momenta of the bodies and the kinetic energy of the system. The chosen values of R and θ indicate the initial conditions of the system.

The behaviour within regions was also identified for various masses of the bodies using the Poincaré sections. It was discovered that in most cases the system breaks apart leaving a bound binary and a single unbound particle [42]. For the scattering orbits it was also examined whether the escaper is a lighter or a heavier body [43, 35], in both directions of time. From the analysis of the results, it was suggested that the Schubart orbit and its stability has global influence on the other regions [35]. For example, the quasiperiodic region and some types of the scattering orbits are absent if the Schubart orbit is unstable.

The results for stability of the Schubart orbit for perturbations in all three dimensions agree with the former results by Hénon [32, 34]. A triangle of masses, similar to Hénon's [34], was produced and analysed, in terms of rectangular coordinates a and b that are related to the three masses. It was shown that the Schubart orbit exists for all choices of masses. The Schubart equal-mass orbit was found to be stable and situated near the intersection of two instability regions. In cases when the central mass is large, a large region of stable Schubart orbits was observed. On the contrary, the stability is restricted to narrow regions for a small central mass [44].

The structure of the Poincaré section and, in particular, the chaotic region was explored later by Tanikawa and Mikkola [77, 78] with the use of symbolic dynamics. Instead of orbits, symbolic sequences of binary collisions were considered. A symbol was assigned to each of three possible kinds of collision in the collinear three-body problem: 1) collision between one of the outer bodies with the middle body, 2) collision between the other outer body with the middle body, 3) triple collision.

It was found that the Poincaré section is further subdivided into an increasing number of regions that are separated by the triple collision curves. Each region was associated with

different digits of symbol sequences. Also, some of the symbol sequences were called inadmissible as they were found to be nonexistent. The numerical experiments showed that the number of non-escape orbits (i.e. periodic in the sense of symbol sequence) in the Schubart region is uncountable.

Similar structures were observed by Boyd and McMillan [9] in their study of gravitational scattering in the planar restricted three-body problem. The system that was considered consisted of a binary pair initially performing a circular orbit, and an incoming star. Boyd and McMillan constructed a two-parameter initial-value space in terms of the initial phase of the binary φ and the impact parameter b, which is a displacement of the incoming star from the line going through the centre of the binary parallel to the velocity vector of that star.

The mapping of the angle of escape of the star leaving the system to its initial conditions showed a particular structure of regions of non-resonant (smooth) motion separated by "rivers" of resonant scattering [9]. The former corresponds to the only one close approach to a system that results in either a simple flyby or an exchange with one of the members of the binary. In resonant scattering the system was bounded for some time before the following ejection of a star. A higher resolution view on the rivers of resonance revealed the existence of bands of smooth behaviour separated by bands of chaotic motion.

One of the orbits from the Broucke - Hénon - Hadjidemetriou family was rediscovered by Moore [48], who introduced the theory of braids as a tool for a topological classification of motion in a three-dimensional space-time. It is now known as the criss-cross orbit [50]. This orbit was numerically found to exist for different masses by Nauenberg [49], and later extended to three-dimensional orbits by Nauenberg and Moore [50]. Some of the orbits, including the criss-cross orbit, are shown to be stable by using a nonlinear simulation. The linear stability of the criss-cross orbit was later studied by Chang, Ouyang and Yan [17] by utilising symmetries of the orbits and using index theory.

The existence of symmetric families of "Schubart-like" orbits has been further studied by Martínez [36, 37] for the case of $n \geq 3$ bodies. The study initially concentrated on the periodic orbits that have two collisions (not necessarily binary collisions) in one period [36]. Martínez

uses the blow-up technique introduced by McGehee [38] which has an effect of replacing the total collision with a collision manifold so that the system can be studied in the neighbourhood of the collision. A following paper by Martínez [37] considers the families of orbits with many singularities in one period. Examples of planar, pyramidal and polygonal systems are provided.

2.2 The symmetric four-body problem

Numerical studies in the four-body problem originate from the last century. However, the four-body problem was first studied as a perturbed three-body problem with an added infinitesimal fourth mass. Some of the first numerical explorations of the interaction of two equal-mass binary stars were performed by Mikkola in the early 1980s. Four types of final motion were identified [1, 39] as:

- a pair of binaries,
- a triple system and one escaper moving away from the system's centre of mass,
- one binary with another two bodies separately escaping the system,
- total disruption of the system into four single masses that move independently.

In the general four-body problem the number of degrees of freedom increases compared to the three-body problem. The dynamics of the problem is even more complicated than for the case of three bodies. In order to reduce the dimensions of the system to manageable levels, yet leave it meaningful to real systems, some special conditions of symmetry can be introduced.

In 1998, Steves and Roy [66, 67] modelled a simplified symmetric problem for a quadruple system. The idea of introducing such a problem lies in utilising possible symmetries of a four-body system, thus reducing the number of equations. Also (Sweatman [74]), because some orbits are symmetric in the general problem, they can be discovered and studied with less effort if considered in a symmetric context.

Two different hierarchies of the system were considered: the linear and the double binary. By hierarchy the authors mean a particular arrangement of the system in terms of a designated number of disturbed two-body motions. For the linear hierarchy two bodies are orbiting each other, while the third body orbits their centre of mass at a great distance from it. The fourth body orbits the centre of mass of the first three bodies, at a far greater distance from them.

The double-binary hierarchy accounts for two symmetrical binaries which rotate about their centre of mass. The problem with a double-binary hierarchy was named the Caledonian four-body problem (after the name of Glasgow Caledonian University where the research was conducted). The Caledonian double-binary four-body problem was later renamed the Caledonian symmetric four-body problem [58].

The Caledonian problem exhibits additional symmetry about the origin [66]; at any time one of the outer (or inner) bodies mirrors the motion other outer (inner) body. The double-binary hierarchy also requires that the distances between two bodies in the binaries are the same, as well as the distances between both centres of mass of the binaries and the centre of mass for the four bodies.

An advantage of the Caledonian model in both hierarchies, compared to the general four-body model, is that it successfully reduces the number of variables. For a general four-body problem the number of variables is 24 with 28 initial parameters (12 for positions, 12 for momenta and 4 for masses). This is reduced to 10 variables (4 for positions, 4 for momenta and 2 for masses) with only 6 initial parameters. The ten classical integrals of motion in the general model are reduced to just two: the energy integral and the integral of the angular momentum of the system.

A connection between the Caledonian symmetric four-body problem and the circular restricted three-body problem was drawn [67]. Steves and Roy studied the symmetrical equilibrium solutions for equal masses in the system in the form of a square, a triangle and a straight line. They showed analytically that when two masses are reduced to zero, then the solutions are reduced to the Lagrange points in the limit.

Steves and Roy [66] (also see Roy [58]) discussed the Caledonian symmetric N-body problem for the cases $N = 2, 4, 6$ and the possible types of motion for the problem. They derive an analytical stability criterion for the Caledonian problem and show that its hierarchical stability depends on a parameter C_0, the Szebehely constant, which is the function of the total energy, angular momentum and the moment of inertia of the system. It was stated that "the system is hierarchically stable if it maintains its initial hierarchical state for all time".

The possibility of studying the Caledonian symmetric problem for odd numbers of bodies was also proposed [58]: by introducing another point-mass at the centre of mass that remains at rest. This allows us to regard the Caledonian problem as a model of a star with a planetary system.

Sweatman [70, 71, 74] studied the collinear symmetric Newtonian four-body problem for which he conducted research similar to that of Mikkola and Hietarinta [42, 43, 44, 35]. The motion of bodies in the symmetrical one-dimensional four-body problem is restricted to a line where they undergo elastic collisions, with a symmetrical distribution of bodies about the system's centre of mass. The total energy of the system is taken to be negative so that at least one pair of bodies will be bound.

It was found that the results resemble the collinear three-body problem results [31, 32, 33, 34, 42, 43, 44, 35]. The orbits form three regions on a Poincaré section similar to those observed by Mikkola and Hietarinta for the three-body problem. For the majority of orbits it was found that the system starts and finishes as distinct subsystems of binaries and single bodies.

The bound-orbit region consists of a periodic orbit similar to the three-body Schubart orbit and quasiperiodic orbits surrounding it. The equal-mass Schubart periodic orbit for four bodies was found to be unstable under two- and three- dimensional perturbations, although stable under collinear perturbations. This contrasts with Hénon's results for three bodies [31, 32, 33, 34].

In a following paper [71], Sweatman generates a family of symmetric periodic interplay

orbits from the equal-mass Schubart periodic orbit discussed above. The stability of the orbits is studied. For this family the total mass of the system is fixed, but the masses of the outer and inner bodies are varied.

The author describes thoroughly the process for determining the stability of the orbits. For each orbit the collinear and transverse perturbations are applied separately. Then, four stability indices are derived: two for collinear perturbations, one for transverse perturbations with a reflective symmetry about the x-axis, and one for transverse perturbations with a rotational symmetry about the centre of mass.

The results of linear stability analysis show that there are three stable regions for the mass range: one region unstable to collinear perturbations and two regions unstable to transverse perturbations. The long-term integrations in one dimension and three dimensions confirm the results. Again, the results look similar to the three-body problem in the sense that if one pair of outer bodies is replaced by a single combined mass, the intervals for stability will be comparatively similar to those for the three-body problem.

The limiting cases for the masses were studied, and it was found that when the outer mass tends to zero, all the energy is contained within the central binary and the system is stable. The case with zero inner mass is collinearly stable but unstable to transverse perturbations.

Sekiguchi and Tanikawa [60] also studied the one-dimensional Newtonian four-body problem with the use of a Poincaré section, McGehee coordinates [38] and symbolic dynamics. Their research was similar to the one for the three-body problem conducted by Tanikawa and Mikkola [77, 78].

The results they gave are in agreement with the collinear three-body problem results [42, 43, 44, 35] and the results of Sweatman [70, 71]. Three regions on the surface of section were discovered: the chaotic region, the fast-scattering region and the quasi-periodic region with the Schubart-like orbit and unstable periodic solutions. Similarly to [77, 78], the stratified structure of the chaotic region was revealed, which was also shown in Sweatman [70].

Ouyang and Yan [51] proved analytically the existence of the Schubart-like orbit for four

bodies. The proof consisted of deriving initial coordinates for the orbit in regularised Levi-Civita-type coordinates, finding the upper bound on the positions of the bodies, showing that the velocities are continuous functions of the coordinates, and then deriving the corresponding positions and velocities for $t = T/2,\ T,\ 3T/2$, etc. It was shown that the half-period coordinates, as well as the coordinates for $t = T$, satisfy the initial conditions, and this holds for all periods.

Bakker et al. [4, 5] studied the linear stability of the Schubart-like four-body orbit for different masses by using the analytic-numerical method of Roberts [55, 56] in regularised Levi-Civita-type coordinates. Use of symmetries in time and regularised coordinates allowed them to reduce the stability analysis of an orbit to a quarter of its regularised period (half-period in real coordinates). The monodromy matrix was then reduced by using the relevant factorisation and symmetries of the problem. The linear stability results confirmed the stability regions, as calculated by Sweatman [70].

Bakker et al. [5] also studied the existence and stability of the planar pairwise symmetric four-body problem with masses $1,\ m,\ m,\ 1$. This problem is also sometimes called the rhomboidal symmetric four-body problem. Two of the bodies are initially on the x-axis, and the other two on the y-axis, all symmetrical with respect to the centre of mass at the origin. The region of stability for different values of mass m was identified with Roberts' method [4] and by using characteristic multipliers [5].

Further studies of the Caledonian symmetric four-body problem were conducted by Sivasankaran, Steves and Sweatman [63, 64] who proposed a suitable regularisation for integrating the problem. They used the Levi-Civita type regularisation with a time-smoothing transformation which enabled them to study close encounters and collision events. The algorithm they used showed good properties in conserving the total energy of the system. It is further explained in Chapter 3.

In 2014 Sweatman [73] found a new planar periodic solution for the problem of four bodies with an orbit similar to the three-body orbits that Hénon derived from the Schubart orbit [32]. This suggested the existence of a four-body family of planar periodic orbits generated from

the Schubart-like orbit. The family of orbits was expected to have similar properties to the three-body family found and examined by Hénon.

The variational approach was first introduced for the figure-eight orbit of three bodies by Chenciner and Montgomery [18]. The four-body 'hip-hop' orbit was discovered in three dimensions [19] using the same principles. This led to a sequence of studies dedicated to searching for the four-body solutions by searching for minimisers of the action functional defined in appropriate spaces under topological constraints.

Chen [20] discovered an interesting planar symmetric four-body star-shaped orbit, in which each pair of bodies shared the same path. An interesting feature of this orbit was that the configuration of the masses changed from square to collinear, and remained a parallelogram for all times [20]. Another set of orbits belonging to the parallelogram four-body problem was proved to exist by Chen [21], and their linear stability were analysed by Peng, Yan, Xu and Ouyang [53]. An interesting pentagon star choreographic solution for equal and unequal masses was considered in Ouyang and Xie [52]. A group of orbits was presented for a double isosceles and an isosceles trapezoid initial configuration by Yan [82].

Broucke [15] gave a thorough classification of the four- and five-body planar periodic orbits regarding the symmetries they possess and presence of choreography solutions. He distinguished five different classes of symmetries for four-body orbits, namely:

- *Class 1*: initial orientation of the bodies is collinear, the orbits are symmetric about the x-axis, but not necessarily about the y-axis,
- *Class 2*: initial orientation of the bodies is collinear, the orbits are symmetric with respect to the system's centre of mass,
- *Class 3*: one pair of bodies is at a right angle to the other pair of bodies, the orbits are symmetric about both the x- and the y- axis; some of the orbits are of choreography and semi-choreography types (bodies sharing the same orbit path),
- *Class 4*: initial positions of the bodies are in the double isosceles triangle configuration,

with two bodies on a line parallel to the x-axis and another two on the y-axis at right angles,

- *Class 5*: initial positions of the bodies are in the trapezoidal configuration, with the appropriate symmetric velocities.

The most common structure of the four-body periodic system was found to be in the form of two binaries rotating about their centre of mass. From the preliminary results of the current work it might be deduced that the four-body Schubart periodic orbit and the corresponding family of orbits belong to the Class 2 periodic orbits.

2.3 Types of regularisation

The classical equations of motion for the N-body problem have the form

$$m_i \frac{d^2\mathbf{r}_i}{dt^2} = \sum_{j \neq i} \frac{m_i m_j (\mathbf{r}_j - \mathbf{r}_i)}{|\mathbf{r}_i - \mathbf{r}_j|^3} \qquad i = 1, 2, \ldots, N, \tag{2.1}$$

where the units are chosen such that the gravitational constant is set to 1, and $\mathbf{r}_i$ is a vector of the i-th body's coordinates. It can be seen that the equations of motion are singular at the collision since the gravitational attraction as well as the acceleration of the bodies are infinite [8, 69]. Thus if the particles approach one another very closely, a *near collision* event happens. Standard numerical techniques fail close to such events.

The theory of regularisation was developed in order to overcome such numerical difficulties. The singularities due to two-body collisions can be eliminated by the appropriate choice of the independent variable [75]. The purpose of regularisation is to eliminate singular behaviour by transforming singular equations into regular ones. When the elimination of singularities is not feasible, often a time transformation is introduced.

Regularisations are accomplished by transformations of the variables occurring in the differential equations of motion. Poincaré was first to propose a technique that transforms the

independent variable in the Hamiltonian system [46, 54]. By defining $dt = gd\tau$, the time is transformed to the new independent variable τ, where $g(\mathbf{p}, \mathbf{q}) > 0$ is a function of position $\mathbf{p}$ and momentum $\mathbf{q}$ variables of the system.

Time is taken to be a canonical coordinate $t = q_0$ by adding the momentum of time (also, binding energy) $p_0 = -E = H(0)$ to the Hamiltonian H [46], where E is the energy of the system ($E = H = \text{const}$). The new Hamiltonian is then taken as

$$\Gamma = g(\mathbf{p}, \mathbf{q})(H(\mathbf{p}, \mathbf{q}, q_0) + p_0), \tag{2.2}$$

which gives the equations of motion [46]

$$\frac{dt}{d\tau} = \frac{\partial \Gamma}{\partial p_0} = g, \qquad \frac{dq}{d\tau} = \frac{\partial \Gamma}{\partial p}, \qquad \frac{dp}{d\tau} = -\frac{\partial \Gamma}{\partial q}.$$

In the original regularisation of the problem of two bodies, as proposed by Sundman in 1913 [8], the usual choice of the new independent variable τ is introduced through a differential relation [62]:

$$dt = qd\tau,$$

where q is the distance between two colliding bodies.

This technique is helpful because it changes the time-step during numerical integration. As q becomes smaller, the time-step of integration, Δt, also decreases in order to accommodate the large changes occurring on the right hand side of the equations to be integrated. Some function g could be used instead of distance q. The choice $g = q^\alpha$ with α as a constant was discussed in Bettis and Szebehely [8]. They found that the selection $\alpha = 3/2$ is the best choice for a transformation. The case $\alpha = 1$ is the classical Sundman's regularisation [8].

Other choices of the function g were suggested later by various investigators. Szebehely [75] discussed the use of the inversion of the velocity vector, Aarseth and Zare [1, 3, 41] proposed

a function of the form

$$g = \prod_{i<j} q_{ij} \qquad q_{ij} = \mathbf{r_i} - \mathbf{r_j}, \quad i = 1, 2, \cdots, N, \tag{2.3}$$

while Heggie [27] considered smoothing transformations for simultaneous collisions of N bodies in the form

$$g = \frac{\prod\limits_{i<j} q_{ij}}{\left(\sum\limits_{i<j} q_{ij}\right)^{\beta}}, \qquad \beta = \frac{N(N-1)-3}{2}, \quad i = 1, 2, \cdots, N. \tag{2.4}$$

The use of function g in the form of the inverse of the potential energy of the system U or the inverse of the Lagrangian of the system $L = T - U$ (where T is the kinetic energy) was also explored [3, 8].

It was also recognised [8] that such transformations on their own do not offer the best formulation for numerical work. Regularisations with transformations involving both the dependent and the independent variables were used to transform the equations of motion into their form suitable for numerical integration. Such regularisation techniques are essentially based on three steps [16]:

1. a coordinate transformation,
2. the introduction of a fictitious time τ by the properly chosen function g,
3. the use of the energy integral (the Hamiltonian H of the system) in order to transform the singular differential equations into regular ones (Equation 2.2).

For planar motion the Levi-Civita transformation is commonly used as the simplest for implementation. In 1920, Levi-Civita introduced a coordinate transformation of the form

$$q_1 = Q_1^2 - Q_2^2,$$
$$q_2 = 2Q_1Q_2,$$

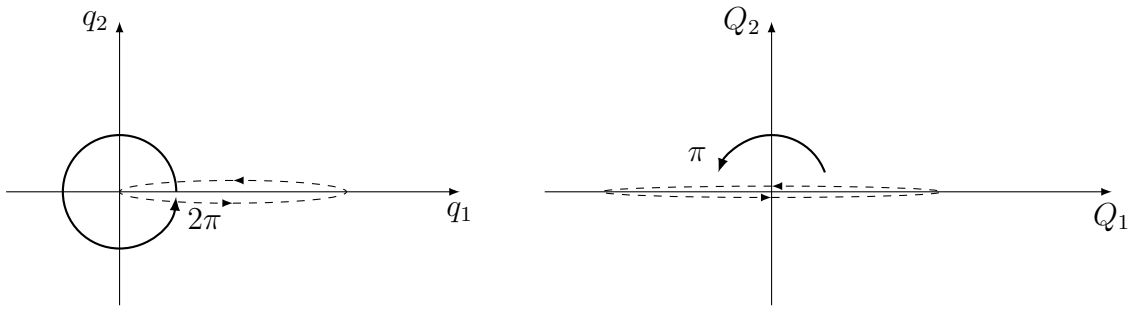

Figure 2.2: The revolution about the centre of mass in real coordinates (left) becomes half the revolution about the centre of mass in regularised coordinates (right). (Reproduction of Figure 4 in Celetti [16])

where q_1 and q_2 are the components of the interbody distance vector $\mathbf{q}$, and Q_1 and Q_2 are the new dependent variables. For the two-body Hamiltonian, this transformation yields the Hamiltonian of a harmonic oscillator [46]. It might be noted that the Levi-Civita coordinate transformation can be written as the conformal squaring

$$z = w^2,$$

where $z = q_1 + iq_2$ and $w = Q_1 + iQ_2$ are complex vectors. It follows that

$$q = Q_1^2 + Q_2^2 = (q_1^2 + q_2^2)^{1/2},$$

i.e. in the Levi-Civita coordinates the expression for the interbody distance R does not require the calculation of a square root.

The angles at the origin are halved in the regularised coordinates [16]. Denoting the angle between the position vector and the origin in the original coordinates by θ and in regularised coordinates by ψ gives

$$\tan\theta = \frac{q_2}{q_1} = \frac{2Q_1Q_2}{Q_1^2 - Q_2^2} = \frac{2 \cdot \frac{Q_2}{Q_1}}{1 - (\frac{Q_2}{Q_1})^2} = \frac{2\tan(\psi)}{1 - \tan^2(\psi)} = \tan 2\psi.$$

Consequently, if in the original coordinates one body makes one revolution about the other, then in the Levi-Civita coordinates this body will make only one half of a revolution [8, 69] (see Figure 2.2).

This type of regularisation was also used effectively in Sivasankaran, Steves and Sweatman [63, 64], although with the time transformation similar to the one proposed by Heggie [27] (Equation 2.4). It was shown to be effective for close two-body encounters by performing a test on preserving energy during numerical integrations. The energy errors were at most of order 10^{-6}.

A new method of regularisation, based on the Levi-Civita transformation, of simultaneous binary collisions, was proposed by Waldvogel [79] for the planar problem of three bodies. The coordinate transformation is performed in terms of fourth degree polynomials. A possibility of a triple collision is avoided by choosing a suitable time transformation so that it can only be approached asymptotically. This regularisation was used by Hénon [31, 32, 33, 34] in his study of the families of planar three-body orbits.

It was shown by Hurwitz in 1933 that the generalisation of the Levi-Civita coordinate transformation to three dimensions is not possible [8]. However, the transformation can be performed in four dimensions. Kustaanheimo and Stiefel [69] generalised Levi-Civita's transformation to the case when motion takes place in three dimensions by using two four-dimensional vectors $\mathbf{q}$ and $\mathbf{Q}$ connected by relations

$$
\begin{aligned}
q_1 &= Q_1^2 - Q_2^2 - Q_3^2 + Q_4^2, \\
q_2 &= 2(Q_1 Q_2 - Q_3 Q_4), \\
q_3 &= 2(Q_1 Q_3 + Q_2 Q_4), \\
q_4 &= 0
\end{aligned}
$$

with a magnitude

$$q = Q_1^2 + Q_2^2 + Q_3^2 + Q_4^2.$$

The Kustaanheimo and Stiefel (K-S) transformation was found to be successful and is widely used for N-body problem integration. It was generalised later by Aarseth and Zare [1, 2] for three-body systems. This was extended for N-body systems by Mikkola and Aarseth [41, 45], now known as the chain method.

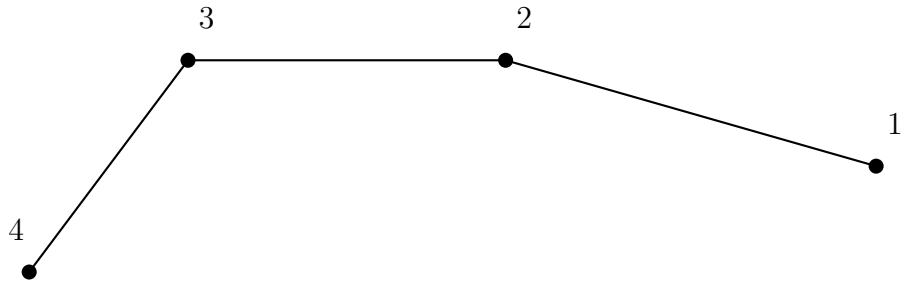

Figure 2.3: An example of a four-body chain

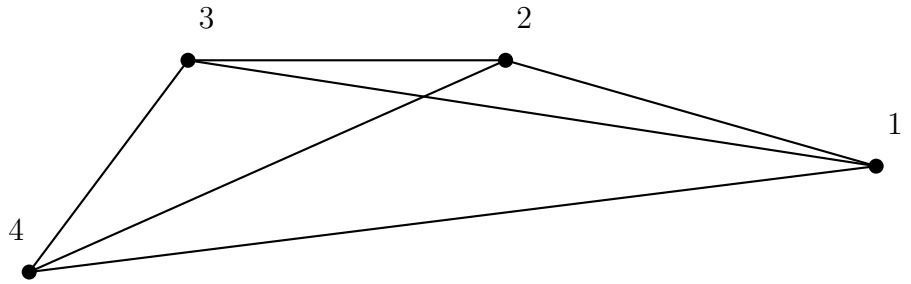

Figure 2.4: Heggie's global regularisation applied to the same example as in Figure 2.3.

The Aarseth-Zare method, or chain method, uses a chain of shortest interbody distance vectors (see Figure 2.3 for the example of a four-body chain). The vectors are labelled and transformed using K-S regularisation. During numerical integration, if particles change their order, or "non-chained" distances become small comparing with "chained" distances, the switching and relabelling of the chain vectors occurs.

At the same time, Heggie [27] found a way to simultaneously regularise all possible two-body collisions and thus invented the global regularisation method for N-body systems. This, however, results in a further increase in the number of variables and the differential equations for the problem. It is seen in Figure 2.4 that Heggie regularisation, applied to the general four-body system, increases the number of equations from 16 (for the positions and velocities of the bodies in the fixed problem) to 24 (for the interbody distances and corresponding momenta in the regularised problem). In comparison, for the chain-formulation of the four-body system the number of equations is 12 (6 for interbody distances and 6 for corresponding momenta).

Heggie's method was not widely used because of the complexity of the original formulation. In 1985 Mikkola [40] employed a modified notation for the coordinates and derived the equations of motions that made the use of the Heggie's global regularisation

convenient. Also, an alternative time transformation was proposed. This adaptation of the Heggie method is further described in Chapter 4.

A comparison of regularisation methods, with different choices of time transformations for binary-single and binary-binary interactions, was conducted by Alexander [3]. The following regularisation schemes were examined: Aarseth-Zare [1, 41, 45], Zare [1], Heggie with Mikkola's formulation [27, 40]. The tested time transformations include those discussed earlier (Equations (2.3) and (2.4)), and functions involving the kinetic energy T as well as the potential energy U of the system.

The conclusion Alexander made is that the most effective schemes of regularisation are the chain regularisation and the Heggie global regularisation along with the time transformation $g = 1/L$ involving the Lagrangian of the system $L = T - U$. However, the Heggie regularisation is computationally expensive because of the large number of equations.

Chapter 3

The Caledonian symmetric four-body problem: the equations and Levi-Civita regularisation

3.1 Equations of motion

The Caledonian Symmetric Four-Body Problem (CS4BP) was introduced by Roy [58] and Steves and Roy [66, 67] in 1998. Sometimes it is also referred to as the Caledonian Symmetric Double Binary Problem [58]. The idea behind this modelling was to build a system analogous to the Copenhagen three-body problem (the circular restricted coplanar three-body problem with two finite equal masses and an infinitesimal particle) for four bodies. Such a system can provide some insight into the general problem of four bodies with the help of the symmetric restrictions introduced.

The original investigation sought to model a restricted four-body problem with a minimum number of variables and initial conditions. The introduced simplifications of the CS4BP model reduce the initial four-body problem with 28 parameters (24 for positions and velocities and 4 for masses of the bodies) to only 18 parameters with only 6 acting as initial parameters [66].

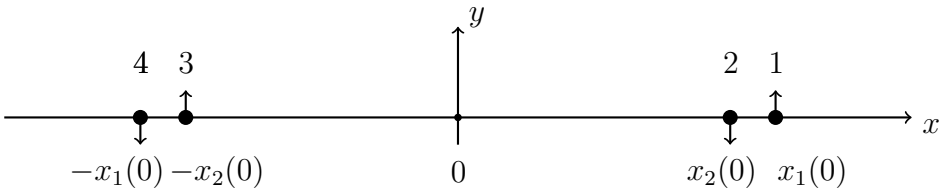

Figure 3.1: The initial configuration of the four bodies

We consider a system of four bodies 1, 2, 3 and 4 which have point masses m_1, m_2, m_3 and m_4 (see Figure 3.1). The four masses move in coplanar orbits about the centre of mass in a fixed plane. Each mass is described by two coordinates, x and y, for positions and two coordinates, u and v, for momenta.

The position coordinates of the four bodies are taken to be $\mathbf{r}_1 = (x_1, y_1)$, $\mathbf{r}_2 = (x_2, y_2)$, $\mathbf{r}_3 = (-x_2, -y_2)$, $\mathbf{r}_4 = (-x_1, -y_1)$ and the corresponding momenta are $(u_1, v_1) = 2m_1\,(\dot{x}_1, \dot{y}_1)$, $(u_2, v_2) = 2m_2\,(\dot{x}_2, \dot{y}_2)$, $(-u_2, -v_2) = 2m_2\,(-\dot{x}_2, -\dot{y}_2)$ and $(-u_1, -v_1) = 2m_1\,(-\dot{x}_1, -\dot{y}_1)$.

The units of the system are the standard N-body units and are chosen so that the gravitational constant $G = 1$ (see Appendix A for details). The centre of mass of the system is fixed at the origin. The value of the total mass is fixed with $M = \sum_{i=1}^{4} m_i = 4$.

The bodies are labelled as 1, 2, 3, 4 according to their initial order, from right to left. The bodies 1 and 4 are referred to as the outer bodies, and the bodies 2 and 3 are called the inner bodies. Although the relative position of the bodies may change as they move, we name them according to their initial configuration.

The bodies form a collinear configuration at $t = 0$, and initially move with velocities perpendicular to the line from which they start. For simplicity we assume that at the start of the integration time, or at time $t = 0$, the bodies are located on the x-axis. The initial velocities of the bodies have opposite orientation and are perpendicular to the x-axis.

The CS4BP has two symmetric restrictions: about the centre of mass at the origin and in time. Symmetry about the origin applies in such a way that the dynamical evolution of two bodies on one side of the system's centre of mass is a rotational image of that of the two bodies on the other side of the centre of mass [66]. So, the bodies 3 and 4 move symmetric to bodies

1 and 2 with

$$m_1 = m_4, \qquad m_2 = m_3.$$

The system is in a mirror configuration, i.e. it satisfies the Roy-Ovenden Mirror theorem that states: "if N point masses are acted upon by their mutual gravitational forces only, and at a certain epoch each radius vector from the centre of mass of the system is perpendicular to every velocity vector, then the orbit of each mass after that epoch is a mirror image of its orbit prior to that epoch" [58].

In other words, the dynamical behaviour of the four-body system after time $t = 0$ is a mirror image of its behaviour before $t = 0$. So, integrating the system backwards in time does not change the description of the system's behaviour.

In general, the planar four-body system is described by 6 classical integrals of motion: 4 for the centre of mass (3.1), 1 for the angular momentum of the system (3.2) and 1 for the total energy of the system (3.3):

$$\begin{aligned} &\sum_{i=1}^{4} m_i x_i = x_0, \qquad \sum_{i=1}^{4} m_i \dot{x}_i = \dot{x}_0 \\ &\sum_{i=1}^{4} m_i y_i = y_0, \qquad \sum_{i=1}^{4} m_i \dot{y}_i = \dot{y}_0 \end{aligned} \qquad \text{(integrals of centre of mass)}, \tag{3.1}$$

$$\sum_{i=1}^{4} m_i (x_i \dot{y}_i - y_i \dot{x}_i) = A \qquad \text{(integral of angular momentum)}, \tag{3.2}$$

$$\sum_{i=1}^{4} \frac{m_i}{2} \left(\dot{x}_i^2 + \dot{y}_i^2\right) - \sum_{i<j} \frac{m_i m_j}{\sqrt{(x_j - x_i)^2 + (y_j - y_i)^2)}} = E \qquad \text{(integral of energy)}. \tag{3.3}$$

By fixing the centre of mass at the origin we take the centre of mass' integrals to be equal to zero ($x_0 = y_0 = \dot{x}_0 = \dot{y}_0 = 0$). The dynamical symmetry then eliminates the integrals of the centre of mass, leaving only two integrals: that of the angular momentum A and energy E.

We take the initial time $t = 0$ to coincide with an extremum of the distance between the inner bodies, and the x-axis is taken parallel to the direction from body 3 to body 2 at that time (see Figure 3.1). Combined with the symmetry properties, these two conditions can be

written as

$$y_2 = 0, \qquad u_2 = 0 \qquad \text{for} \quad t = 0. \tag{3.4}$$

The total energy of the system is constant and is taken to be $E = K + U = -1$, where

$$K = m_1\dot{x}_1^2 + m_1\dot{y}_1^2 + m_2\dot{x}_2^2 + m_2\dot{y}_2^2 = \frac{1}{4m_1}\, u_1^2 + \frac{1}{4m_1}\, v_1^2 + \frac{1}{4m_2}\, u_2^2 + \frac{1}{4m_2}\, v_2^2$$

is the kinetic energy of the system, and

$$U = -\frac{2m_1m_2}{r_{12}} - \frac{2m_1m_2}{r_{13}} - \frac{m_1^2}{r_{14}} - \frac{m_2^2}{r_{23}},$$

is the potential energy of the system with

$$\begin{aligned}
r_{12} &= \left((x_1 - x_2)^2 + (y_1 - y_2)^2\right)^{\frac{1}{2}} = r_{34}, \\
r_{13} &= \left((x_1 + x_2)^2 + (y_1 + y_2)^2\right)^{\frac{1}{2}} = r_{24}, \\
r_{14} &= \left((2x_1)^2 + (2y_1)^2\right)^{\frac{1}{2}}, \\
r_{23} &= \left((2x_2)^2 + (2y_2)^2\right)^{\frac{1}{2}}.
\end{aligned}$$

The choice of negative potential energy is dictated by the convention that for gravitational systems the reference point, at which the potential energy is zero, is at infinite separation. Since the potential energy increases as a mass moves away from another mass, it should be negative at any finite distance.

By fixing the total energy with a negative value we require that in magnitude the system possesses more potential energy than kinetic energy. This ensures that at least one pair of bodies will stay bounded for all time. Hietarinta and Mikkola [35] cite Hopf who showed that "the system actually stays bound forever or breaks up in both directions of time, with the exception of a set of measure zero".

Sweatman [72] (citing Mikkola [39]) outlines four possible outcomes in the case of even a small positive energy:

1. two separate binaries moving independently,

2. three bound together masses and an isolated single mass,

3. one binary with two single masses,

4. four isolated masses, moving independently (also called full ionisation).

In other words, when the total energy is positive, the system falls apart with at least one body moving away. Sweatman [72] notes that the case leading to full ionisation can only occur when the energy is divided evenly among the masses in the original configuration.

The system is symmetric and its Hamiltonian is

$$H = \frac{1}{4m_1}\left(u_1^2 + v_1^2\right) + \frac{1}{4m_2}\left(u_2^2 + v_2^2\right) - \frac{2m_1m_2}{r_{12}} - \frac{2m_1m_2}{r_{13}} - \frac{m_1^2}{r_{14}} - \frac{m_2^2}{r_{23}}. \tag{3.5}$$

The differential equations corresponding to the Hamiltonian are

$$\frac{dx_i}{dt} = \frac{\partial H}{\partial u_i}, \qquad \frac{dy_i}{dt} = \frac{\partial H}{\partial v_i}, \qquad \frac{du_i}{dt} = -\frac{\partial H}{\partial x_i}, \qquad \frac{dv_i}{dt} = -\frac{\partial H}{\partial y_i}, \qquad i = 1, 2 \tag{3.6}$$

with initial conditions that the bodies start at $t = 0$ on the x-axis with coordinates $(x_1(0), 0)$, $(x_2(0), 0)$, $(-x_2(0), 0)$, $(-x_1(0), 0)$ and transverse momenta $(0, v_1(0))$, $(0, v_2(0))$, $(0, -v_2(0))$, $(0, -v_1(0))$.

3.2 Levi-Civita regularisation

The differential equations are difficult to solve directly near close encounters because of the singularity that occurs at a two-body collision. The precision of the numerical integration near the collision event will inevitably become poor. The integration process becomes extremely long: the step-size of a numerical integrator decreasing significantly to compensate numerical errors at each step. This leads to the accumulation of round-off errors.

In order to enable integration through these events, we transform the singular differential equations into regular ones by means of a variable transformation [69]. In this section we follow closely the approach of Sivasankaran, Steves and Sweatman [63, 64] for regularising two-body collisions in the planar symmetric system of four bodies. The proposed regularisation scheme is an adaptation of the global regularisation developed by Heggie [27]. It makes use of a Levi-Civita type transformation and a rescaled time.

In the general planar four-body problem there are six possible collisions between two bodies. There are only four possible collisions in the CS4BP, namely:

- between the bodies 1 and 2 and between the bodies 3 and 4 - when the interbody distances r_{12} or r_{34} are equal to zero,
- between the bodies 1 and 3 and between the bodies 2 and 4 - when the interbody distances r_{13} or r_{24} are equal to zero,
- between the outer bodies 1 and 4 - when the interbody distance r_{14} is equal to zero,
- between the inner bodies 2 and 3 - when the interbody distance r_{23} is equal to zero.

In order to regularize the singularities that occur during collisions, we use the Levi-Civita coordinate transformation. First, we introduce the interbody coordinates q_j, $j = 1, \ldots, 8$ which are the x and y coordinates of the interbody vectors, by

$$\begin{aligned} q_1 &= x_1 - x_2, & q_5 &= 2x_1 \\ q_2 &= y_1 - y_2, & q_6 &= 2y_1, \\ q_3 &= x_1 + x_2, & q_7 &= 2x_2, \\ q_4 &= y_1 + y_2, & q_8 &= 2y_2. \end{aligned}$$

The corresponding momenta p_j are defined as related to the original momenta, u_i and v_i, by means of the generating function F_1 given by

$$u_i = \frac{\partial F_1}{\partial x_i}, \qquad v_i = \frac{\partial F_1}{\partial y_i}, \qquad \text{where } F_1 = \sum_{j=1}^{8} p_j q_j(x_1, x_2, y_1, y_2), \quad i = 1, 2, 3, 4.$$

So, the generating function F_1 is

$$F_1 = p_1(x_1 - x_2) + p_2(y_1 - y_2) + p_3(x_1 + x_2) + p_4(y_1 + y_2) + 2p_5x_1 + 2p_6y_1 + 2p_7x_2 + 2p_8y_2$$

and the relations between original momenta and the conjugate momenta take the following form:

$$u_1 = \frac{\partial F_1}{\partial x_1} = p_1 + p_3 + 2p_5, \qquad v_1 = \frac{\partial F_1}{\partial y_1} = p_2 + p_4 + 2p_6,$$
$$u_2 = \frac{\partial F_1}{\partial x_2} = -p_1 + p_3 + 2p_7, \qquad v_2 = \frac{\partial F_1}{\partial y_2} = -p_2 + p_4 + 2p_8.$$

This gives four equations for eight momentum coordinates. For the inverse transformation we require another four relations. We note from the definition of q_j that

$$q_5 = q_1 + q_3, \qquad q_7 = q_3 - q_1,$$
$$q_6 = q_2 + q_4, \qquad q_8 = q_4 - q_2.$$

In order to eliminate the degeneracy found in the momentum coordinates, we choose a similar relation to hold for the momenta

$$p_5 = p_1 + p_3, \qquad p_7 = p_3 - p_1,$$
$$p_6 = p_2 + p_4, \qquad p_8 = p_4 - p_2.$$

After summarising the above formulas, the conjugate momenta are derived using the formulae:

$$p_1 = \frac{1}{6}(u_1 - u_2), \qquad p_5 = \frac{1}{3}u_1,$$
$$p_2 = \frac{1}{6}(v_1 - v_2), \qquad p_6 = \frac{1}{3}v_1,$$
$$p_3 = \frac{1}{6}(u_1 + u_2), \qquad p_7 = \frac{1}{3}u_2,$$
$$p_4 = \frac{1}{6}(v_1 + v_2), \qquad p_8 = \frac{1}{3}v_2.$$

We finally perform the Levi-Civita regularisation by introducing the new coordinates (Q_k, P_k) such that

$$q_k = Q_k^2 - Q_{k+1}^2, \qquad q_{k+1} = 2Q_kQ_{k+1}, \qquad k = 1, 3, 5, 7.$$

So,

$$\begin{aligned} q_1 &= Q_1^2 - Q_2^2, & q_2 &= 2Q_1Q_2, \\ q_3 &= Q_3^2 - Q_4^2, & q_4 &= 2Q_3Q_4, \\ q_5 &= Q_5^2 - Q_6^2, & q_6 &= 2Q_5Q_6, \\ q_7 &= Q_7^2 - Q_8^2, & q_8 &= 2Q_7Q_8. \end{aligned}$$

For the inverse transformation we use the relation

$$Q_1 = \left(q_1^2 + q_2^2\right)^{\frac{1}{4}} \cos\left(\frac{\arctan\frac{q_2}{q_1}}{2}\right), \qquad Q_2 = \left(q_1^2 + q_2^2\right)^{\frac{1}{4}} \sin\left(\frac{\arctan\frac{q_2}{q_1}}{2}\right).$$

which originates from solving the equation $z = w^2$, or $w = \pm\sqrt{z}$, where $z = q_1 + iq_2$, $w = Q_1 + iQ_2$, $z,\ w \in \mathbb{C}$.

Since $x_1(0) > x_2(0) > 0$ by assumption, then $q_1(0)$ and $q_2(0)$ are positive too, so we can make a choice of neglecting the negative square root case. We then represent a complex solution in a trigonometric form as $z = re^{i\theta}$, where $r = \sqrt{q_1^2 + q_2^2}$, $\theta = \arctan\frac{q_2}{q_1}$, or $w = \sqrt{r}\left(\cos\frac{\theta}{2} + i\sin\frac{\theta}{2}\right)$. The same consideration applies to the other interbody distances. All q_j are positive, so the negative square root case is neglected.

An alternative inverse transformation involves only the use of square roots and is represented by

$$Q_1 = \sqrt{\frac{\sqrt{q_1^2 + q_2^2} + q_1}{2}} \qquad Q_2 = \sqrt{\frac{\sqrt{q_1^2 + q_2^2} - q_1}{2}}.$$

We tested both expressions, and they produced similar results in terms of computational errors and simulation time. In the actual computations the first expression was used.

The corresponding conjugate momenta P_k are found using the generating function F_2 by

$$P_k = \frac{\partial F_2}{\partial Q_k}, \qquad \text{where } F_2(p_k, Q_k) = \sum_{j=1}^{8} p_j q_j(Q_1, \ \ldots, \ Q_8), \qquad k = 1, ..., 8$$

that is

$$P_j = 2p_j Q_j + 2p_{j+1}Q_{j+1}, \qquad P_{j+1} = 2p_{j+1}Q_j - 2p_j Q_{j+1}, \qquad j = 1, 3, 5, 7,$$

or, explicitly,

$$\begin{aligned} P_1 &= 2p_1Q_1 + 2p_2Q_2, & P_5 &= 2p_5Q_5 + 2p_6Q_6, \\ P_2 &= -2p_1Q_2 + 2p_2Q_1, & P_6 &= -2p_5Q_6 + 2p_6Q_5, \\ P_3 &= 2p_3Q_3 + 2p_4Q_4, & P_7 &= 2p_7Q_7 + 2p_8Q_8, \\ P_4 &= -2p_3Q_4 + 2p_4Q_3, & P_8 &= -2p_7Q_8 + 2p_8Q_7. \end{aligned}$$

The inverse formulas are

$$\begin{aligned} p_1 &= -\frac{1}{2}\frac{P_2Q_2 - P_1Q_1}{Q_1^2 + Q_2^2}, & p_5 &= -\frac{1}{2}\frac{P_6Q_6 - P_5Q_5}{Q_5^2 + Q_6^2}, \\ p_2 &= \frac{1}{2}\frac{P_1Q_2 + Q_1P_2}{Q_1^2 + Q_2^2}, & p_6 &= \frac{1}{2}\frac{P_5Q_6 + P_6Q_5}{Q_5^2 + Q_6^2}, \\ p_3 &= -\frac{1}{2}\frac{P_4Q_4 - P_3Q_3}{Q_3^2 + Q_4^2}, & p_7 &= -\frac{1}{2}\frac{P_8Q_8 - P_7Q_7}{Q_7^2 + Q_8^2}, \\ p_4 &= \frac{1}{2}\frac{P_3Q_4 + P_4Q_3}{Q_3^2 + Q_4^2}, & p_8 &= \frac{1}{2}\frac{P_7Q_8 + P_8Q_7}{Q_7^2 + Q_8^2}. \end{aligned}$$

We additionally introduce a rescaled time τ, similar to one proposed by Heggie [27], which includes a modification by the exponent power of $\frac{5}{2}$. This was found to produce a better performance in conserving energy [64],

$$\frac{dt}{d\tau} = g = \frac{r_{12}r_{13}r_{14}r_{23}}{(r_{12} + r_{13} + r_{14} + r_{23})^{\frac{5}{2}}} = \frac{(Q_1^2 + Q_2^2)(Q_3^2 + Q_4^2)(Q_5^2 + Q_6^2)(Q_7^2 + Q_8^2)}{(Q_1^2 + Q_2^2 + Q_3^2 + Q_4^2 + Q_5^2 + Q_6^2 + Q_7^2 + Q_8^2)^{\frac{5}{2}}}.$$

The final time-transformed Hamiltonian takes the form

$$\Gamma = g(Q_i)\left(H'(Q_i, P_i) - H(0)\right), \tag{3.7}$$

where H' is the original Hamiltonian considered as a function of regularised coordinates Q_i and P_i, $H(0)$ is the initial value of the Hamiltonian, $H(0) = E$.

The new regularised equations are

$$\frac{dQ_i}{d\tau} = \frac{\partial \Gamma}{\partial P_i}, \qquad \frac{dP_i}{d\tau} = -\frac{\partial \Gamma}{\partial Q_i}, \qquad \frac{dt}{d\tau} = g, \qquad i = 1, 2, 3, 4. \tag{3.8}$$

Their implementation showed satisfactory results in conserving the integrals of motion with relative errors of order 10^{-15} over several periods and within a reasonable computational time.

3.3 Orbital period

When we use the terms "periodic solution" or "periodic orbit", we mean that the relative configuration of the bodies at the beginning and end of a period is the same. The considered orbits are not strictly speaking periodic because the whole system of four bodies is rotating around the system's centre of mass [31, 32]. This means that the start and end of the period do not necessarily coincide in physical coordinates.

The standard definition of a periodic orbit for a three-body problem is found in Whittaker [81] which states: "In the problem of three bodies, a solution is said to be periodic if the mutual distances of the bodies are periodic functions of the time, although the bodies may not necessarily have the same orientation at the end of a period as at its beginning".

Following Hénon [32] and Sweatman [71], we use a rotating frame with constant angular velocity ω about the centre of mass, so the positions of the bodies at the end of the period are rotated by some angle θ with respect to their initial positions. Such a system of coordinates is called "rotating coordinates" by Hénon [31, 32], and this kind of orbit is sometimes referred to

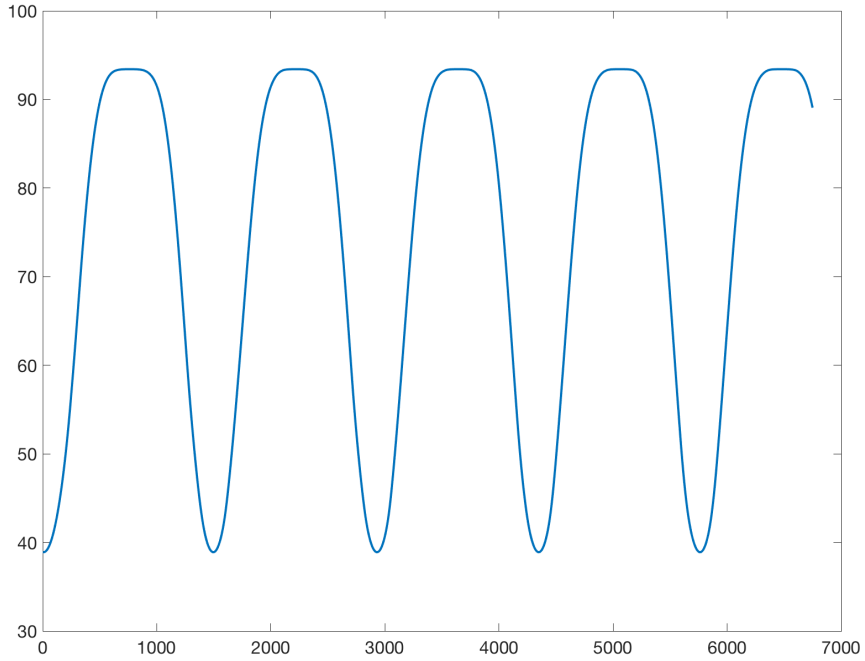

Figure 3.2: Distance r_{23} between bodies 2 and 3 against the number of its calculations over about four full periods.

as a "relatively periodic orbit" [12, 13].

In our setting, the bodies' initial conditions imply that the inner bodies are at extrema at $t = 0$. Thus if we denote by r_{23} the distance between inner bodies with $r_{23}(0) = 2x_2$, then $\dot{r}_{23}(0) = 0$. The next time when $\dot{r}_{23} = 0$ is a half-period of the orbit and r_{23} is minimal. Distance r_{23} is again at maximum when bodies complete one period, and so on (see Figure 3.2). Thus, the relation that is used to determine the end of a period for stability analysis is $\dot{r}_{23} = 0$, or in regularised form,

$$(Q_7\dot{Q}_7 + Q_8\dot{Q}_8) = 0. \tag{3.9}$$

Taking into account the symmetries of the CS4BP, we use a special case of the period's definition that relies on the fact that the bodies are on the same $y = 0$ line at the start of integration. If integration starts at time $t = 0$, then at time $t = T$, or at the end of the period, they must be lined up again in the same configuration. Using the line equation $y = kx$, we can derive the following relation for the coordinates of the two bodies, and then apply the symmetry

of the problem to the other two bodies on the other side of system's centre of mass:

$$\frac{y_2}{x_2} = \frac{y_1}{x_1} = k,$$

or

$$y_1 x_2 - y_2 x_1 = 0. \tag{3.10}$$

Thus, we say that when the relation (3.10) becomes true then the bodies have completed one revolution one around another. It should be noted that the bodies are on a line not only at the beginning and end of one period, but also at the half-period. However, since they are in a different configuration, this crossing is skipped. For the purpose of increasing the speed of computations the relation (3.10) is implemented in the regularised form

$$(Q_6 Q_7 - Q_5 Q_8)(Q_5 Q_7 + Q_6 Q_8) = 0.$$

However, in the calculations that break the initial collinear configuration, the former definition of a period (Equation 3.9) is used. A similar relation to (3.9) is constructed for the general four-body problem and used in the calculations that do not take into account the symmetries of the problem. For instance, during the stability analysis we introduce non-symmetric perturbations to test the orbit's survival (see Section 5.4 for details). Also, in the case of transverse or vertical perturbations the bodies are not on a line any more (see Section 5.5 for details).

3.4 Rotating coordinates

As it was discussed in the previous section, the system rotates around the centre of mass (see Figure 3.3) with constant angular velocity ω. This means that the bodies deviate from their original coordinates during one period by some fixed angle θ. We can represent this using a rotating frame with constant angular velocity $\omega = \theta/T$, where T is the period of an orbit.

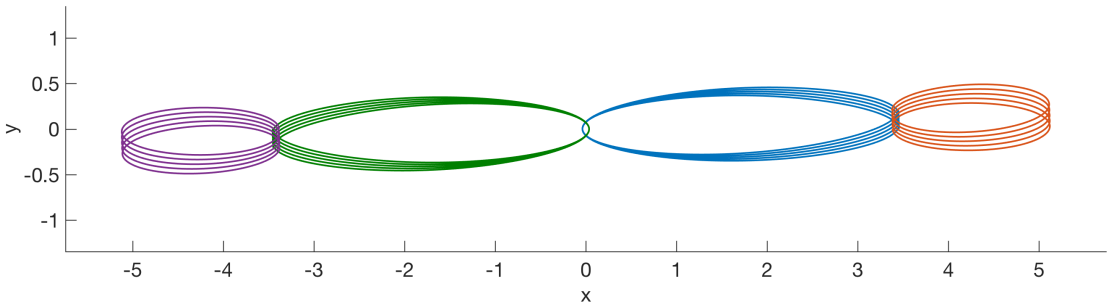

Figure 3.3: Bodies plotted in a non-rotating frame in fixed coordinates (about five periods are shown)

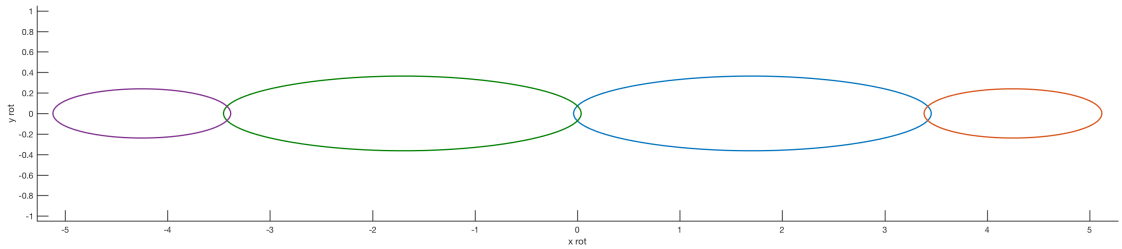

Figure 3.4: Bodies plotted in a rotating frame in rotating coordinates (about five periods are shown)

The rotation of the physical coordinates by $-\theta$ around the origin during one period makes all successive periods of the orbits match one another (see Figure 3.4). It also helps us to see the periodicity clearer, because for some orbits it is not obvious that the orbits are actually periodic in the relative sense.

So, after tracking an orbit for one period T we measure the angle θ between the x-axis and the line going through all bodies and the origin. We set the angle to be in the region $\theta \in [-\pi, \pi]$. We then find the angular velocity ω and introduce the rotating coordinates by means of the rotation matrix for the time of integration $t \in [0, T]$,

$$R(t) = \begin{bmatrix} \cos \omega t & \sin \omega t \\ -\sin \omega t & \cos \omega t \end{bmatrix}.$$

The rotating coordinates are essential to use during the search for orbits or in the stability analysis of an orbit, as they allow us to determine the relative value by which the body deviated from its initial position as it moves along its orbit. Some of the restricted three-body problems

are defined and modelled within the rotating frame. This enables us to remove the rotation of the system and search for periodic orbits of the reduced system.

We should note here that the way of representing the orbits in rotating coordinates is not unique because angle θ is defined only modulo 2π. We utilise this idea later in Section 7.5 in order to observe the orbits from different perspectives.

Chapter 4

The general four-body problem: a three-dimensional view

4.1 Equations of motion

In this chapter we provide a description of the general problem of four bodies moving under their mutual gravitational interaction. Although we aim to study symmetric systems, we should include the possibility for non-symmetric behaviour. Even for symmetric motion, if an external object affects the system, the chance that it will have a symmetric effect on the system is extremely small.

It is important to determine whether the symmetric family of orbits survives under any type of perturbation. In order to consider non-symmetric effects, we introduce and study the influence of general perturbations within the general four-body problem. These can be planar perturbations or those in three-dimensional space.

The classical four-body problem is formulated as for the many-body problem for the case when the number of bodies is four. Each body has a mass m_i, $i = 1, \ldots, 4$ and is described by three coordinates, $\mathbf{r}_i = (x_i, y_i, z_i)$, for positions and three coordinates, $m_i\dot{\mathbf{r}}_i = (u_i, v_i, w_i)$, for momenta in a fixed coordinate frame.

The general problem in three dimensions is described by 10 integrals of motion: two more integrals for the centre of mass are added for the third dimension, and the angular momentum of the system is now described as three projections of the angular momentum vector,

$$\begin{aligned}
&\sum_{i=1}^{4} m_i x_i = x_0, \qquad \sum_{i=1}^{4} u_i = u_0, \\
&\sum_{i=1}^{4} m_i y_i = y_0, \qquad \sum_{i=1}^{4} v_i = v_0, \qquad \text{(integrals of centre of mass)}, \qquad (4.1)\\
&\sum_{i=1}^{4} m_i z_i = z_0, \qquad \sum_{i=1}^{4} w_i = w_0,
\end{aligned}$$

$$\begin{aligned}
&\sum_{i=1}^{4} (x_i v_i - y_i u_i) = A_{xy}, \\
&\sum_{i=1}^{4} (y_i w_i - z_i v_i) = A_{yz}, \qquad \text{(integrals of angular momentum)}, \qquad (4.2)\\
&\sum_{i=1}^{4} (z_i u_i - x_i w_i) = A_{xz},
\end{aligned}$$

$$\sum_{i=1}^{4} \frac{(u_i^2 + v_i^2 + w_i^2)}{2m_i} - \sum_{i<j} \frac{m_i m_j}{\sqrt{(x_j - x_i)^2 + (y_j - y_i)^2 + (z_j - z_i)^2}} = E(\text{energy integral}). \qquad (4.3)$$

The centre of mass is at (x_0, y_0, z_0) and moves with constant momentum (u_0, v_0, w_0). We fix the centre of mass by setting all the six integrals of the centre of mass to be zero. The energy integral is fixed at the level -1, as before.

Now, when we apply the initial conditions for the targeted orbits (see previous chapter), without stating specifically the symmetry of the orbits, we add the following modifications: since the motion of the four bodies is entirely planar, both z and w coordinates of each body are zero, unless there are any perturbations of them. This sets two of the angular momentum integrals, A_{yz} and A_{xz}, to zero.

To make sure that the Mirror theorem [57] is satisfied, we set the bodies to be in a collinear configuration at $t = 0$ and to have velocities perpendicular to the line from which they start. Also, to set time and initial angle of rotation for the system, we take the initial time $t = 0$ to coincide with an extremum of the distance between the inner bodies, and the x-axis is taken

parallel to the direction from body 3 to body 2 at that time. These two conditions can be written as

$$\begin{aligned} r_{23} &= y_2 - y_3 = 0, \\ \dot{r}_{23} &= u_2 - u_3 = 0 \end{aligned} \qquad \text{for} \quad t = 0,$$

which simplifies to

$$\begin{aligned} y_2 &= y_3, \\ u_2 &= u_3, \end{aligned} \qquad \text{for} \quad t = 0. \tag{4.4}$$

The value of the total mass is fixed as $\sum_{i=1}^{4} m_i = 4$ with $m_1 = m_4$ and $m_2 = m_3$. The energy integral (4.3) is the Hamiltonian of the system, and the differential equations corresponding to the Hamiltonian are

$$\frac{dx_i}{dt} = \frac{\partial H}{\partial u_i}, \qquad \frac{dy_i}{dt} = \frac{\partial H}{\partial v_i}, \qquad \frac{du_i}{dt} = -\frac{\partial H}{\partial x_i}, \qquad \frac{dv_i}{dt} = -\frac{\partial H}{\partial y_i}, \qquad i = 1, \ldots, 4 \tag{4.5}$$

with initial conditions that the bodies start at $t = 0$ on the x-axis with coordinates $(x_1(0), 0, 0)$, $(x_2(0), 0, 0)$, $(x_3(0), 0, 0)$, $(x_4(0), 0, 0)$, where $x_1(0)$, $x_2(0) > 0$ and $x_3(0)$, $x_4(0) < 0$ and transverse momenta $(0, v_1(0), 0)$, $(0, v_2(0), 0)$, $(0, v_3(0), 0)$, $(0, v_4(0), 0)$, where $v_1(0) > 0$, $v_2(0) < 0$, $v_3(0) > 0$, $v_4(0) < 0$.

4.2 Heggie regularisation

For the general three-dimensional four-body problem we use the regularisation proposed by Heggie [27]. Similar to the previous section, in order to regularise the singularities arising in a close encounter of any two bodies of the system, we map the three-dimensional physical space onto a four-dimensional parametric space using a sequence of transformations.

As discussed in Chapter 2, the generalisation of the Levi-Civita regularisation cannot be performed in three dimensions. However, a three- to four-dimensional mapping is possible. This kind of coordinate transformation is called the Kustaanheimo-Stiefel transformation [1, 69]. In this section we repeat steps from Mikkola [40] for obtaining the regularised Hamiltonian and

the regularised equations of motion.

First, we introduce the interbody coordinate vectors $\mathbf{q}_{ij} = (q_1, q_2, q_3)$, which now represent all six possible interbody distances in the four-body system as compared to the four required for the symmetric problem. The indices i and j indicate the bodies between which the distance is taken. These indices are replaced by a single index k for interbody coordinate vectors $\hat{\mathbf{q}}_k$ in the equations:

$$\hat{\mathbf{q}}_k = \mathbf{q}_{ij} = \mathbf{r}_i - \mathbf{r}_j, \quad k = 4(i-1) - i(i+1)/2 + j, \quad 1 \leq i < j \leq 4.$$

The corresponding momenta $\mathbf{p}_{ij}$ are related to the original velocities of the bodies by

$$\hat{\mathbf{p}}_k = \mathbf{p}_{ij} = (m_i\dot{\mathbf{r}}_i - m_j\dot{\mathbf{r}}_j)/4, \quad k = 4(i-1) - i(i+1)/2 + j, \quad 1 \leq i < j \leq 4.$$

It is important to mention that, although the vectors $\hat{\mathbf{q}}_k$ and $\hat{\mathbf{p}}_k$ are three-dimensional, we introduce the fourth components to both of these vectors for the purpose of Kustaanheimo-Stiefel regularisation. These fourth components are set to be always zero.

The inverse tranformation back to the real coordinates is represented for the positions by

$$\mathbf{r}_i = \frac{1}{M}\left[\sum_{j=i+1}^{4} m_j\mathbf{q}_{ij} - \sum_{j=1}^{i-1} m_j\mathbf{q}_{ji}\right], \qquad M = \sum_{e=1}^{4} m_e,$$

and for the momenta as

$$\dot{\mathbf{r}}_i = \frac{1}{m_i}\sum_{j=i+1}^{4}\mathbf{p}_{ij} - \frac{1}{m_i}\sum_{j=1}^{i-1}\mathbf{p}_{ji}.$$

The generalisation of the Levi-Civita coordinate transformation gives rise to a 4-by-4 matrix

$$\mathcal{L}(\mathbf{Q}_k) = \begin{pmatrix} Q_1 & -Q_2 & -Q_3 & Q_4 \\ Q_2 & Q_1 & -Q_4 & -Q_3 \\ Q_3 & Q_4 & Q_1 & Q_2 \\ Q_4 & -Q_3 & Q_2 & -Q_1 \end{pmatrix}, \tag{4.6}$$

where each $\mathbf{Q}_k$ is the Kustaanheimo-Stiefel regularised interbody distance and defined as $\mathbf{Q}_k =$

(Q_1, Q_2, Q_3, Q_4). The Kustaanheimo-Stiefel transformation [1, 69] transforms the coordinates $\hat{\mathbf{q}}_k$, $\hat{\mathbf{p}}_k$ into variables $\mathbf{Q}_k$, $\mathbf{P}_k$ by

$$\hat{\mathbf{q}}_k = \mathcal{L}(\mathbf{Q}_k)\mathbf{Q}_k, \tag{4.7}$$

$$\hat{\mathbf{p}}_k = \frac{1}{2}\mathcal{L}(\mathbf{Q}_k)\mathbf{P}_k/|\mathbf{Q}_k|^2. \tag{4.8}$$

It can be seen, as mentioned in Section 2.3, that the square root, involved in the interbody distances, in Kustaanheimo-Stiefel coordinates becomes

$$R = |\hat{\mathbf{q}}_k| = \sqrt{q_1^2 + q_2^2 + q_3^2} = |\mathbf{Q}_k|^2 = Q_1^2 + Q_2^2 + Q_3^2 + Q_4^2. \tag{4.9}$$

Since, as we go from three dimensions into four, one of the components of $\mathbf{Q}_k$ is arbitrary, there is some freedom of choice when it comes to specifying the initial coordinates [1]. If $q_1 > 0$, we combine the equation for q_1 from (4.7) with (4.9) [1] so that $q_1 + R = Q_1^2 - Q_2^2 - Q_3^2 + Q_4^2 + R = 2Q_1^2 + 2Q_4^2$ and

$$\begin{aligned}
Q_1 &= \sqrt{\frac{1}{2}(q_1 + R)}, \\
Q_2 &= \frac{1}{2}q_2/Q_1, \\
Q_3 &= \frac{1}{2}q_3/Q_1 \\
Q_4 &= 0.
\end{aligned}$$

If $q_1 < 0$, we then subtract the equation for q_1 (4.7) from (4.9) which results in $R - q_1 = R - Q_1^2 + Q_2^2 + Q_3^2 - Q_4^2 = 2Q_2^2 + 2Q_3^2$ and

$$\begin{aligned}
Q_2 &= \sqrt{\frac{1}{2}(R - q_1)}, \\
Q_1 &= \frac{1}{2}q_2/Q_2, \\
Q_3 &= 0, \\
Q_4 &= \frac{1}{2}q_3/Q_2.
\end{aligned}$$

The initial regularised momenta are found using

$$\mathbf{P}_k = 2\mathcal{L}^T(\mathbf{Q}_k)\hat{\mathbf{p}}_k,$$

where $\mathcal{L}^T(\mathbf{Q}_k)$ is the transpose matrix of $\mathcal{L}(\mathbf{Q}_k)$ (4.6).

The function g used for the rescaled time τ is the inverse of the Lagrangian of the system, $L = K - U$ with K as the kinetic energy of the system and U as potential energy of the system, derived in regularised coordinates. Alexander [3] found that this relation of the rescaled time produces the best efficiency in terms of the accuracy and time for the calculations. Thus, the relation for time is

$$\frac{dt}{d\tau} = g = \frac{1}{L} = \frac{1}{K - U}. \tag{4.10}$$

Similar to the previous section, we derive the regularised Hamiltonian Γ from the original Hamiltonian H considered as a function H' of regularised coordinates Q_k and P_k with $H(0)$ as the initial value of H',

$$\Gamma = g(Q_k, P_k)\left(H'(Q_k, P_k) - H(0)\right).$$

We derive the regularised equations of motion for the general four-body problem. As Heggie regularisation takes into account all six of the interbody distances, the number of equations for the regularised position coordinates is 24 (6 distances considered in the four-dimensional space). Including the 24 equations for the regularised momenta coordinates and the equation for the rescaled time, we obtain a system of 49 regularised equations of motion:

$$\frac{dQ_k}{d\tau} = \frac{\partial \Gamma}{\partial P_k}, \qquad \frac{dP_k}{d\tau} = -\frac{\partial \Gamma}{\partial Q_k}, \qquad \frac{dt}{d\tau} = g, \qquad k = 1, \ldots, 24. \tag{4.11}$$

4.3 A discussion on rotating coordinates in 3D

Referring back to Section 3.3, we seek solutions that are periodic within the introduced rotating frame that moves around the centre of mass with constant angular velocity. This angular

velocity is associated with the value of rotation angle and period of the system. There is also a connection with the angular momentum of the system (Equations (6.1), (7.1), [32]).

This gets more complicated for the general problem when three-dimensional motion is possible. The conservation of three angular momentum integrals must be taken into consideration. To define a three-dimensional rotating frame, we need to take into account three Euler angles. The difficulty is to make sure that all ten integrals of the problem remain conserved for both fixed and rotating coordinate systems.

However, we simplify this problem, because our aim is to separately introduce either planar or vertical perturbations to the components (positions and momenta) of the system, one at a time. In the case of planar perturbations the approach stays the same as before: only one angle θ is used and this is defined on a plane. For vertical perturbations two situations are possible:

1. when perturbing the initial position coordinate z of a body: we may note from (4.2) that when this perturbation is applied, the integral for A_{yz} becomes non-zero (because $y_i = 0$ and $v_i \neq 0$ in the initial configuration of bodies $i = 1, \ldots, 4$)

2. when perturbing the initial momentum coordinate w of a body: for this perturbation $A_{yz} = 0$, but the integral for A_{xz} becomes non-zero (because $u_i = 0$ and $x_i \neq 0$ in the initial configuration of bodies $i = 1, \ldots, 4$)

We then perform two rotations: the first in the $x - z$ plane to confine the motion to a plane, and the second in the $x - y$ plane by the angle θ measured in a similar way as described in Section 3.4.

Introducing the rotating frame in the general three-body problem might be tricky, because the performed orbits themselves can be three-dimensional. However, because for our purposes we only introduce small perturbations, we thus know that the perturbed motion will not deviate much from the plane. The orbital period is defined as before, in terms of the inter-body distances of bodies 2 and 3.

Chapter 5

Periodic orbits: procedures for orbit search and stability analysis

5.1 Introduction

In this work we have used various techniques in order to search for periodic solutions that satisfy the conditions mentioned in Chapter 3, and to conduct further analysis of these periodic solutions. The current chapter is devoted to the explanation of algorithms and procedures that were used in the study.

The first section outlines the differential corrections procedure that is used for searching for periodic orbits in principle. Here we follow the approach described in Broucke [11, 12] and Hénon [32] for three-body orbits in general and restricted elliptic problems.

We should note here that in principle the differential corrections can be applied in different ways to different parameters of the system. For instance, we have tested an implementation of the differential corrections performed in regularised coordinates. This was as successful as when applied to physical coordinates of the system.

The second section provides a sketch of the automatic search procedure, that utilises the differential corrections and describes the idea of searching for the complete branch of the

family, all at once. Most of the rest of the chapter is devoted to the algorithms for linear and vertical stability analysis of orbits. Finally, a nonlinear stability analysis check is presented as introduced by Mikkola and Hietarinta [42].

All of the described methods and algorithms have been implemented in the MATLAB environment (versions from `R2015a` to `R2017a`) during this study. These are also used for integrating orbits that are described later in Chapters 6 and 7.

In our simulations we use the standard MATLAB's `ode45` integrator which is based on the explicit Dormand-Prince method of order 4 [23] from the family of Runge-Kutta methods. Our usual choice of absolute and relative error tolerance for orbit integration is 10^{-12}, as we aim to obtain the orbit with high accuracy. This sets the local truncation error ϵ of the numerical integration to be within $|\epsilon| \leq \max(10^{-12} * |\mathbf{y}|, 10^{-12})$, where $\mathbf{y}$ is the solution vector.

5.2 Differential corrections: a search for a periodic orbit

In the general four-body problem each body is described by three position and three momenta coordinates, giving us a 24-dimensional phase space. In addition to that, each body has a certain mass and volume: the latter is neglected by assuming point masses. Thus, when searching for a periodic orbit, we manipulate a 28-parameter space.

In order to compute orbits of the desired type, we reduce the system and apply restrictions, as discussed previously in Chapters 3 and 4. The motion is restricted to a plane, so the positions and momenta corresponding to the third dimension are zero. The symmetry conditions reduce the number of parameters to 10. This also sets the four centre-of-mass integrals (3.1) to zero and fixes the centre of mass to be at the origin.

At the same time we define the origin of time and initial configuration of the system by the relations (3.4). These relations also overlap with the initial collinear configuration that comes from agreement with the Mirror theorem [58]. If the time or the initial angle are not set, we could achieve an infinity of periodic solutions by simply changing the initial point on the orbit

or by rotating the initial configuration by different angles [31].

By applying the initial configuration, we restrict another 4 parameters (position y and momentum u coordinates). The masses are related by fixing the total mass: $m_2 = 2 - m_1$. We keep the values of both masses fixed and use m_1 as a parameter.

Another two coordinates can be derived by fixing the integrals of total energy E (3.3) and total angular momentum A (3.2) of the system. The energy integral is fixed at the level -1, and angular momentum is used as another parameter in the search.

So, in other words, when we search for a periodic orbit, we search for a periodic solution with particular properties for the specified values of parameters m_1 and A. In order to define the initial state of the system, we need to specify another 2 parameters, x_1 and x_2. This is done by utilising the process of differential corrections.

In general, the periodicity conditions are defined by

$$\mathbf{r}(t) = \mathbf{r}(t+T), \qquad \dot{\mathbf{r}}(t) = \dot{\mathbf{r}}(t+T),$$

where $\mathbf{r}$ is a coordinate vector containing the positions of all bodies, t is time, and T is the period of the orbit. These conditions imply that the distances between the initial coordinates and the coordinates after one period should be zero.

In our setting the desired solutions are not periodic in real physical coordinates: the vectors $\mathbf{r}(T)$ and $\dot{\mathbf{r}}(T)$ are rotated and translated with respect to the initial vectors $\mathbf{r}(0)$ and $\dot{\mathbf{r}}(0)$ [32]. We think of the orbit as periodic with respect to the reduced system with rotating axes (see Section 3.4 for details), and vectors $\mathbf{r}$ and $\dot{\mathbf{r}}$ are defined within the rotating frame. However, if the orbit is not quite periodic, then a small correction $\Delta\mathbf{r}_0$ might be introduced to the initial vector $\mathbf{r}_0 = \mathbf{r}(0)$ so that [13]

$$\mathbf{r}_0 + \Delta\mathbf{r}_0 = \mathbf{r}(T, \mathbf{r}_0 + \Delta\mathbf{r}_0). \tag{5.1}$$

We assume that the correction is so small that the linear theory is valid. Expanding the

right-hand side in $\Delta\mathbf{r}_0$ about the point $(T, \mathbf{r}_0)$ and considering only the first-order terms gives

$$\mathbf{r}_0 + \Delta\mathbf{r}_0 = \mathbf{r}(T, \mathbf{r}_0) + \frac{\partial \mathbf{r}}{\partial \mathbf{r}_0}\Delta\mathbf{r}_0.$$

Rearranging the equation gives

$$\Delta\mathbf{r}_0 = \left[\frac{\partial \mathbf{r}}{\partial \mathbf{r}_0} - I\right]^{-1}(\mathbf{r}_0 - \mathbf{r}(T, \mathbf{r}_0)), \tag{5.2}$$

where I is the identity matrix, $\frac{\partial \mathbf{r}}{\partial \mathbf{r}_0}$ is the matrix of partial derivatives, calculated at $t = T$, and -1 indicates the inverse of a matrix.

The corrections for the coordinates are obtained by solving the linear system (5.2). The matrix of partial derivatives is found by perturbing each of the coordinates of vector $\mathbf{r}$ by a small number (usually of order $10^{-6} - 10^{-8}$). The system is solved iteratively using Newton's method, until the corrections are close enough to zero. The differential corrections process is similar to solving the minimisation problem for differences $d\mathbf{r}$, $d\dot{\mathbf{r}}$ between the initial coordinates and the coordinates after one period ([76]):

$$\sum_{i=1}^{4}\left[(d\mathbf{r}_i)^2 + (d\dot{\mathbf{r}}_i)^2\right] \to 0,$$

where $d\mathbf{r} = \mathbf{r}(t+T) - \mathbf{r}(t), d\dot{\mathbf{r}} = \dot{\mathbf{r}}(t+T) - \dot{\mathbf{r}}(t)$.

The practical procedure is as follows. The differential corrections are applied on the initial values of x_1 and x_2 coordinates. The initial momenta $v_1(0)$, $v_2(0)$ are obtained with 10^{-14} accuracy from the energy (3.3) and angular momentum (3.2) integrals using Newton's method by

$$v_1^{i+1}(0) = v_1^i(0) - \frac{H(x_1(0),\ x_2(0),\ v_1^i(0),\ v_2^i(0)) + 1}{\frac{\partial H(x_1(0),\ x_2(0),\ v_1^i(0),\ v_2^i(0))}{\partial v_1}},$$
$$v_2^{i+1}(0) = \frac{A - 2x_1(0)v_1^{i+1}(0)}{2x_2(0)},$$

where i is the iteration counter. On each iteration we first generate the variational matrix

R comprised of the partial derivatives that have been calculated numerically as follows. We calculate four perturbed orbits with:

1. the initial coordinate $x_1(0)$, perturbed by ξ,
2. the initial coordinate $x_1(0)$, perturbed by $-\xi$,
3. the initial coordinate $x_2(0)$, perturbed by ξ,
4. the initial coordinate $x_2(0)$, perturbed by $-\xi$,

where ξ is the value of the applied perturbation.

For increased accuracy, we apply perturbations in a symmetrical order. We follow the perturbed orbits around for one period and obtain the coordinates at the end of the period. Then we produce central differences by

$$\frac{\partial x_i(T)}{\partial x_j(0)} = \frac{dx_{i,x_j+\xi} - dx_{i,x_j-\xi}}{2\xi}, \qquad i,j = 1,2,$$

where $dx_{i,x_j+\xi} = x_{i,x_j+\xi}(T) - x_{i,x_j+\xi}(0)$ and $x_{i,x_j+\xi}(t)$ is the i-th coordinate, taken at time t and produced as a result of applied perturbation ξ on the x_j coordinate.

The variational matrix R is constructed as

$$R = \begin{bmatrix} a_{11} & a_{12} \\ a_{21} & a_{22} \end{bmatrix} = \begin{bmatrix} \frac{\partial x_1(T)}{\partial x_1(0)} & \frac{\partial x_1(T)}{\partial x_2(0)} \\ \frac{\partial x_2(T)}{\partial x_1(0)} & \frac{\partial x_2(T)}{\partial x_2(0)} \end{bmatrix},$$

and we introduce the matrix C as

$$C = (R-I)^{-1} = \frac{1}{|R-I|} \begin{bmatrix} a_{22}-1 & -a_{12} \\ -a_{21} & a_{11}-1 \end{bmatrix}.$$

Then the corrected values of x_1 and x_2 are obtained from the differential corrections equations as in (5.2):

$$\begin{pmatrix} x_1^{i+1} \\ x_2^{i+1} \end{pmatrix} = \begin{pmatrix} x_1^i \\ x_2^i \end{pmatrix} - C \begin{pmatrix} dx_1^i \\ dx_2^i \end{pmatrix} \tag{5.3}$$

and the process is repeated with the new values of x_1 and x_2.

The iterative process continues until the relative errors of the distances $d\mathbf{r}$ between the initial coordinates and the coordinates after one period become less than 10^{-15}. After the orbit has been found, we integrate it one more time and launch its stability analysis, which is discussed in Sections 5.4, 5.5. The overall algorithm for differential corrections is presented in the diagram in Figure 5.1. It is further extended in the diagram in Figure 5.2 and referred to as "the orbit search".

The chosen value of ξ is usually 10^{-7}, but can vary between $10^{-7} - 10^{-9}$ depending on how far away the initial configuration is from the collision. It should also be noted that in some cases a variable size of perturbations is used; for example, when the bodies are in a close encounter and their initial coordinates are close to each other. If a perturbation is too big, then it might be the case that bodies change their hierarchy which would lead to a different solution.

Depending on the order of magnitude of the variables, different values of ξ can be applied to the different variables. As mentioned at the beginning of this chapter, the differential corrections can be applied to other combinations of variables of the system: for example, the position x_1 and momentum v_1 coordinates of the outer body 1. In this situation, when it comes to searching for a near-collisional orbit, the position coordinate needs to be perturbed by only a tiny amount (10^{-12}). For the momentum coordinate, the perturbation size can reach 10^3 because the bodies move infinitely fast in the limit.

In calculating the orbits that are close to collinear, a variable size of perturbation, dependent on the distance between the bodies, is introduced to handle the challenges of integrating close encounters. We use a prediction of the parameter d_{12}, which is the difference between starting values of x_1 and x_2 in the iterational process, and choose $\xi = 10^{-7}\ d_{12}$. Knowing how far away the two nearby masses are, we safely perturb them by a much smaller distance. This is mostly done by manual change of the perturbation size.

It was mentioned at the beginning of this chapter that an implementation of the differential corrections performed in regularised coordinates was tested. The idea behind this was to improve the performance time by removing the transformations between real and regularised

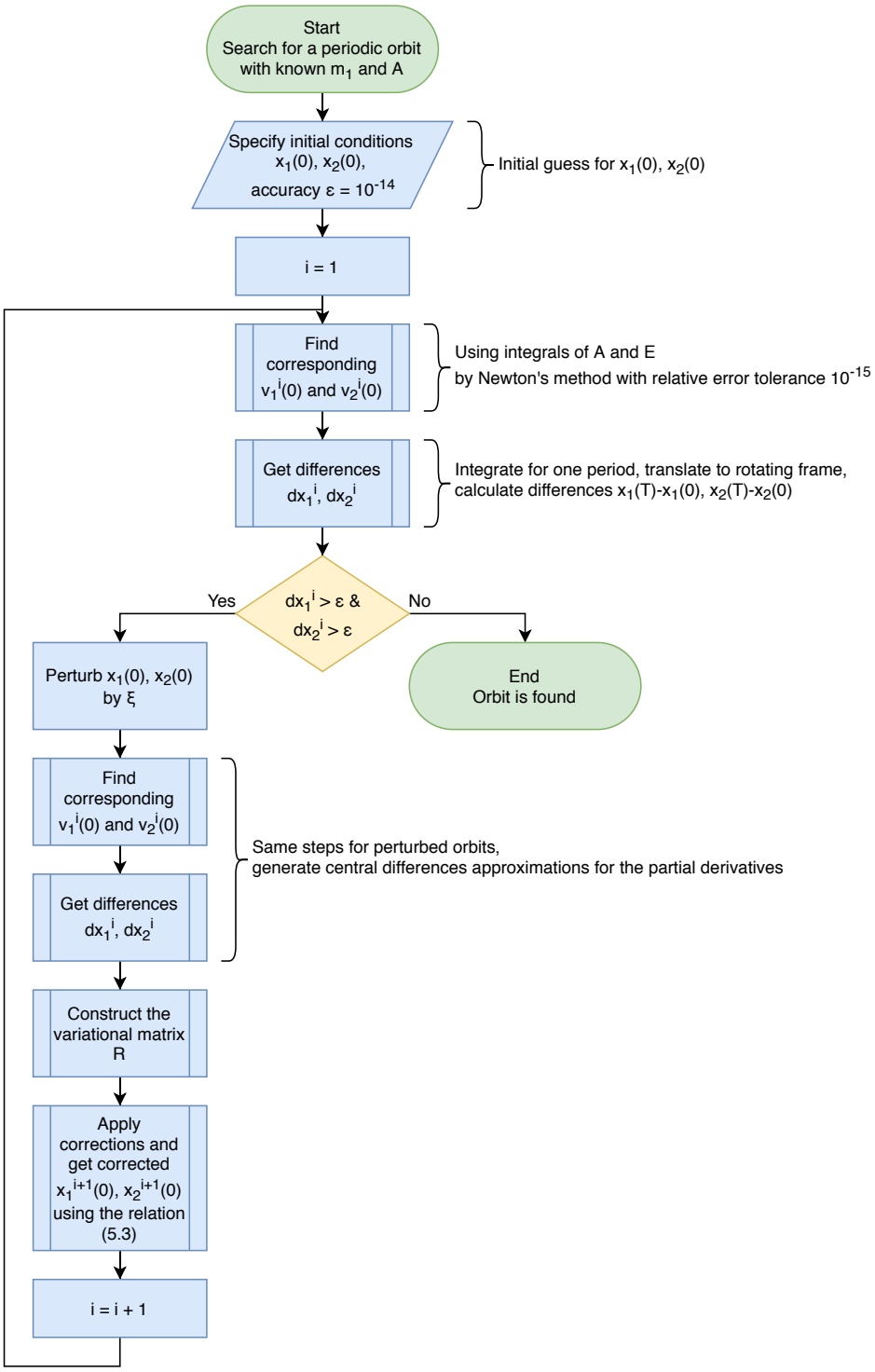

Figure 5.1: The algorithm for orbit search using differential corrections

coordinates. Also, working in regularised coordinates would allow us to initiate a search close to the collisional orbits. However, this implementation was not used in practice because of the increased number of variables and the inability to use relative differences in physical coordinates as a criterion for differential corrections.

5.3 Automatic orbit search for various masses

For this study we aim to generate the family of planar Schubart-like periodic orbits. We first generate the branch of the family with the mass $m_1 = 1.000$. By branch we mean a part of the family with the specified value of the mass m_1. The equal mass solutions are mostly found manually by applying small changes to the angular momentum of the system and by small perturbations of the initial coordinates x_1, x_2.

The idea behind the automatic search is to generate the whole branch of the family for a chosen value of m_1. It is partially derived from Broucke [11]. The important feature of the program is that it stores and uses all previously found orbits of the same class. They are later used to provide predictions for new orbits.

The program is designed in such a way that it is enough to specify the value of the mass m_1 to start producing new orbits. Let us denote the mass m_1 for which the search is being performed by $\tilde{m}_1$. The equal-mass orbits and the boundaries (see Sections 6.1 and 7.1 for details) are loaded by default. We also load previously found branches, if there are any.

We start the search at the equal-mass orbits and decide whether the search is going to increase or decrease the mass m_1. Then we introduce a stepsize Δm_1 and, depending on the previous choice, add or subtract it from the initial mass. Thus, for example, if the search is going down, then $\tilde{m}_1 = m_1 - \Delta m_1$. In our program we initially chose $\Delta m_1 = 0.001$ to produce a thorough coverage of the family. Partially our choice is dictated by previous studies by Sweatman [71] who used the same stepsize in mass.

From the loaded branches we search for the one which has closest m_1 to $\tilde{m}_1$ (variable

$Nfound$). The orbits with the closest m_1 are then used as predictions for new orbits. We take their initial coordinates and, by changing m_1 to $\tilde{m}_1$, initiate differential corrections for every single orbit with m_1. Because m_1 and $\tilde{m}_1$ are neighbouring masses, the coordinates for the orbit with m_1 are considered as perturbed coordinates for the orbits with $\tilde{m}_1$. In doing so, we also assume that the physical parameters are continuous along the family.

After this part of the program is completed, we take the newly generated orbits for $\tilde{m}_1$ and check how uniformly they are located and how many there are found (variable $Norbits$). This is done in order to detect whether the orbits are far apart from each other, and if there is a necessity to fill a gap, i.e. search for more orbits. In this part we use a fixed stepsize Δd_{12} for the parameter d_{12} which constantly increases along one branch of the family. The usual choice is $\Delta d_{12} = 0.01$, but sometimes Δd_{12} is decreased. This is done in order to meet better accuracy in the behaviour of the family: for example, when the orbits are located on the boundaries of stability regions.

If the program decides that two neighbouring orbits of the new branch are far away from each other (distance between their parameters d_{12} is bigger than Δd_{12}), then it performs a search between the orbits. The number of orbits to find is determined by the variable $NorbitsBetween$. To get the best prediction for an orbit, we pick $n + 1$ neighbouring orbits and use polynomial interpolation with degree up to $n = 5$. The initial guess for variables A, x_1 and x_2 is achieved from interpolation along the parameter d_{12}.

Even though both stages of the search are important, sometimes the second part is skipped. This is mainly to speed up the family generation. In some regions, mostly for the middle range of masses, when the properties of the family change smoothly and no particular behaviour is observed, we also omit the interpolation part. This is done by defining, in the program, the minimum number of orbits that we find sufficient for the branch. If this number is reached during the computations, then the process stops and switches to another branch.

We also introduce some alterations to the stopping criteria for finding the periodic orbit. For example, if during the orbit search the number of differential corrections' iterations reaches 50 and the process still does not reach the desired accuracy, then we mark the orbit as 'not

found' and switch to a subsequent orbit. The search routine is also set to fail immediately in the cases that the relative errors increase with interations or decrease too slowly. These criteria were again found to be successful in accelerating the family generation.

The flowchart of the algorithm performed is presented in Figure 5.2. The pseudocode of the algorithm is also attached (see Algorithm 1). The program is designed in a way that the search can be initiated in every part of the family. This feature was extensively used when a smaller grid was necessary for interpreting the properties of the family. It is also planned for later use to improve the grid on which the family is generated.

Algorithm 1 The algorithm for generating the family of orbits

$\tilde{m}_1[] \leftarrow$ array of desired masses
$\Delta d_{12} \leftarrow$ max step for orbit search dd12
$\Delta m_1 \leftarrow$ the step size in mass
for each $\tilde{m}_1$in $\tilde{m}_1[]$ **do**
    $m_1 \leftarrow$ closest mass to $\tilde{m}_1$(with Δm_1) that already has orbits
    $Nclosest \leftarrow$ number of existing orbits for m_1
    for $i = 1,\ i < Nclosest,\ i = i + 1$ **do**
        perform orbit search with $\tilde{m}_1$ and A, x_1, x_2 from existing $i-$th orbit for m_1
        perform stability analysis of the found orbit
    $Nfound \leftarrow$ number of found orbits
    if $Norbits < 150$ **then**
        for $j = 1,\ j < Norbits,\ j = j + 1$ **do**
            if $d_{12}(j+1) - d_{12}(j) < \Delta d_{12}$ **then**
                $NorbitsBetween \leftarrow$ number of orbits between $d_{12}(j)$ and $d_{12}(j+1)$ with interval Δd_{12}
                for $k = 1,\ k < NorbitsBetween,\ k = k + 1$ **do**
                    predict A, x_1, x_2 for $d_{12} = d_{12} + k \cdot \Delta d12$ by polynomial interpolation
                    perform orbit search for orbit with $\tilde{m}_1$ and A, x_1, x_2 predicted
                    perform stability analysis of the found orbit

For each discovered orbit the planar symmetric stability analysis is conducted automatically. This is mostly done because both orbit search and symmetric stability derivations require use of the symmetric code (see Chapter 3). Also, half of the perturbations, needed for symmetric stability, are applied with differential corrections. Thus, it is only a matter of applying another half of the perturbations to get the planar symmetric stability results.

We also added the possibility of performing the whole linear stability analysis, that includes

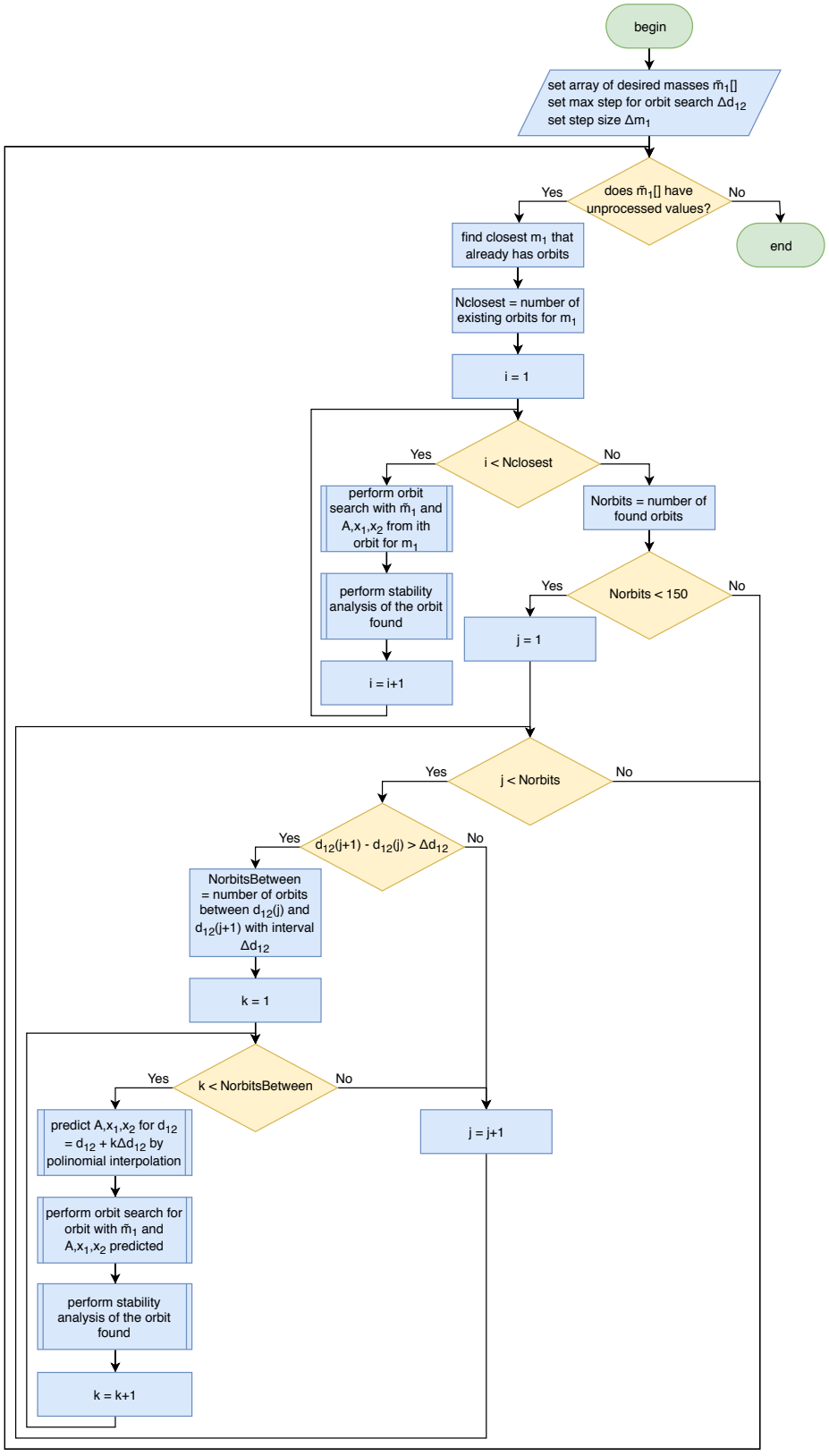

Figure 5.2: The algorithm for generating the family of orbits. The variables i, j, k are only used as counters in `for`-loops.

both planar linear stability (Section 5.4) and vertical linear stability (Section 5.5). These are conducted using the general four-body code (see Chapter 4).

We should note that there are many ways to improve the algorithm shown in Figure 5.2. One of the easiest modifications we could think of would be to update the number of stored orbits in Part 2 every time a new orbit is found. The updated orbits could then be used to improve prediction for other orbits. With this improvement the program would use its output for achieving better results, i.e. learning from its outputs.

5.4 Planar linear stability analysis

The linear stability analysis is conducted by applying the perturbations that preserve symmetry of the problem and complementary perturbations that do not. This follows the approach described by Hénon [32, 34] for the general three-body problem. Small perturbations are applied to each of the initial coordinates of the outer bodies.

From the 16 parameters that define the general four-body problem, 8 are specified by the integrals of motion (four from the centre of mass, one from the angular momentum and one from the total energy) and definition of the initial time and rotation angle. The other 8 parameters are subject to perturbations that we introduce on the outer bodies 1 and 4. The specified parameters then provide the constraints that are required to find the perturbed coordinates of the inner bodies 2 and 3 when the outer bodies are perturbed [22].

The linear stability analysis is performed in the same way as we produced the variational matrix for differential corrections, discussed in Section 5.2. From the introduced perturbations we generate an 8×8 monodromy matrix composed of the local values of the partial derivatives of the system. Figure 5.3 illustrates these perturbations. As before, we introduce alternating perturbations in order to compute central differences (perturbations (1a) and (1b) in Figure 5.3, also perturbations (2a) and (2b)). Thus, overall, we compute 16 perturbed orbits.

We introduce perturbations on the outer bodies related to longitudinal displacement (on

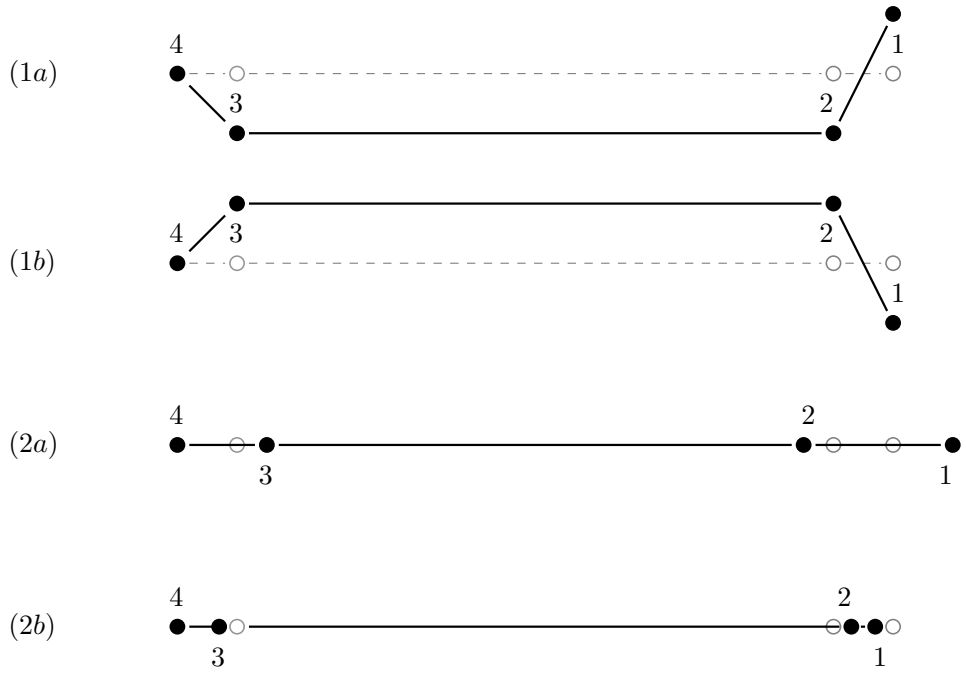

Figure 5.3: Example of the perturbations applied on the position coordinates of the body 1. Similar perturbations are applied on the body 4 and momenta of both bodies 1 and 4.

x- and u- coordinates) and transverse displacement (on y- and v- coordinates), as shown in Figure 5.3. The four perturbations are applied on the outer body 1 and then similarly on the outer body 4. No symmetry is assumed to persist.

Half of the perturbations, however, are of the form that the resulting stability parameters corresponds to symmetric perturbations. They are determined by the planar symmetric stability analysis, which is based on the same algorithm as discussed in this section, but performed with the symmetric code from Chapter 3. Thus, we distinguish 4 symmetric and 4 non-symmetric perturbations.

The coordinates for inner bodies are found from the integrals of motion (4.1)-(4.3) and initial conditions (4.4) in a Newton's iterational process by

$$y_2 = -\frac{1}{m_2 + m_3}(m_1 y_1 + m_4 y_4),$$
$$u_2 = -\frac{1}{m_2 + m_3}(m_1 u_1 + m_4 u_4),$$

$$
\begin{aligned}
y_3 &= y_2, \\
u_3 &= u_2, \\
x_{2,i+1} &= x_{2,i} - \frac{H(x_{2,i},\ x_{3,i},\ v_{2,i},\ v_{3,i}) + 1}{\frac{\partial H(x_{2,i},\, x_{3,i},\, v_{2,i},\, v_{3,i})}{\partial x_2}}, \\
x_{3,i+1} &= -\frac{1}{m_3}(m_1 x_1 + m_2 x_{2,i+1} + m_4 x_4), \\
v_{2,i+1} &= \frac{A + \sum_{j=1}^{4} y_j u_j - v_1 x_1 + v_1 x_{3,i+1} + v_4 x_{3,i+1} - v_4 x_4}{x_{2,i+1} - x_{3,i+1}} \\
v_{3,i+1} &= -v_1 - v_{2,i+1} - v_4.
\end{aligned}
$$

The resulting 8×8 matrix B of partial derivatives is similar to the matrix R for differential corrections, except that perturbations are applied on all four coordinates of the outer bodies and the system is not bound by symmetry conditions. It takes the following form:

$$
B = \begin{bmatrix}
\frac{\partial x_1(T)}{\partial x_1(0)} & \frac{\partial x_1(T)}{\partial x_4(0)} & \frac{\partial x_1(T)}{\partial y_1(0)} & \frac{\partial x_1(T)}{\partial y_4(0)} & \frac{\partial x_1(T)}{\partial u_1(0)} & \frac{\partial x_1(T)}{\partial u_4(0)} & \frac{\partial x_1(T)}{\partial v_1(0)} & \frac{\partial x_1(T)}{\partial v_4(0)} \\
\frac{\partial x_4(T)}{\partial x_1(0)} & \frac{\partial x_4(T)}{\partial x_4(0)} & \frac{\partial x_4(T)}{\partial y_1(0)} & \frac{\partial x_4(T)}{\partial y_4(0)} & \frac{\partial x_4(T)}{\partial u_1(0)} & \frac{\partial x_4(T)}{\partial u_4(0)} & \frac{\partial x_4(T)}{\partial v_1(0)} & \frac{\partial x_4(T)}{\partial v_4(0)} \\
\frac{\partial y_1(T)}{\partial x_1(0)} & \frac{\partial y_1(T)}{\partial x_4(0)} & \frac{\partial y_1(T)}{\partial y_1(0)} & \frac{\partial y_1(T)}{\partial y_4(0)} & \frac{\partial y_1(T)}{\partial u_1(0)} & \frac{\partial y_1(T)}{\partial u_4(0)} & \frac{\partial y_1(T)}{\partial v_1(0)} & \frac{\partial y_1(T)}{\partial v_4(0)} \\
\frac{\partial y_4(T)}{\partial x_1(0)} & \frac{\partial y_4(T)}{\partial x_4(0)} & \frac{\partial y_4(T)}{\partial y_1(0)} & \frac{\partial y_4(T)}{\partial y_4(0)} & \frac{\partial y_4(T)}{\partial u_1(0)} & \frac{\partial y_4(T)}{\partial u_4(0)} & \frac{\partial y_4(T)}{\partial v_1(0)} & \frac{\partial y_4(T)}{\partial v_4(0)} \\
\frac{\partial u_1(T)}{\partial x_1(0)} & \frac{\partial u_1(T)}{\partial x_4(0)} & \frac{\partial u_1(T)}{\partial y_1(0)} & \frac{\partial u_1(T)}{\partial y_4(0)} & \frac{\partial u_1(T)}{\partial u_1(0)} & \frac{\partial u_1(T)}{\partial u_4(0)} & \frac{\partial u_1(T)}{\partial v_1(0)} & \frac{\partial u_1(T)}{\partial v_4(0)} \\
\frac{\partial u_4(T)}{\partial x_1(0)} & \frac{\partial u_4(T)}{\partial x_4(0)} & \frac{\partial u_4(T)}{\partial y_1(0)} & \frac{\partial u_4(T)}{\partial y_4(0)} & \frac{\partial u_4(T)}{\partial u_1(0)} & \frac{\partial u_4(T)}{\partial u_4(0)} & \frac{\partial u_4(T)}{\partial v_1(0)} & \frac{\partial u_4(T)}{\partial v_4(0)} \\
\frac{\partial v_1(T)}{\partial x_1(0)} & \frac{\partial v_1(T)}{\partial x_4(0)} & \frac{\partial v_1(T)}{\partial y_1(0)} & \frac{\partial v_1(T)}{\partial y_4(0)} & \frac{\partial v_1(T)}{\partial u_1(0)} & \frac{\partial v_1(T)}{\partial u_4(0)} & \frac{\partial v_1(T)}{\partial v_1(0)} & \frac{\partial v_1(T)}{\partial v_4(0)} \\
\frac{\partial v_4(T)}{\partial x_1(0)} & \frac{\partial v_4(T)}{\partial x_4(0)} & \frac{\partial v_4(T)}{\partial y_1(0)} & \frac{\partial v_4(T)}{\partial y_4(0)} & \frac{\partial v_4(T)}{\partial u_1(0)} & \frac{\partial v_4(T)}{\partial u_4(0)} & \frac{\partial v_4(T)}{\partial v_1(0)} & \frac{\partial v_4(T)}{\partial v_4(0)}
\end{bmatrix}.
$$

As discussed in Sweatman [71], because of the symmetry of the system and the applied perturbations, $\frac{\partial x_1(T)}{\partial x_1(0)} = \frac{\partial x_4(T)}{\partial x_4(0)}$, $\frac{\partial x_1(T)}{\partial x_4(0)} = \frac{\partial x_4(T)}{\partial x_1(0)}$, etc. Thus, matrix B consists of 16 blocks of 2×2 symmetric matrices.

One complication arises when transverse perturbations are applied. Our earlier condition for starting or completing a period requires that the bodies are collinear (see Section 3.3 for details). However, it can be seen in Figure 5.3 that this is not the case for perturbations ($1a$) and ($1b$). For this reason, a general definition of a period in terms of interbody distances

(Section 3.3) is used for the linear stability analysis. We performed a test for the period computed with both definitions and confirmed that the results differ by no more than 10^{-13}.

As mentioned in Section 5.2, the monodromy matrix B has the following important properties: it has a unit determinant and its eigenvalues occur in reciprocal pairs [13, 26, 65, 81]. Depending on the form of the eigenvalues of B, the orbit belongs to a stability region as described by Broucke [10] for the case of a system with four degrees of freedom (see Chapter 2 for details).

The feature of having a unit determinant provides the possibility of an accuracy test for the matrix B. In our simulations we first compute the matrix and then, depending on how accurately it is calculated, we keep the stability results for future analysis of the family. In general, the monodromy matrix is calculated with accuracy 10^{-3} for equal masses, 10^{-2} for pairwise symmetric unequal masses.

Out of the eight eigenvalues of the monodromy matrix, four eigenvalues correspond to collinear perturbations whereas the other four correspond to transverse perturbations. It is, however, tricky to relate the eigenvalues to the type of an introduced perturbation: this requires further analysis of the eigenvectors of the matrix B [72], which was not part of our research. Also, for planar orbits the perturbations are coupled together, which makes it more difficult to distinguish the influence of a particular type of perturbation over other types.

For these reasons, we assumed that the eigenvalues and the stability parameters, derived from them, are continuous along the orbits from the same family. We used the results by Sweatman [70, 71], who calculated the stability for the collinear Schubart orbits, and related them to the perturbations for the planar problem by linear interpolation. When considering the collinear problem, the planar and collinear perturbations can be applied independently [32, 71]. Thus, identification of a perturbation type is apparent.

The stability parameters take the form

$$k_1 = \lambda + \frac{1}{\lambda}, \qquad k_2 = \mu + \frac{1}{\mu}, \qquad k_3 = \nu + \frac{1}{\nu}, \qquad k_4 = \gamma + \frac{1}{\gamma},$$

where λ, $1/\lambda$, μ, $1/\mu$, ν, $1/\nu$, γ, $1/\gamma$ are the eigenvalues of matrix B. It can be seen that the stability parameters are real in case of the real eigenvalues or complex eigenvalues on the unit circle (regions I, III - VII in Figure 2.1).

However, if there are four related complex eigenvalues λ, $1/\lambda$, μ, $1/\mu$ that are not on the unit circle (region II in Figure 2.1), the stability parameters will be complex according to the formula above (Note: λ and μ, as well as $1/\lambda$ and $1/\mu$, are complex conjugates). This region is called the complex instability region (Broucke [10]) and it can only appear in systems with at least four degrees of freedom [26].

After the stability parameters are constructed, we say that the orbit is stable (on the plane) if all $k_1,\ k_2,\ k_3,\ k_4$ are real and $|k_1|,\ |k_2|,\ |k_3|,\ |k_4| < 2$, i.e. the eigenvalues are on a unit circle in the complex plane. This can only be observed in the case of all eight eigenvalues (region I in Figure 2.1) lying on the unit circle. When matrix B has real eigenvalues equal to $+1$ or -1 (i.e. also on the unit circle), one of its stability indices is equal to 2. Such orbit is called "critical" and is located on the boundary between stable and unstable regions.

5.5 Vertical linear stability analysis

In our analysis of the orbits we introduce not only planar perturbations to see if the orbits survive in the plane, but also perturbations into three-dimensional space. They are also often called vertical; and the planar perturbations are then considered as horizontal. As Hénon [30] states, any actual orbit will inevitably deviate from the theoretical periodic orbit, not only in the plane, but also out of the plane. Thus, in order to consider an orbit as stable, it must be stable with respect to three-dimensional perturbations.

According to Hénon [30], Barrabes and Mikkola [6], the problem of getting an orbit's stability is separable when dealing with planar orbits: the horizontal and vertical perturbations are not coupled. The monodromy matrix S for the general planar orbit considered in three

dimensions takes the following form:

$$S = \begin{bmatrix} B & 0 \\ 0 & D \end{bmatrix}$$

where B and D are the planar and vertical monodromy matrices, respectively. The matrix D has the same properties as the matrix B discussed in previous section: it has a unit determinant and its eigenvalues appear in conjugate pairs.

In order to calculate matrix D we need only to estimate the influence of four different perturbations applied to the system. Although the considered system is three-dimensional, and the number of variables increases, they are compensated by introduction of another 2 integrals of angular momentum (4.2) and 2 integrals of the centre of mass (4.1). There are, however, three rotation angles that are associated with the angular momentum components: θ_{xy}, θ_{xz} and θ_{yz}, where the subscript letters indicate the axes, between which the angle is defined.

The initial values of all three angles are chosen as zero: $\theta_{xy} = \theta_{xz} = \theta_{yz} = 0$; we also set $A_{yz} = A_{xz} = 0$, $A_{xz} = A$ with $A = \sqrt{A_{xy}^2 + A_{xz}^2 + A_{yz}^2} = A_{xy}$. We introduce the same type of perturbations as for the previous problem of finding linear stability in the plane. These are now applied to the third position and momentum coordinate for each of the outer bodies 1 and 4, one at a time. The 4×4 matrix D is generated, and the eigenvalues give rise to two vertical stability indices, k_5 and k_6.

Depending on the perturbing coordinate, one of the angular momentum components, associated with motion in 3D, becomes nonzero. We, in turn, restrict it to zero value by means of the angular momentum integrals (5.2). As before, the four coordinates of the inner bodies are found using the integrals of motion (4.1)-(4.3) and the initial conditions (4.4):

$$y_2 = y_3 = 0,$$

$$u_2 = u_3 = 0,$$

$$x_{2,i+1} = x_{2,i} - \frac{H(x_{2,i},\ x_{3,i},\ z_{2,i},\ z_{3,i},\ v_{2,i},\ v_{3,i},\ w_{2,i},\ w_{3,i}) + 1}{\frac{\partial H(x_{2,i},\ x_{3,i},\ z_{2,i},\ z_{3,i},\ v_{2,i},\ v_{3,i},\ w_{2,i},\ w_{3,i})}{\partial x_2}},$$

$$x_{3,i+1} = -\frac{1}{m_3}(m_1 x_1 + m_2 x_{2,i+1} + m_4 x_4),$$

$$w_{2,i+1} = -\frac{w_1 x_1 - w_1 x_{3,i+1} - w_4 x_{3,i+1} + w_4 x_4}{x_{2,i+1} - x_{3,i+1}},$$

$$w_{3,i+1} = -w_1 - w_{2,i+1} - w_4,$$

$$v_{2,i+1} = \frac{A - v_1 x_1 + v_1 x_{3,i+1} + v_4 x_{3,i+1} - v_4 x_4}{x_{2,i+1} - x_{3,i+1}}$$

$$v_{3,i+1} = -v_1 - v_{2,i+1} - v_4,$$

$$z_{2,i+1} = -\frac{m_1 v_{3,i+1} z_1 - m_3 v_1 z_1 - m_3 v_4 z_4 + m_4 v_{3,i+1} z_4}{m_2 v_{3,i+1} - m_3 v_{2,i+1}},$$

$$z_{3,i+1} = -\frac{1}{m_3}(m_1 z_1 + m_2 z_{2,i+1} + m_4 z_4).$$

Each perturbed system is integrated by one period and then rotated first by $-\theta_{xz}$ in order to confine the motion to a plane, and then by $-\theta_{xy}$, as before. Thus, by performing these two rotations, we make sure that the conditions for time and angle of rotation (4.4) are satisfied in the rotating system too.

The stability indices k_5 and k_6 are generated from four eigenvalues of the matrix D by adding each pair of related eigenvalues together. Since the original orbit exists only within the plane, the only driving force for the orbit to incline into the three-dimensional space is the applied perturbation. The perturbations are then of the form that, if two similar perturbations on body 1 and body 4 are combined together or subtracted one from another, they become either rotationally or reflectionally symmetric [71].

5.6 The nonlinear stability analysis technique

Along with the linear stability analysis we perform the nonlinear stability check used by Mikkola and Hietarinta [44], Sweatman [70, 71]. We integrate the orbit from its initial conditions forward in time over a long duration. In general, the simulation is not constrained to be symmetrical or on a plane. It is necessary to initially rotate the system by some angle in the plane or into 3D

space so that the bodies start with nonzero coordinate components for their initial positions and initial momenta. If instability is present, then, together with the numerical errors, it will gradually lead to the break-up of the system.

In the current research the nonlinear simulation is done by simulating both the symmetrical planar code and general 3D code for 10000 periods, the same number of periods as used by Sweatman [71]. The initial rotation by an arbitrary angle is also applied: the usual choice is a rotation around the x-axis by $\pi/8$.

In our study we have checked all orbits with four equal masses (271 orbits) and confirmed the linear stability results. In the case of unequal masses the check was performed for a limited range of masses m_1: we checked orbits with masses $m_1 = 0.750$, 0.500, 0.250, 0.072 and every orbit for masses smaller than 0.020. This covers 1.3% of the whole dataset of orbits (2154 out of $164,215$ orbits).

The nonlinear stability technique can be viewed as an instant stability/instability check with perturbations introduced to the orbit every time it reaches a period. Because the orbit is rotated in 3D space, the perturbations are both vertical and horizontal. A visual inspection of the results is then required to detect any deviations from the regular pattern of encounters among bodies.

Chapter 6

An equal-mass family of planar Schubart-like periodic orbits and their stability

6.1 A family description and examples

A continuous family of planar Schubart-like periodic orbits has been generated using the algorithms and methods described in the previous chapters. The current chapter considers the case of orbits with four equal masses. This will be extended later to the cases of different symmetric mass ratios. The equal-mass family is described in a very detailed form in order to distinguish properties and peculiarities of the equal mass solutions.

Selected orbits from the family are shown in Figures 6.1 - 6.4 in real and rotating coordinates, respectively. Each orbit is identified by an individual letter. The details of each orbit are summarised in Table 6.1. This includes the angular momentum A, initial separation d_{12}, angle of rotation θ, period T, initial coordinates x_1, x_2 and initial momenta v_1,v_2. In order to get a good perspective on the orbits and the behaviour of the bodies with time, the graphs of these orbits against time are shown in Figures 6.5 and 6.6 in rotating coordinates.

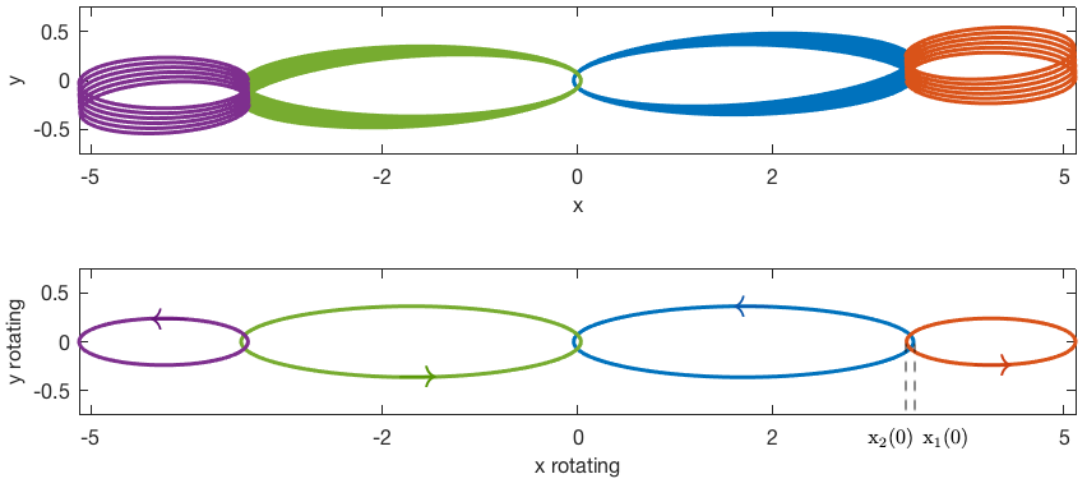

Figure 6.1: The initial orbit for the search, plotted in fixed $x - y$ coordinates (top) and in rotating $x_{\text{rot}} - y_{\text{rot}}$ coordinates (bottom), about five periods are shown. The lower figure indicates the initial coordinates $x_1(0)$ and $x_2(0)$. The arrows indicate the direction of motion.

We start with the planar orbit that was found by Sweatman in 2014 [73]. This orbit is relatively close to the equal-mass Schubart interplay orbit within the family (see Figure 6.1, also orbit C in Figures 6.3 - 6.5, Table 6.1). The orbit has initial positions $x_1 = 3.45413106$, $x_2 = 3.38409367$ with transverse velocities $\dot{y}_1 = 3.79430129$, $\dot{y}_2 = -3.70734831$. The angular momentum of the orbit is $A = 1.12$. The angle of rotation θ has the value of 0.01192373 (rad).

This orbit belongs to the type of orbit with interplay motion, where all four bodies interact with one another. Although the bodies 2 and 3 (shown in red and purple paths) closely interact only with bodies 1 and 4, respectively (shown in blue and green paths), the latter bodies also closely interact with each other. In the rectilinear four-body problem the orbit that exhibits the same type of motion is the Schubart orbit, also found and studied by Sweatman [70].

Using the approach presented in Chapter 5, we perform a search for periodic solutions. First orbits are produced by introducing small alterations to the angular momentum and initial coordinates of the starting orbit. The search process is used for a range of orbits. Suitable values for the angular momentum are found by extrapolation from the values for neighbouring family members. The extrapolations are made using polynomials of degree up to 4.

During the search procedure it was found that a parameter d_{12}, which is the initial distance

between the two bodies 1 and 2, plays an important role in the family of orbits. Despite all other parameters changing their behaviour during passage through the family (i.e. they are not monotonic), the parameter d_{12} constantly increases from zero, for the Schubart orbit, to its final value at the end of the family. The constant growth makes d_{12} a suitable parameter for the family, although it does not appear in the equations of motion explicitly. In the following analysis the other variables of interest are plotted against d_{12}.

The search is initially performed by decreasing the angular momentum from that of the orbit in Figure 6.1. We move the initial coordinates x_1 and x_2 closer together so that the orbits become closer to collinear and collisional motion. Once the first orbits are found, they can be used for extrapolation, in order to predict the best possible location to search for a new orbit. This also allows us to connect the planar orbit from [73] (Figure 6.1) with the collinear Schubart orbit from [70] (Figure 6.2). The search resumes from the initial orbit, by increasing the angular momentum and moving x_1 and x_2 apart from each other, until the whole family is obtained.

The size of the perturbation used in the differential corrections is restricted by the distance between the bodies 1 and 2, d_{12}. The application of a perturbation that is larger than d_{12} would lead to a change in the order of the bodies. This becomes very significant when the search is performed in the near-collision orbits at the beginning or end of the family. The size of the perturbation varies between 10^{-7} and 10^{-11}: for most orbits it is 10^{-7}, but for the first ones a variable size is applied as described in Section 5.2.

It was verified that the family starts with the collinear Schubart periodic orbit [70]. The orbit is shown in Figure 6.2 in fixed coordinates and with coordinates x and y as functions of time t. Since in the collinear problem the bodies are always on the line, they are not allowed to change their order.

One may note from Figure 6.2 that the bodies 1 and 2, as well as the bodies 3 and 4, are swapped for the collinear orbit. This is because the motion starts from simultaneous binary collisions of bodies 1 and 2, and bodies 3 and 4 on the two sides of the system's centre of mass. In other words, the bodies 1 and 2 are exactly at one point, and there is no difference whether

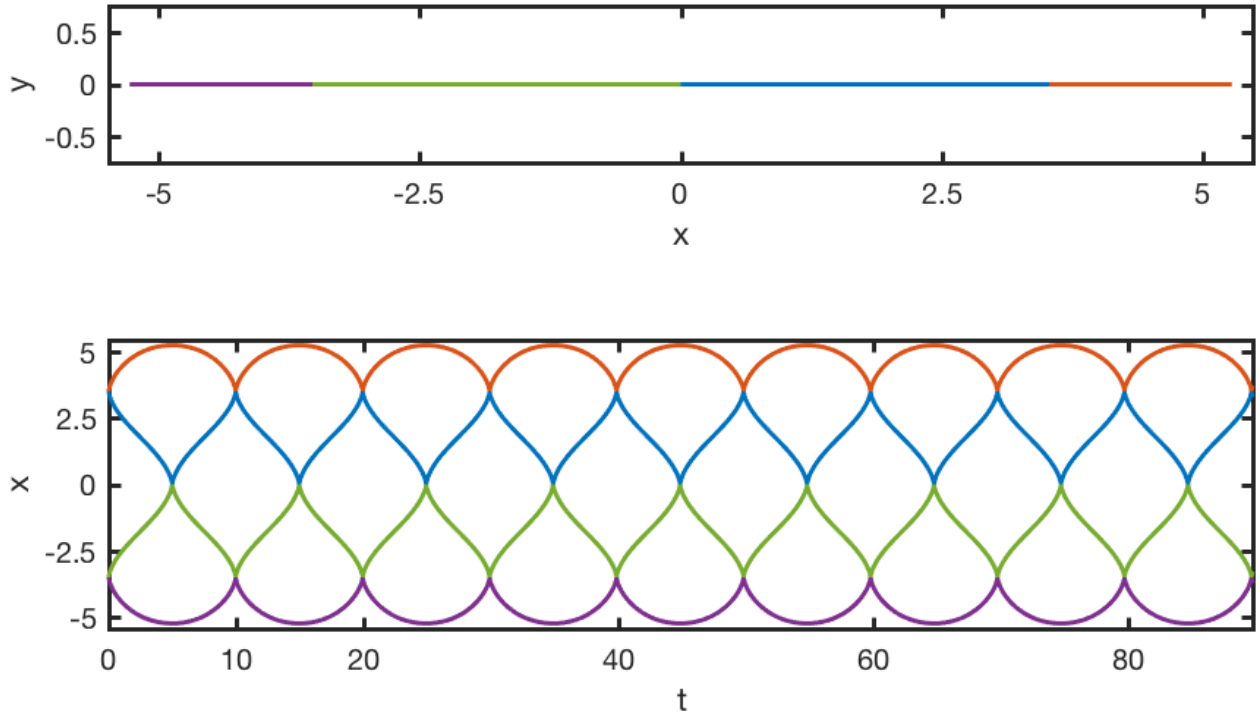

Figure 6.2: The Schubart four-body orbit: plotted in fixed x-y coordinates (top), x-coordinate against time t (bottom).

the bodies are ordered as 1-2-3-4 or 2-1-4-3. These collisions are followed by another collision of the inner bodies 2 and 3 at the system's centre of mass, after which the inner bodies turn back to collide with the outer masses again.

The interplay periodic motion for the Schubart four-body orbit is purely one-dimensional, and, thus, the momentum components are collinear. There is no rotation present and both the angle of rotation θ and the angular momentum A are zero. However, if we consider the collinear Schubart orbit as a limit of the family of orbits, the collinear components of the bodies' momentum, u_1 and u_2, corresponding to colliding bodies, are zero.

These initial conditions correspond to the moment of collision, when the bodies are, in the line of motion, instantaneously at rest. These components are infinite in magnitude immediately before and after collision. Similarly the transverse components of the momentum, v_1 and v_2, are instantaneously infinite in magnitude in their initial conditions. Apart from the instantaneous collisions, v_1 and v_2 are zero [22].

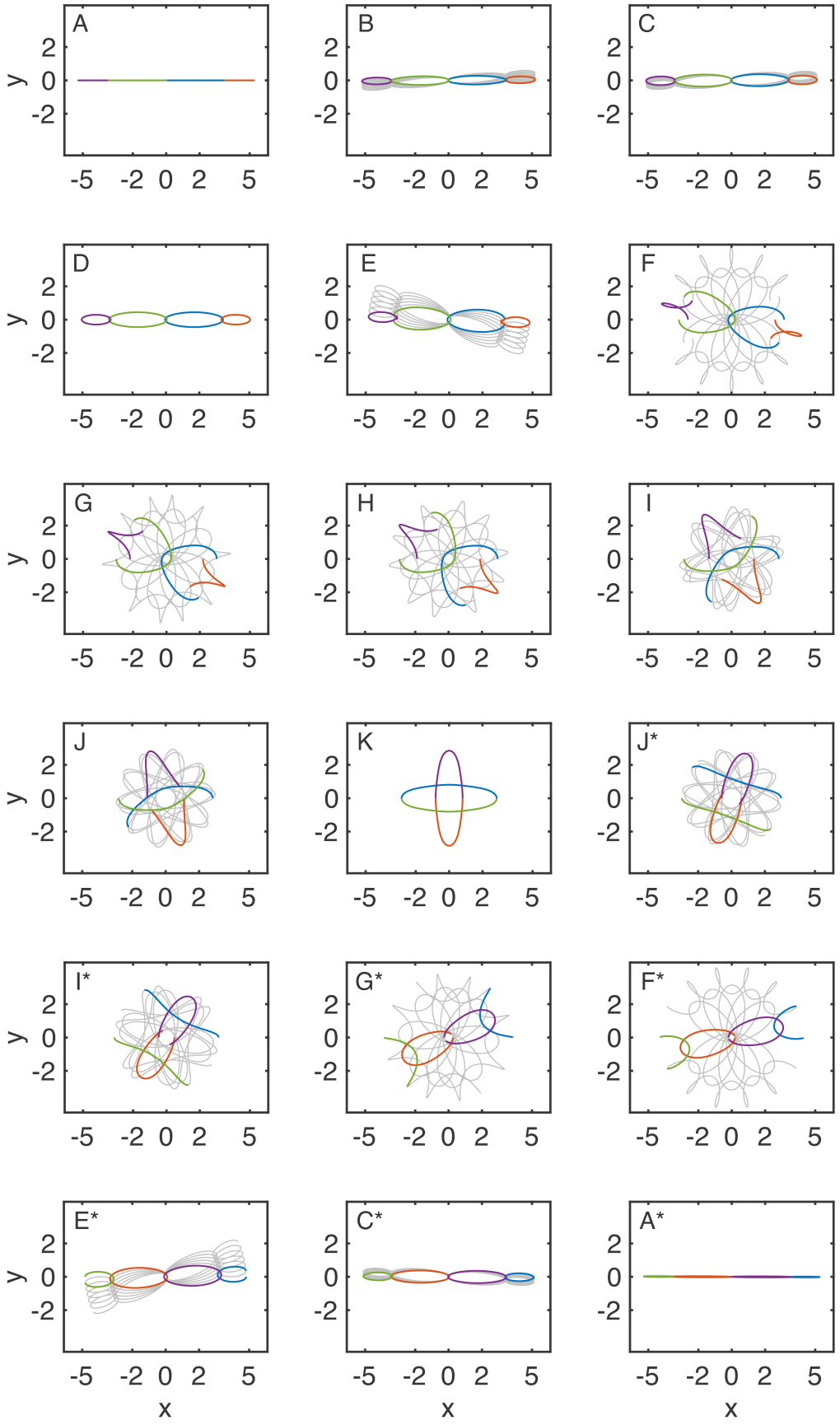

Figure 6.3: A selection of orbits in the planar family. The motion starts from the x-axis. Bodies 1 and 4 follow blue and green paths, and bodies 2 and 3 follow red and purple paths, respectively. One period is shown with coloured paths. Grey lines show a further five periods.

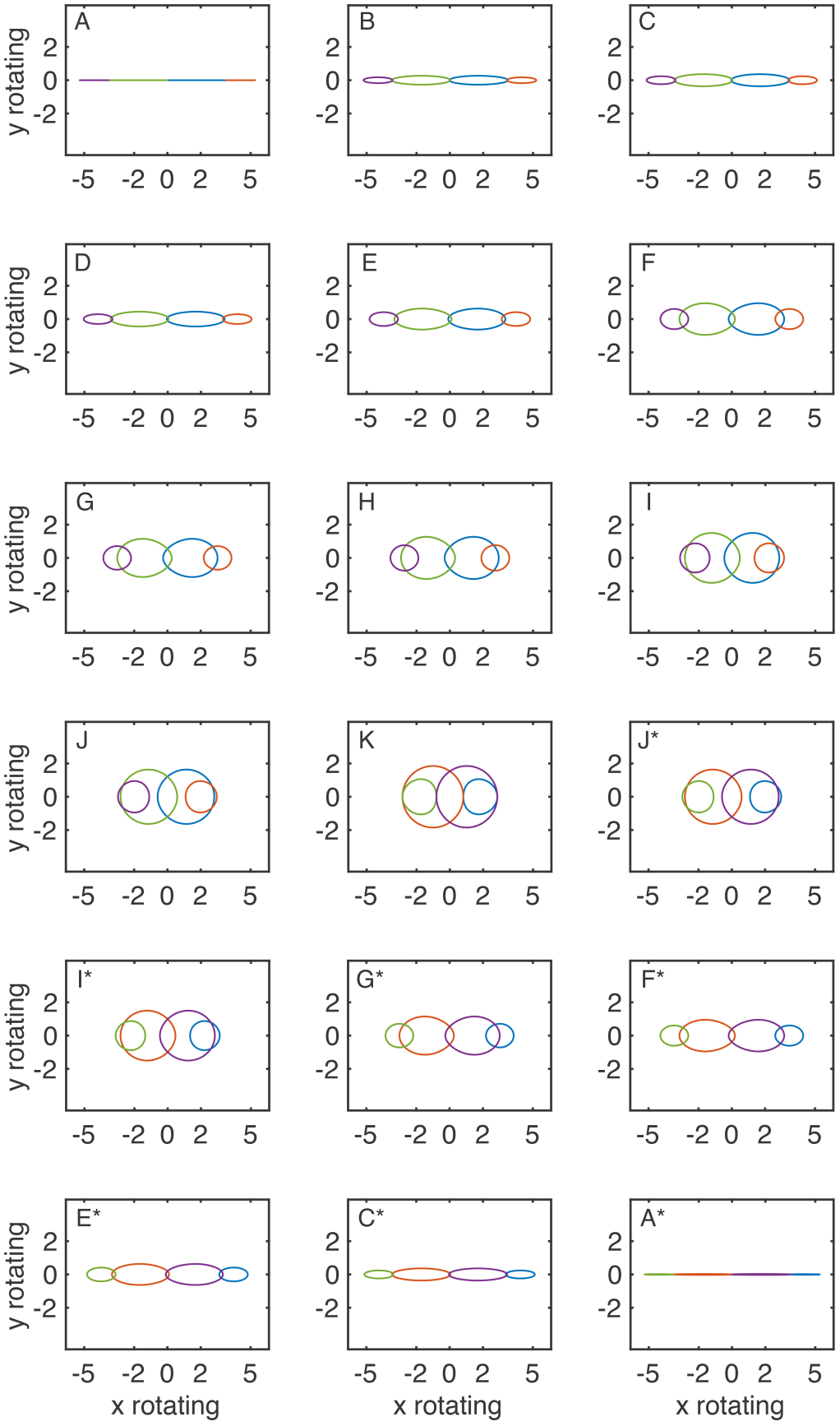

Figure 6.4: The same orbits as in Figure 6.3, but plotted in rotating coordinate frames. The colour code is the same as for Figure 6.3.

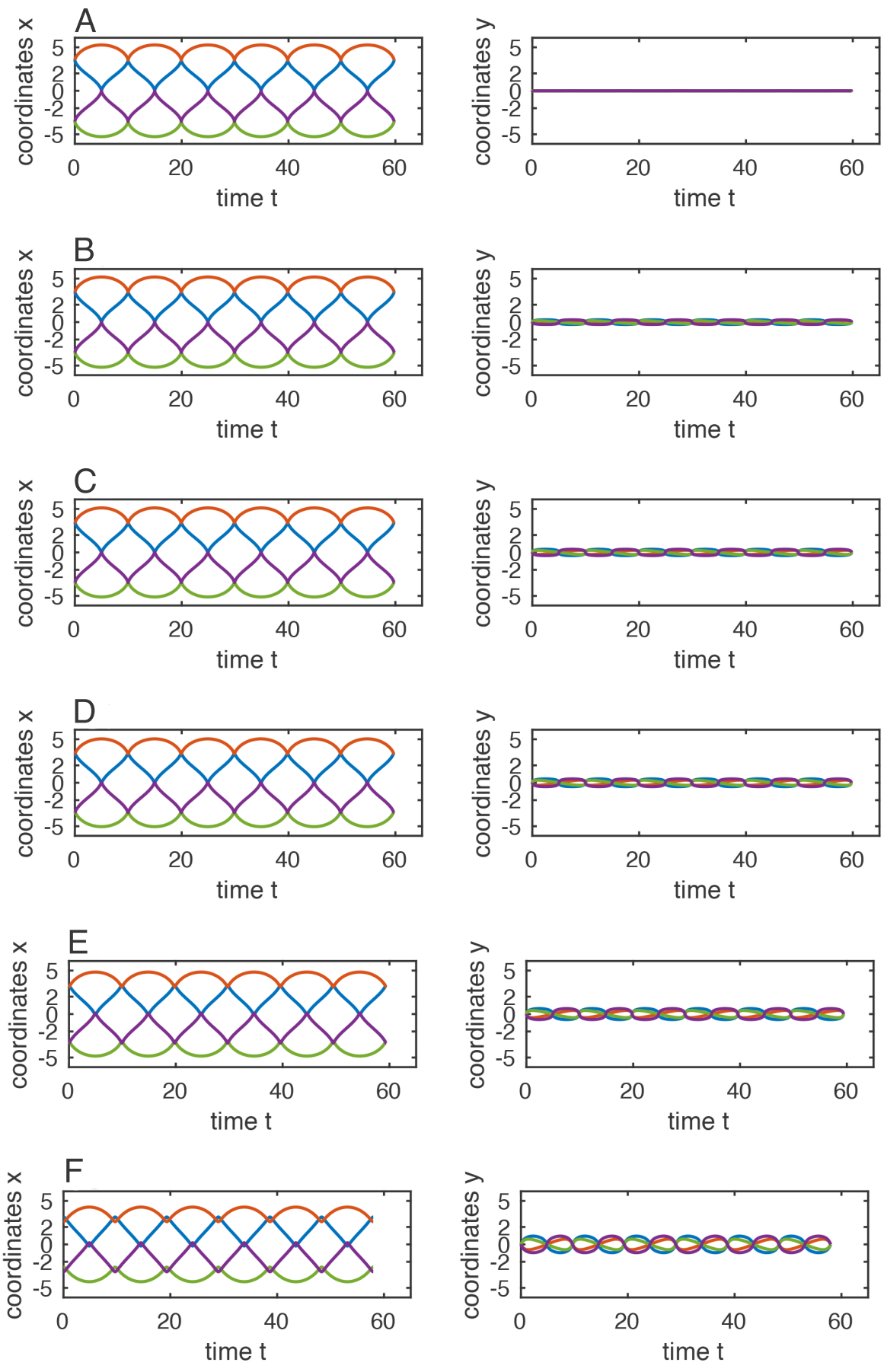

Figure 6.5: The same orbits as in Figure 6.3 and Figure 6.4, plotted in rotating coordinates against time.

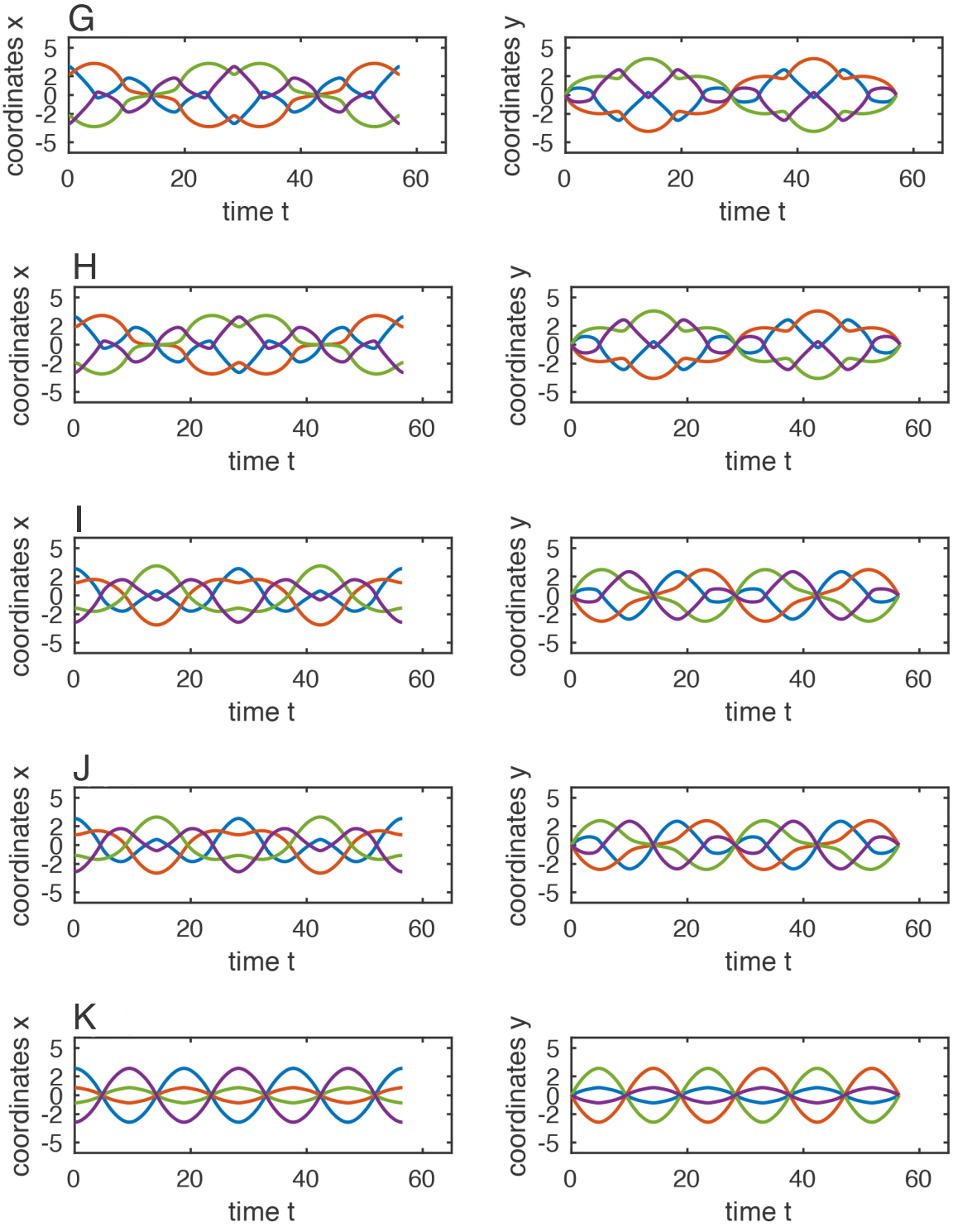

Figure 6.6: The same orbits as in Figure 6.3 and Figure 6.4, plotted in rotating coordinates against time.

Table 6.1: Details of the planar family

Orbit	A	d_{12}	θ	T	x_1	x_2	$\dot{y}_1$	$\dot{y}_2$
S	0	0	0	9.95878144	3.52357315	3.52357314	∞	$-\infty$
...	...	...	...	...	...	...	...	...
A	0.10	0.0004	0.00261799	9.95884506	3.52357197	3.52357087	952.78665461	-952.78665461
B	0.86586	0.037	0.01604439	9.96152658	3.48535279	3.44802692	5.19010502	-5.19010502
C	1.12	0.07	0.01192373	9.95973776	3.45413106	3.38409367	3.79430130	-3.70734831
D	1.28810791	0.106	0	9.95211030	3.42218248	3.31627555	3.08702368	-2.99139932
E	1.46037387	0.220	-0.07513642	9.89887270	3.33383754	3.11386858	2.12884571	-2.04473588
F	1.0	0.535	-0.44802602	9.66406524	3.14692086	2.61196866	1.27541436	-1.34520300
G	0.5	0.828	-0.87353729	9.50829878	3.01273841	2.18466730	0.92320386	-1.15869896
H	0.25	1.044	-0.87353730	9.44643156	2.93595243	1.89239311	0.74962835	-1.09695664
I	0	1.488	-2.00503424	9.40856152	2.83425450	1.34600285	0.50214984	-1.05736806
J	-0.026140227	1.724	-2.47906567	9.41281088	2.81666030	1.09287860	0.40948238	-1.06731238
K	0	2.041	π	9.41821298	2.84979157	0.80789733	0.31343372	-1.10561172
J*	0.026140227	2.381	2.47906567	9.41281088	2.96898683	0.58823696	0.23588653	-1.16836228
I*	0	2.659	2.00503424	9.40856152	3.12522260	0.46581849	0.18308676	-1.22834727
G*	-0.5	3.592	0.87353729	9.50829878	3.85039308	0.25882612	0.03258016	-1.45057394
F*	-1.0	4.099	0.44802602	9.66406524	4.28923521	0.19005505	-0.04403469	-1.63702484
E*	-1.46037387	4.728	0.07513642	9.8988727	4.82755189	0.09954850	-0.10540295	-2.22352640
C*	-1.12	5.083	-0.01186824	9.95973776	5.11918082	0.03670241	-0.08305437	-3.67359133
A*	-0.10	5.268	-0.00261800	9.95884506	5.26876120	0.00024726	-0.00737962	-44.96662955
...	...	...	...	...	...	...	...	...
S*	0	0	0	9.95878144	5.26974382	0	0	$-\infty$

As we observe the family from its beginning (the Schubart orbit) the orbits start to extend in the y-direction making the orbits more recognisably elliptic at first (see Figure 6.1 for example), and then more circular. We notice a peculiar change in the direction of rotation at the beginning of the family. The initial rotation is anticlockwise with a positive angle of rotation θ. The angle θ reaches a maximum value $\theta_{max} \approx 0.01604439$ (orbit B) and then decreases. After some orbits it changes to a clockwise motion with negative angle of rotation. The planar orbit that has a zero angle of rotation (orbit D) looks the same in fixed and rotating coordinates. This type of solution is called an"absolute periodic orbit" by Broucke's categorisation [12, 13].

At the same time, the angular momentum of the system grows rapidly from zero, for the Schubart orbit, until its maximum value $A_{max} \approx 1.46037387$ (orbit E). Then the angular momentum decreases steadily (for orbits F, G, H) back to zero (orbit I) and towards negative values, reaching a local minimum of $A_{min} \approx -0.026140227$ (orbit J), after which it increases to $A = 0$ (see Figure 6.9, also orbit K). The angle of rotation continues to decrease from orbit D until it reaches a limit of $-\pi$ (orbit K, see Figure 6.10).

The limit orbit (orbit K) with angle of rotation of $-\pi$, or π, and zero angular momentum (Figure 6.7) is a double choreography orbit [7]. That is, the bodies are split into two groups and within each group the member bodies perform a simple choreography (i.e. they follow the same path) [22]. This orbit has been studied independently by Chen [20] as an action-minimising orbit. Chen [20] also gives an analytical proof of the existence of the orbit.

This orbit is periodic even in fixed coordinates because its angle of rotation $\theta = \pi$. It still, however, looks different in the rotating coordinate system. That is because the definition of the period (and angle of rotation) is based on the order of the bodies and does not take into account the possibility of two or more bodies sharing the same path. If we consider the period of the orbit K as $\hat{T} = 2T$, instead of T, as for the other orbits, then the outer bodies 1 and 4, as well as the inner bodies 2 and 3, share the same path, respectively. According to our definition of a period, the four bodies only have to come back to their initial ordering for the period to be completed.

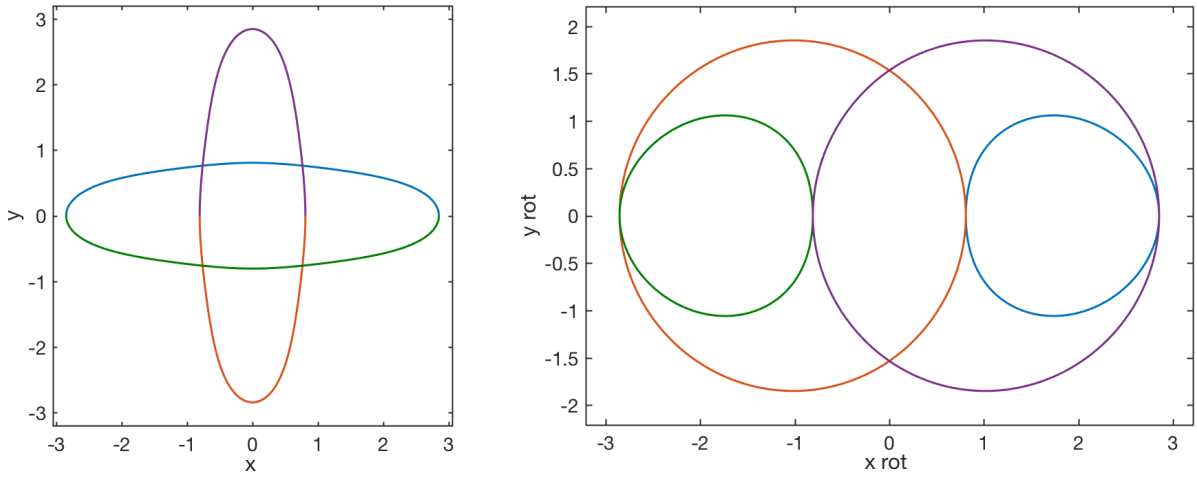

Figure 6.7: The double choreography $A = 0$ orbit from the family of orbits: in fixed coordinates (left) and in rotating coordinates (right).

After the double choreography orbit, the orbits that we encounter are the same orbits but in reverse order to those that appear before the double choreography. They differ in that the initial conditions are the half-period coordinates and that the motion is reversed. So, orbits J and J^* are essentially the same, and so are orbits I and I^*, G and G^*, F and F^*, E and E^*, C and C^*, A and A^*. Also, the family finishes with the Schubart orbit (S and S^* in Table 6.1) which it starts with.

This can be explained using the schematic plot for an orbit belonging to the family of the Schubart-like orbits (Figure 6.8). After integrating the orbit from the initial position through half of its period the orbits are on a line again with momentum vectors perpendicular to that line. This indicates that the positions and velocities at time $t = T/2$ satisfy the initial conditions, as defined for the family (Figure 6.8), although with the relabelling of masses and the reversing of motion. In principle, taking these coordinates as initial ones results in the same orbit with a shift in time.

Thus, the family can be regarded as symmetric with limits of the Schubart orbit as the start and the double choreography orbit as the end. The other orbits, that appear after the double choreography orbit, have the same properties as the orbits that come before the double choreography orbit. Thus, from this perspective they are considered as belonging to the duplicate family. We may then consider the central orbit (Figure 6.7) as the end of the

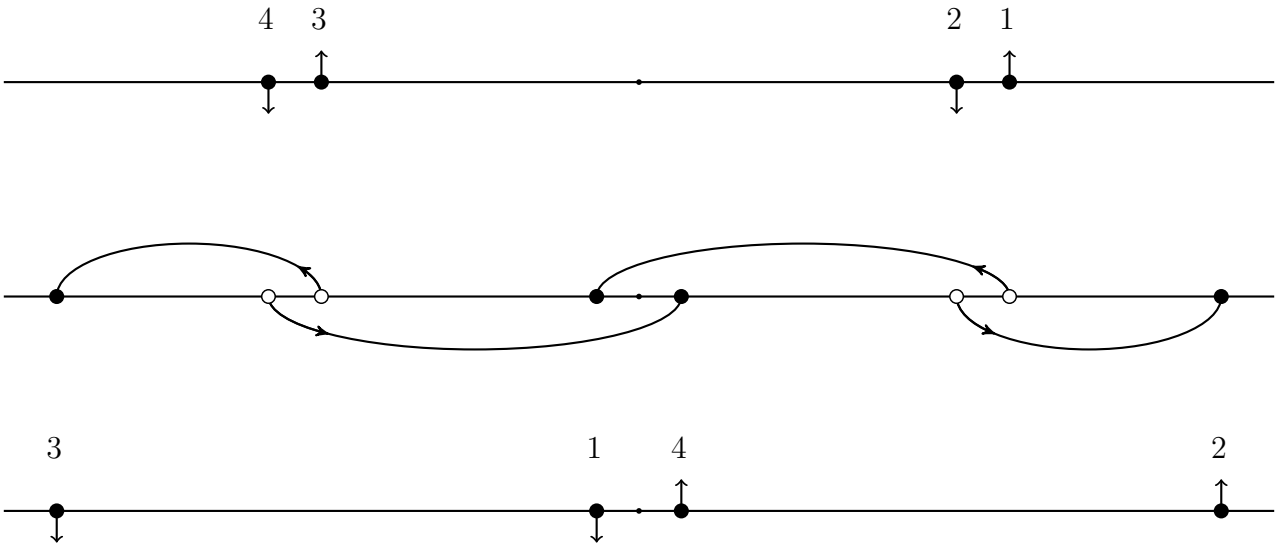

Figure 6.8: A schematic example of an orbit: the four bodies' positions with velocity vectors $t = 0$ (top). The motion of four bodies from time $t = 0$ to time $t = T/2$. Arrows indicate the direction of motion. Open circles indicate initial positions and filled circles account for positions of bodies at time $t = T/2$ (middle). The positions of bodies with velocity vectors at time $t = T/2$ (bottom).

family, since further continuation of orbits would reverse the search of orbits back to the Schubart four-body orbit.

In the study we rather adopt a different view of the family. The discovered family of orbits can also be regarded as being generated from the Schubart four-body orbit, continuing to the central double choreography orbit, then returning back to the Schubart four-body orbit. Since the orbits from the two regions of the family, before and after the double choreography, are essentially the same, they should have the same properties and stability type. Our research showed that in some situations it is more convenient to consider the orbits starting from either the first or the second regions of the family. This is especially true for the near-collisional orbits, which are easier to analyse when only two bodies are close to each other at the centre, rather than when the system is in double binary collision on the outside.

The angular momentum graph along the continuous family is presented in Figure 6.9. The values corresponding to the specific orbits from Table 6.1 are marked. Because all of the orbits that we encounter after the central orbit K, are essentially the same as the orbits before the

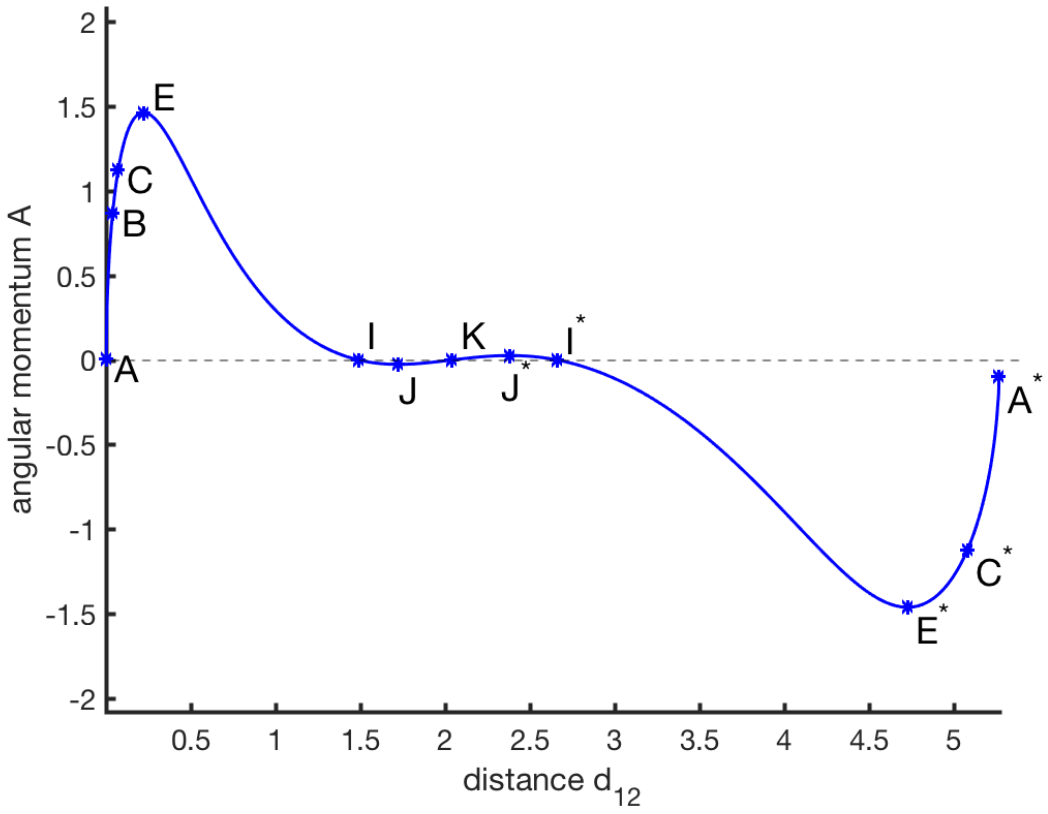

Figure 6.9: Angular momentum A against d_{12} (along the family). The dashed line indicates where the angular momentum is 0.

central orbit K, the angular momentum behaves similarly before and after orbit K. Reversing of velocity vectors, however, reverses the sign of the angular momentum for the other half of the family. Thus, the maximum value of A, that we encountered nearer the beginning (orbit E), turns out to be the minimum towards the end (orbit E^*). Similarly, the local minimum for orbit J transforms into the local maximum for orbit J^*.

A similar behaviour is noted for the angle of rotation θ (Figure 6.10). The maximum value of angle $\theta_{max} = 0.01586303$ for orbit B becomes the minimum $\theta_{min} = -0.01586303$ for orbit B^*. The central orbit K is shown in the middle for both angles $\theta = \pi$ and $\theta = -\pi$.

The period (shown in Figure 6.11) does not change significantly along the family; it varies between values 4.98076329 and 4.70640544. It is noticed that the maximum of the angle of rotation θ coincides with the maximum of the period T (orbits B and B^*). The orbits associated with the minimum (orbits I and I^*) and the local maximum of the period (orbit K)

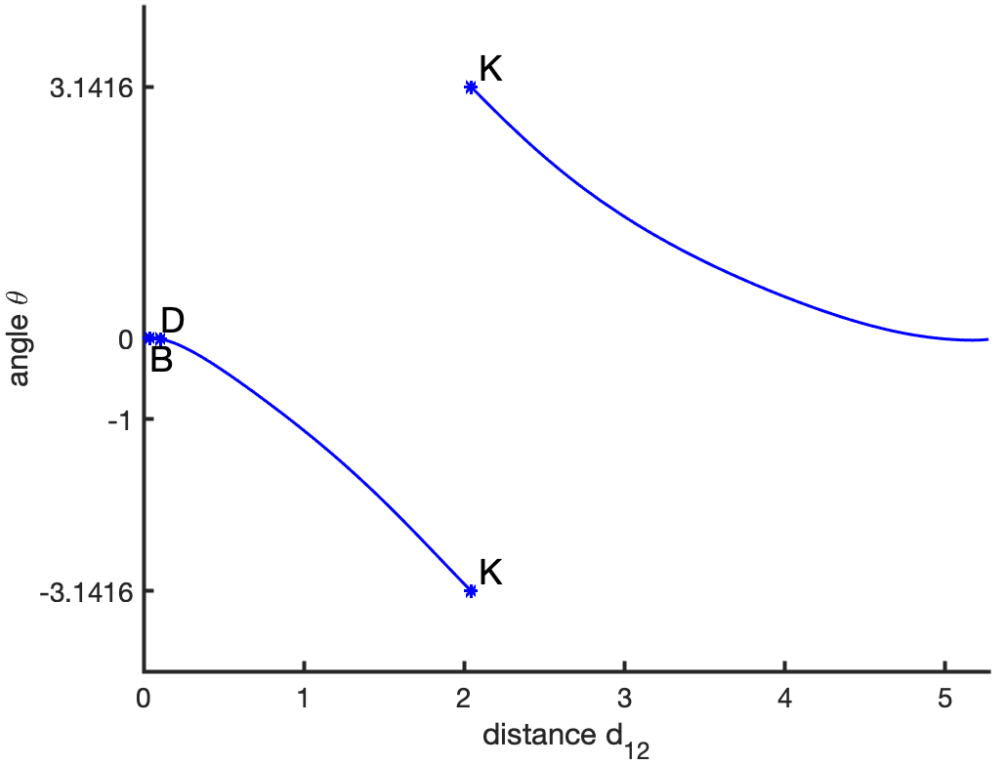

Figure 6.10: Angle θ against d_{12} (along the family), radians.

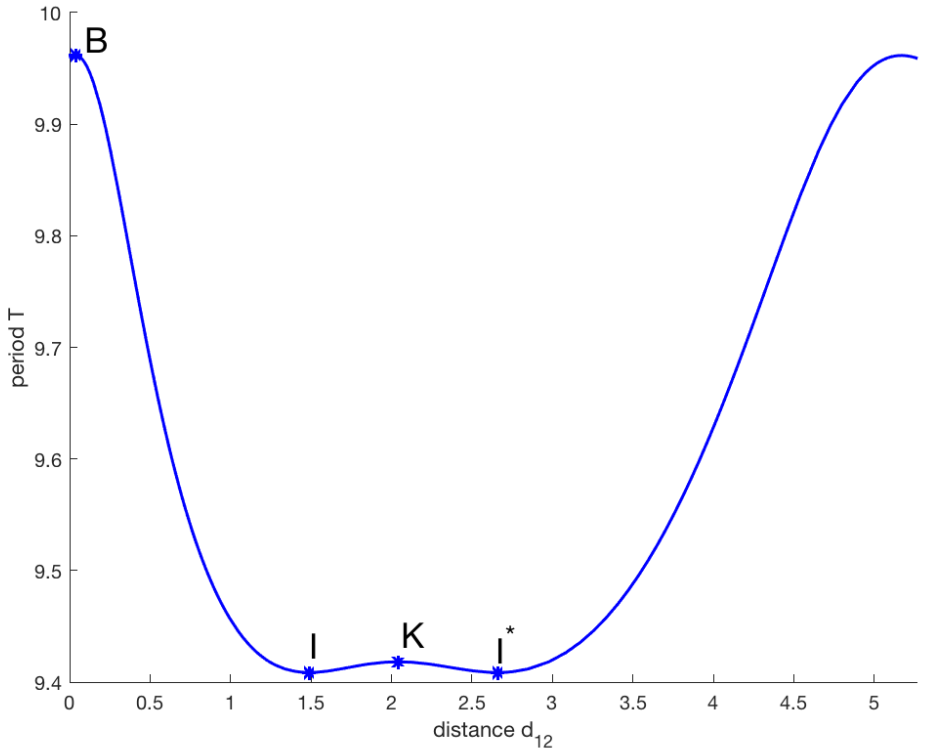

Figure 6.11: Period T against d_{12} (along the family).

have a zero angular momentum.

Hénon noted the same behaviour for the planar three-body problem [32], which led to the discovery and proof [33] of the relation

$$\frac{dT}{dA} = -\frac{A}{2E}\frac{d\theta}{dA}, \tag{6.1}$$

where the derivatives with respect to A are taken along the family. This relation shows that an extremum of angle θ must be an extremum of period T. Alternatively, an extremum of period T must be either an extremum of angle θ or have a zero angular momentum.

For the Schubart orbit, the initial positions of the bodies on either side of the system's centre of mass are the same: the bodies are at a collision. As we continue along the family, both of the initial positions decrease: more rapidly for the inner body than for the outer body (see Figure 6.12). The outer body's initial position reaches a threshold at some point and starts increasing again. Further continuation of the family back to the Schubart orbit leads to a collision of the inner bodies at the system's centre of mass with the outer two bodies reaching their furthest distance from one another. The initial transverse momenta are shown in Figure 6.13.

6.2 Planar linear stability results

A linear stability analysis of the family was conducted in accordance to the approach covered in Chapter 5. As discussed in Section 5.4, we introduce 8 different planar perturbations on the outer bodies of the system, one at a time. The integrals of energy, angular momentum and centre of mass of the system provide the constraints needed to find the positions and momenta of the inner bodies of the system. Each perturbation is applied twice, with opposite signs, in order to estimate central difference derivatives from the perturbation.

From these perturbations the 8×8 monodromy matrix was generated for each orbit. Since both original and perturbed systems are Hamiltonian, the eigenvalues occur in reciprocal pairs

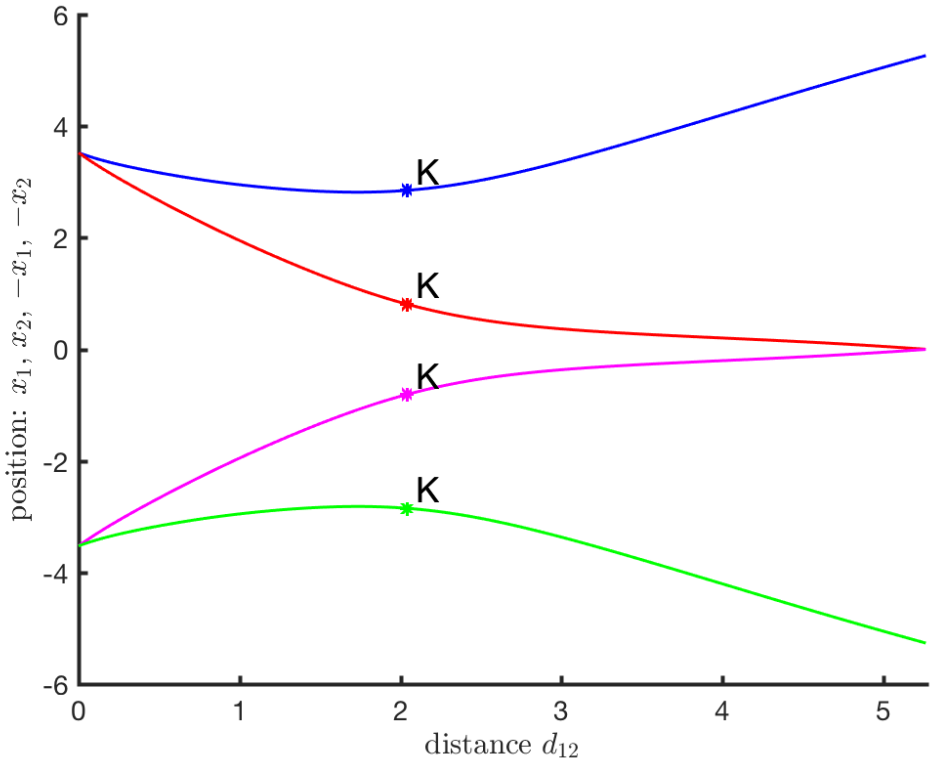

Figure 6.12: The x-coordinates of the four bodies against d_{12} (along the family).

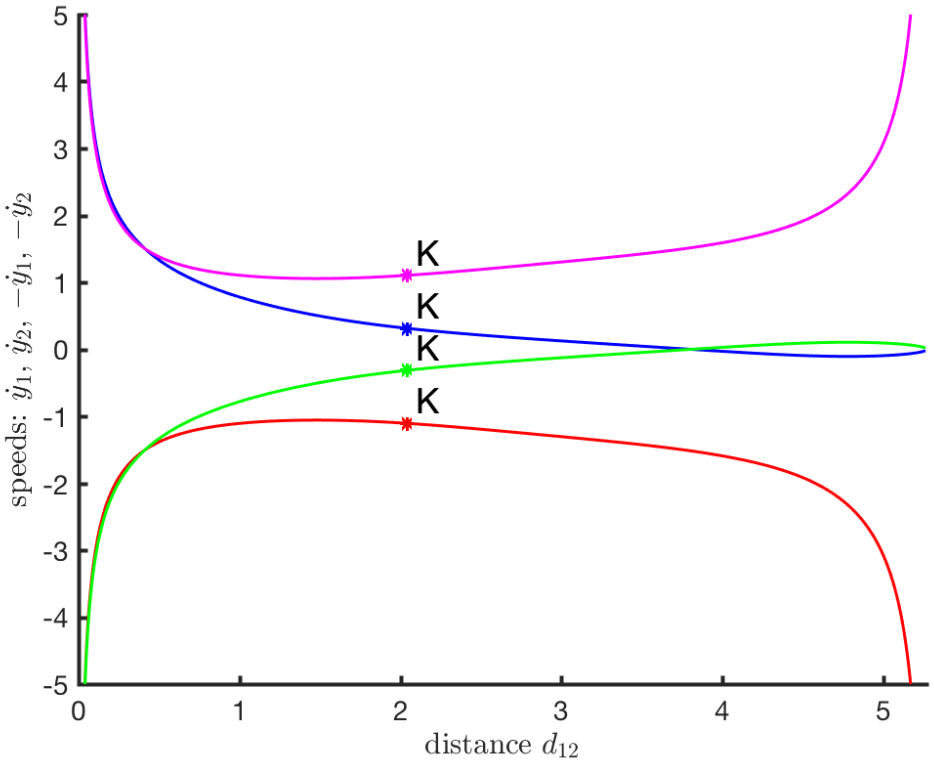

Figure 6.13: The transverse momenta v-coordinates of the four bodies against d_{12} (along the family).

λ, $1/\lambda$, μ, $1/\mu$, ν, $1/\nu$, γ, $1/\gamma$. By adding the reciprocal pairs together, we obtain the stability parameters $k_1 = \lambda + \lambda^{-1}$, $k_2 = \mu + \mu^{-1}$, $k_3 = \nu + \nu^{-1}$, $k_4 = \gamma + \gamma^{-1}$ [81]. The eight eigenvalues then produce the four stability parameters. A periodic orbit is stable when all its stability parameters are less than 2 in magnitude. According to Broucke's [10] analysis of the types of stability for different types of eigenvalues and stability parameters, in order to have a stable orbit, the corresponding eigenvalues should be complex numbers and lie on a unit circle.

We also perform a symmetric linear stability analysis on the plane, to confirm the general results and to distingush the symmetric stability parameters. This introduces a 4×4 monodromy matrix and two stability parameters. For each stability analysis we perform a check that all generated monodromy matrices have a determinant equal to 1, as expected in Hamiltonian systems.

Each stability parameter corresponds to a type of introduced perturbation. The stability parameters k_1 and k_4 correspond to symmetric perturbations whereas the stability parameters k_2 and k_3 correspond to non-symmetric perturbations. Also, parameters k_1 and k_2 show the effect of a collinear perturbation on an orbit, and parameters k_3 and k_4 indicate the influence of transverse perturbations. These are shown along the family in Figure 6.14 and in Table 6.2.

The accuracy of the results is in general 10^{-3}: this is measured by calculating the determinant of the monodromy matrix. However, the simulations showed that it can reach 10^{-1} for orbits with bodies 1 and 2 starting close together, compared to initial conditions with bodies 2 and 3 near the centre of mass with the outer bodies far away in the system. This can be explained by the fact that in the second situation the total energy of the system is mostly concentrated about the inner bodies in the middle. Thus, perturbing the outer bodies does not have such significant effect on the system in total, compared to the first case where we start with a close encounter of the outer and inner bodies.

Examples of such differences in the results can be seen in Table 6.2, for instance, for orbit C and C^*. Since it is essentially the same orbit, it is expected that the stability parameters are the same without any dependence on starting coordinates and integration time. However, because of the problem discussed above, the parameters $k_1 - k_4$ are different up to 10^{-2} (10^{-1}

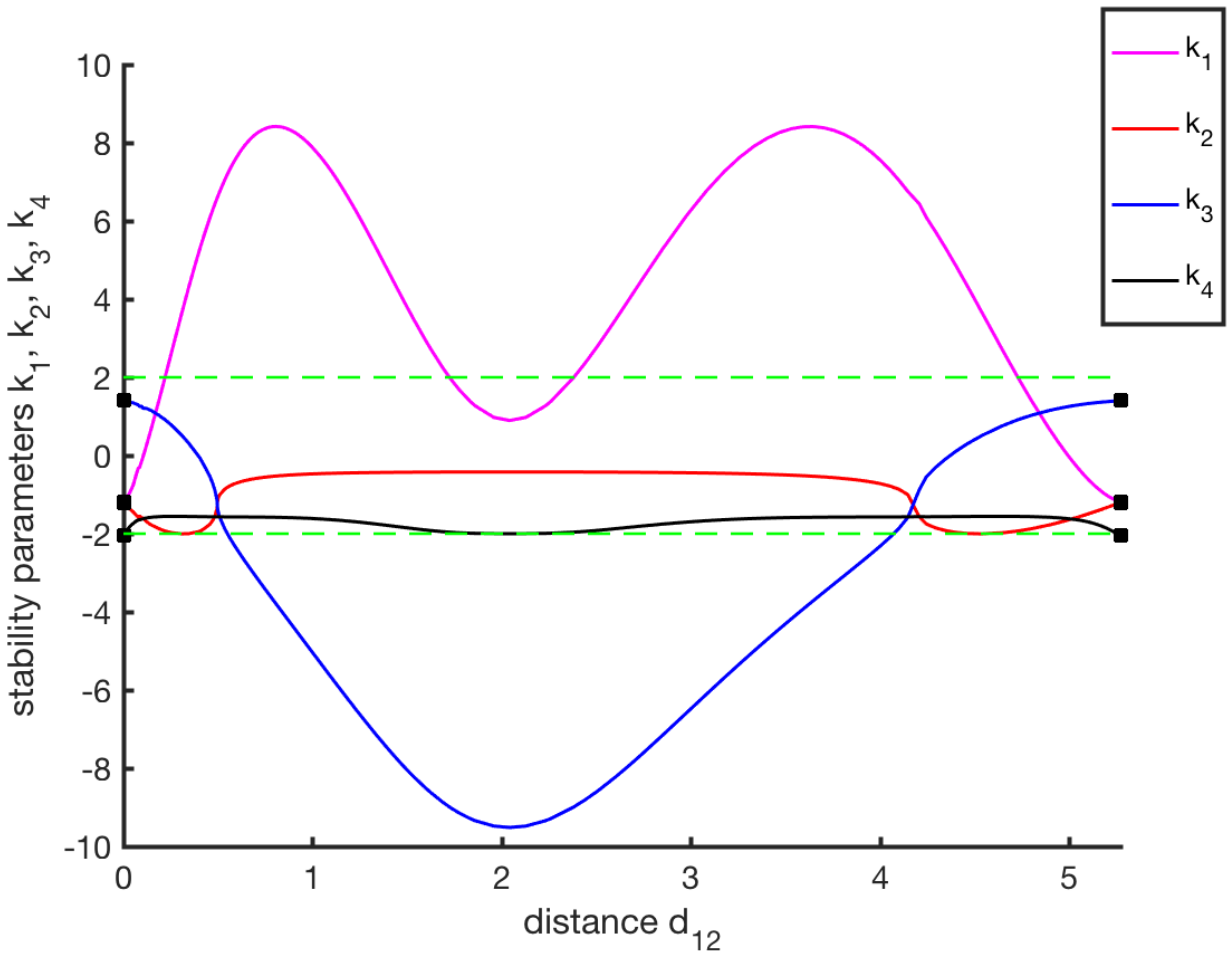

Figure 6.14: The stability parameters plotted against d_{12} (as taken along the family). Green dotted lines at 2 and -2 indicate the regions of stability: the orbits are stable when the stability parameters are between -2 and 2. The black squares indicate the four stability parameters for the collinear Schubart orbit (taken from [70], also in Table 6.2).

for stability index k_1). The monodromy matrix discriminant check along with the explanation above confirms that the results for orbit C^* are more accurate than those for orbit C.

The collisional Schubart orbit and the orbits closely related to it are unstable with the transverse stability parameter $k_4 < -2$. This agrees with and confirms Sweatman's results [70, 71] for the Schubart orbit: that it is unstable under symmetric transverse perturbations. The k_4 parameter then increases and it reaches the stable region when $d_{12} = 0.00667080$ and angular momentum $A = 0.385$. It then stays near the critical value of -2 but remains in the stable region until the end of the family.

The other symmetric stability parameter k_1 steadily increases from negative values to the critical value of 2 and then further into the unstable region. The crossing between stability

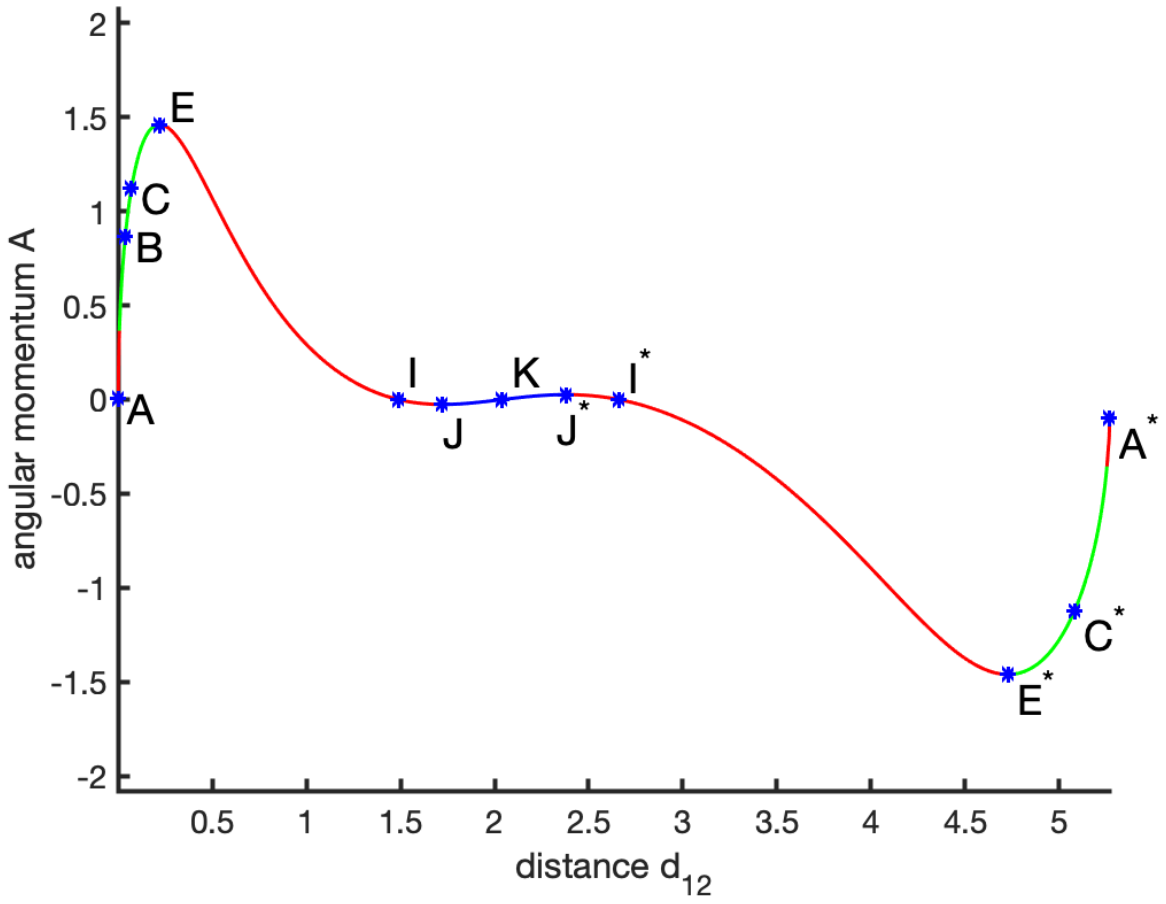

Figure 6.15: The regions of planar linear stability for different values of angular momentum along the family: red and blue (blue is stable symmetrically) lines indicate the instability of orbits, green lines account for the stable orbits.

and instability regions coincides with the local maximum of $A = 1.46037387$. After that, the stability parameter k_1 increases and reaches its maximum $k_1 \approx 8.4162$, corresponding to the orbit with $A \approx 0.53$. It then decreases back to the stable region.

Both non-symmetric parameters k_2 and k_3 start in the stable region. They meet once at a point close to the orbit with $A \approx 1.076$ at $d_{12} \approx 0.4959$. After that the transverse stability parameter k_3 decreases down to the unstable region. The collinear stability parameter k_2 stays in the stable region throughout the whole family of orbits.

In principle, we distinguish four regions of different types of stability / instability in the family from the Schubart orbit until the double choreography orbit on the plane. This is shown in Figure 6.15 of the angular momentum A along the family in different colours.

The first region with $0 \leq A < 0.385$ and $0 \leq d_{12} < 0.00667080$ is unstable (red colour) under transverse symmetric perturbations. The second region with $0.385 \leq A < 1.46037387$, $0.00667080 \leq d_{12} < 0.21996896$ is stable (green colour) as all four planar stability parameters are in the stable region (see Figure 6.14). It is the only stable region in the family of orbits on the plane.

The third region with $1.46037387 \leq A < -0.025$, $0.21996896 \leq d_{12} < 1.72378169$ is unstable (red colour) under symmetric collinear perturbations and, also, non-symmetric transverse perturbations, starting from $d_{12} \approx 0.54525845$, $A \approx 0.98$.

The fourth region ($-0.02614023 \leq A \leq 0$, $1.72378169 \leq d_{12} \leq 2.04189423$) is stable symmetrically, however it is unstable under non-symmetric perturbations (blue colour). These four regions are then repeated in the reverse order on the way from the double choreography back to the Schubart orbit.

6.3 Vertical linear stability results

A vertical stability analysis was conducted using the same approach as the linear stability analysis. This involves the possibility of perturbing the system in a three-dimensional space which gives a rather more realistic view of the family of orbits.

We introduce the third dimension as z_i for the position and w_i for the momenta coordinate of each of the bodies. Similarly to the linear stability analysis, we consider only perturbations of the outer bodies, one at a time, into the vertical space. A total of eight vertical perturbations are applied which results in a 4×4 vertical stability matrix for each orbit. From its eigenvalues, we derive two stability parameters, k_5 and k_6 (see Figure 6.16), in a way similar to that for the planar stability parameters. The same check with a unit discriminant, as in the planar linear stability analysis, applies to the vertical stability analysis.

For the vertical stability parameters we don't distinguish the ones resulting from rotationally or reflectionally symmetric perturbations. We could, however, get some insight

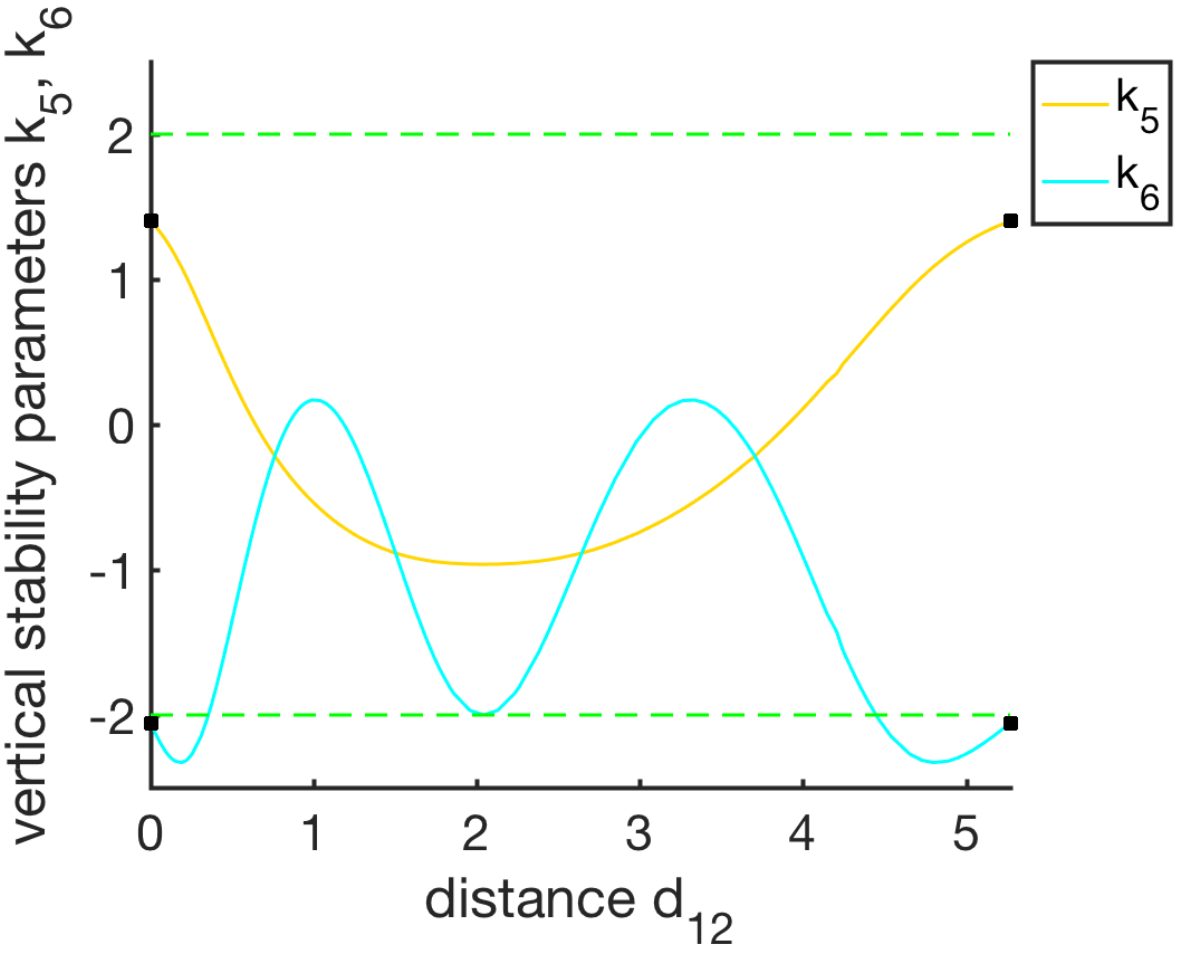

Figure 6.16: The stability parameters plotted against d_{12} (as taken along the family). Green dotted lines at 2 and -2 indicate the region of stability: the orbits are stable when the parameters are between -2 and 2. The black squares indicate the vertical stability parameters for the collinear Schubart orbit (taken from [70], also in Table 6.2).

from the collinear orbits at both ends of the family. As Hénon [32] points out, for purely collinear orbits the application of transverse perturbations have the same effect on the orbit as perturbing it into the vertical space. Thus, the transverse and vertical stability parameters should join together at the ends of the family, where the orbits become collinear.

It can be seen in Figure 6.17, with all six stability parameters, that k_3 and k_5 start from the same point and merge at the end; the same applies to the parameters k_4 and k_6. From that we deduce that k_5 as well as k_3 carries the effect of the reflectionally symmetric perturbations, while k_6 and k_4 result from the rotationally symmetric perturbations.

The results show that the stability parameter k_5 lies in the stable region for the whole range of orbits, whereas the stability parameter k_6 starts and ends in the unstable region and is unstable for the first and last orbits. It moves into the stable region and stays there for the range of orbits in the middle of the family. Thus, the orbits are unstable vertically in only one region of the family.

Combining all six stability parameters in one plot (Figure 6.17) shows that, because of the influence of unstable k_6, the only stable region on the plane (green in Figure 6.15) turns out to be unstable when considered in three-dimensional space. The other regions, although unstable in the plane, are stable vertically. Overall, the whole equal-mass family turns out to be unstable if considered under the influence of every possible type of a perturbation.

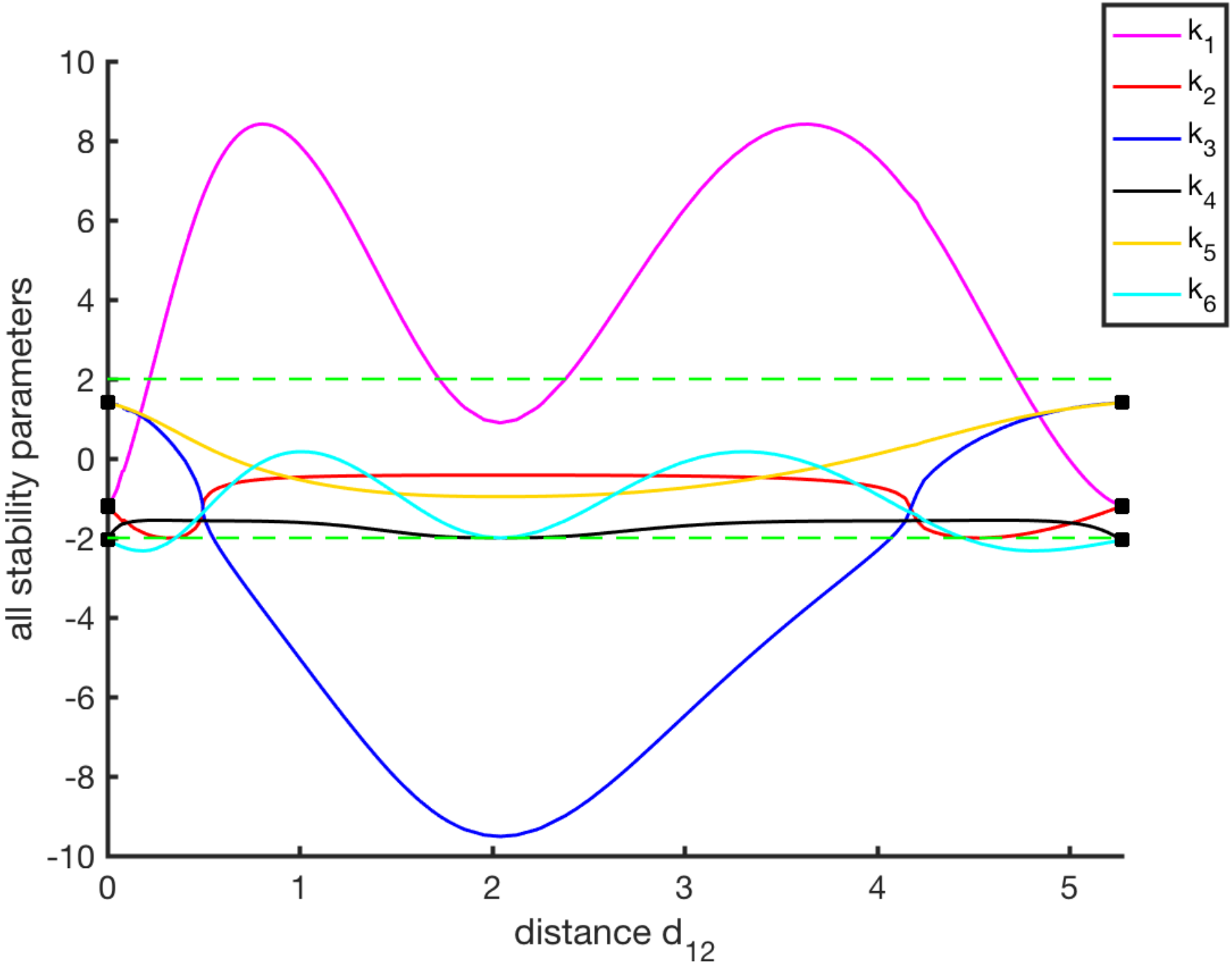

Figure 6.17: All six stability parameters plotted against d_{12}.

Table 6.2: Stability parameters of the planar family

Orbit	d_{12}	k_1	k_2	k_3	k_4	k_5	k_6
S	0	-1.197	-1.202	1.400	-2.057	1.400	-2.057
...	...	...	...	...	...	...	...
A	0.004	-1.180	-1.183	1.400	-2.052	1.400	-2.020
B	0.037	-0.9104	-1.383	1.364	-1.800	1.355	-2.145
C	0.07	-0.4500	-1.541	1.309	-1.668	1.308	-2.213
D	0.106	0.004816	-1.615	1.204	-1.605	1.249	-2.272
E	0.220	2.000	-1.931	0.9149	-1.558	1.015	-2.312
F	0.535	7.042	-0.8613	-1.867	-1.570	0.2317	-1.175
G	0.828	8.408	-0.5167	-3.933	-1.583	-0.3201	-0.0342
H	1.044	7.633	-0.4630	-5.322	-1.624	-0.5847	0.1640
I	1.488	3.897	-0.4282	-7.987	-1.844	-0.8799	-0.8413
J	1.724	2.000	-0.4225	-8.991	-1.961	-0.9407	-1.565
K	2.041	0.8949	-0.4204	-9.515	-1.999	-0.9625	-2.000
J*	2.381	2.000	-0.4225	-8.991	-1.961	-0.9407	-1.565
I*	2.659	3.897	-0.4282	-7.987	-1.844	-0.8799	-0.8413
G*	3.592	8.408	-0.5167	-3.933	-1.583	-0.3201	-0.0342
F*	4.099	7.042	-0.8621	-1.867	-1.570	0.2317	-1.175
E*	4.728	2.000	-1.931	0.9148	-1.558	1.015	-2.312
C*	5.083	-0.5211	-1.521	1.318	-1.680	1.308	-2.213
A*	5.268	-1.180	-1.183	1.400	-2.052	1.400	-2.057
...	...	...	...	...	...	...	...
S*	0	-1.197	-1.202	1.400	-2.057	1.400	-2.057

6.4 Discussion

To sum up, in this chapter we generate and show a family of planar equal-mass four-body periodic orbits that connects the collinear Schubart orbit [70] with the nearby planar orbit found by Sweatman [73]. This family starts and ends with the Schubart orbit, and has a double choreography, with zero angular momentum, in the middle.

We provide a description of the physical properties of the system, such as the angular momentum, period, angle of rotation and starting coordinates for the bodies. Selected orbits from the family are described. We find that the orbits are symmetric to each other about the double choreography orbit in a way that the orbits on both sides are the same but start from different initial conditions.

We analyse the linear stability of the orbits by introducing perturbations within the plane of motion and into three dimensions. The family is shown to be unstable overall, although it has some stable regions when considered on the plane alone or when the symmetry is preserved.

We also perform the non-linear stability analysis in a similar fashion to Mikkola and Hietarinta ([35], also Section 5.6). This is done by the direct integration of the orbits from their initial conditions using the symmetric code and also integration of the same orbits rotated by 45° in the space using the general four-body code for as many periods as the system stays bound together. The approximate maximum number of periods for the integration is chosen to be 10000.

The results of both non-linear stability checks agree, both in the plane and three dimensions, with the data and regions of stability determined by the linear stability analysis. The direct integration of the orbits from "green" stable regions (in Figure 6.15) for 10000 periods showed that these orbits remained stable. The same orbits integrated from rotated initial conditions, using the general four-body code, disintegrated after some time. Also, the energy errors were small (about 10^{-8} in absolute value) which works as a good test for the numerical accuracy of calculations. For instance, the double choreography orbit (orbit K in Figures 6.7, 6.3, 6.4, 6.6), which is stable in symmetric direct integration in Figure 6.18, is

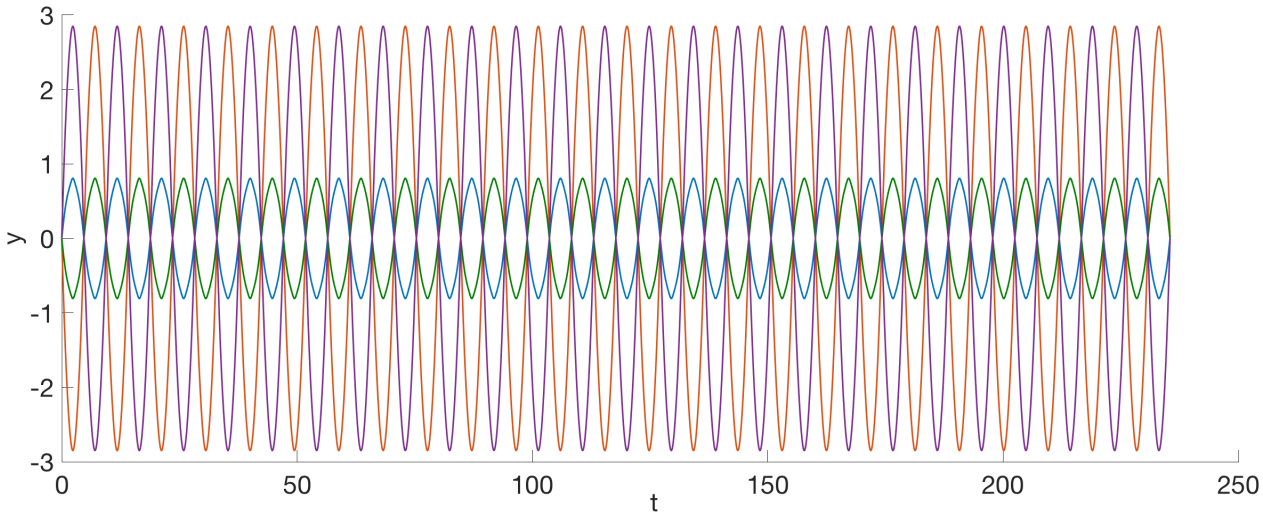

Figure 6.18: The y-coordinates of the four bodies against time for the symmetrically stable double choreography orbit K. The behaviour over about 50 periods is shown.

unstable when considered in three-dimensional space (Figure 6.19).

In contrast, the system showed itself to be unstable in the "red" unstable regions. The orbits in the unstable regions for which the stability parameters are considerably larger in absolute value than 2 were found to fall apart after a few periods: for example, the orbit that corresponds to the maximum of k_1 disintegrates after 18 periods in the direct integration. The orbit H from Figures 6.3 - 6.5 diverges after 20 periods (see Figure 6.20). The unstable orbits that are near the boundary of stability exhibit periodic properties for longer times: for instance, the orbit with angular momentum $A = 1.46$ and $d_{12} = 0.22628317$ only disintegrates into two escaping binaries after 300 periods (see Figure 6.21).

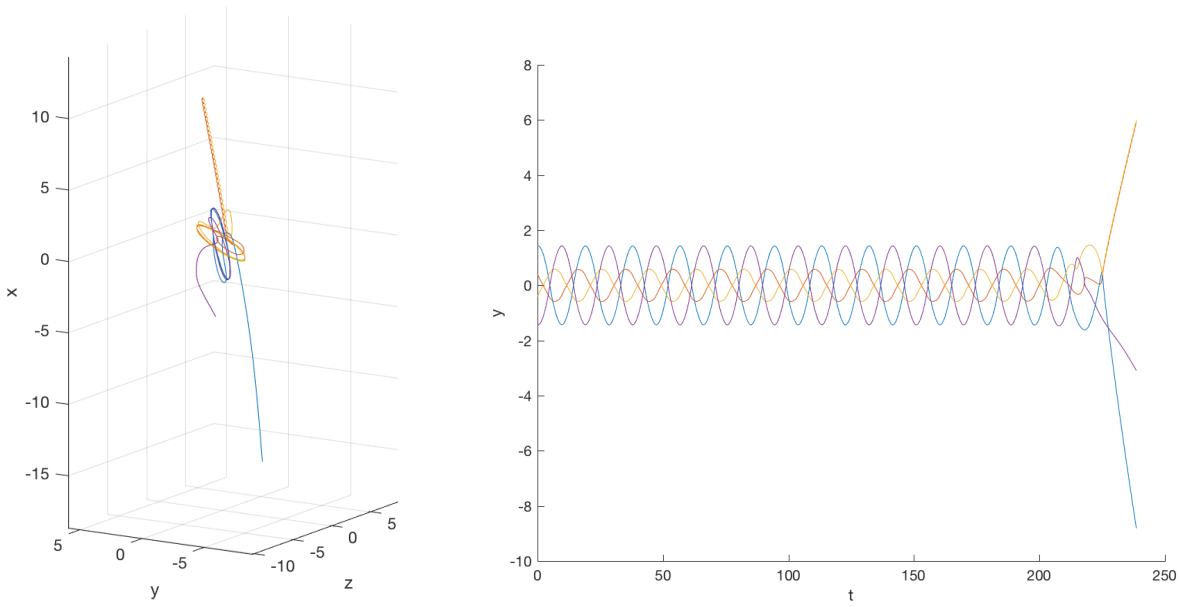

Figure 6.19: Orbit K integrated from rotated initial conditions in a space. The xyz graph (left) and the y-coordinates against time show that the orbit disintegrates into a binary and two single stars after approximately 20 periods.

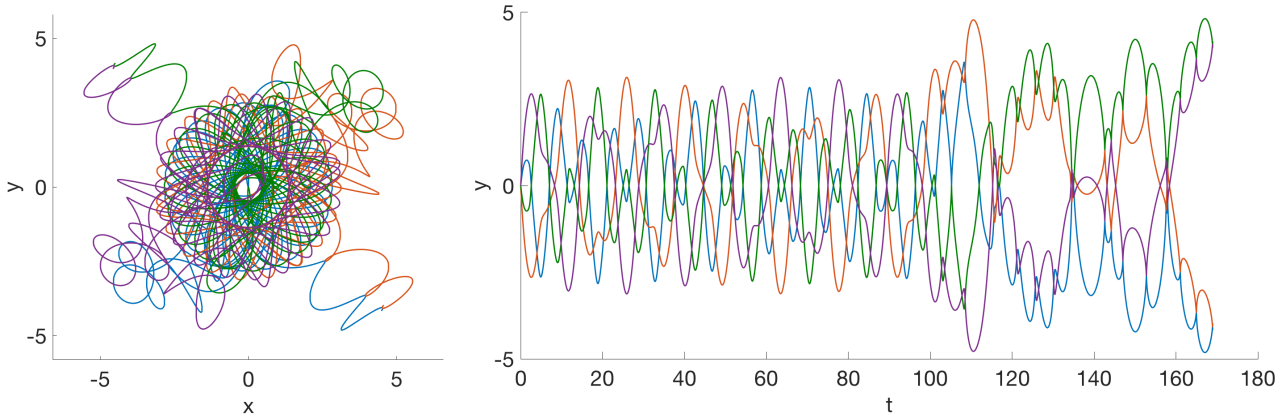

Figure 6.20: The unstable orbit H on the fixed x-y plane (left). The fixed y-coordinates of the four bodies against time for the unstable $A = 0.0025$ orbit (right). The behaviour over about 35 periods time is plotted. The orbit diverges after 20 periods.

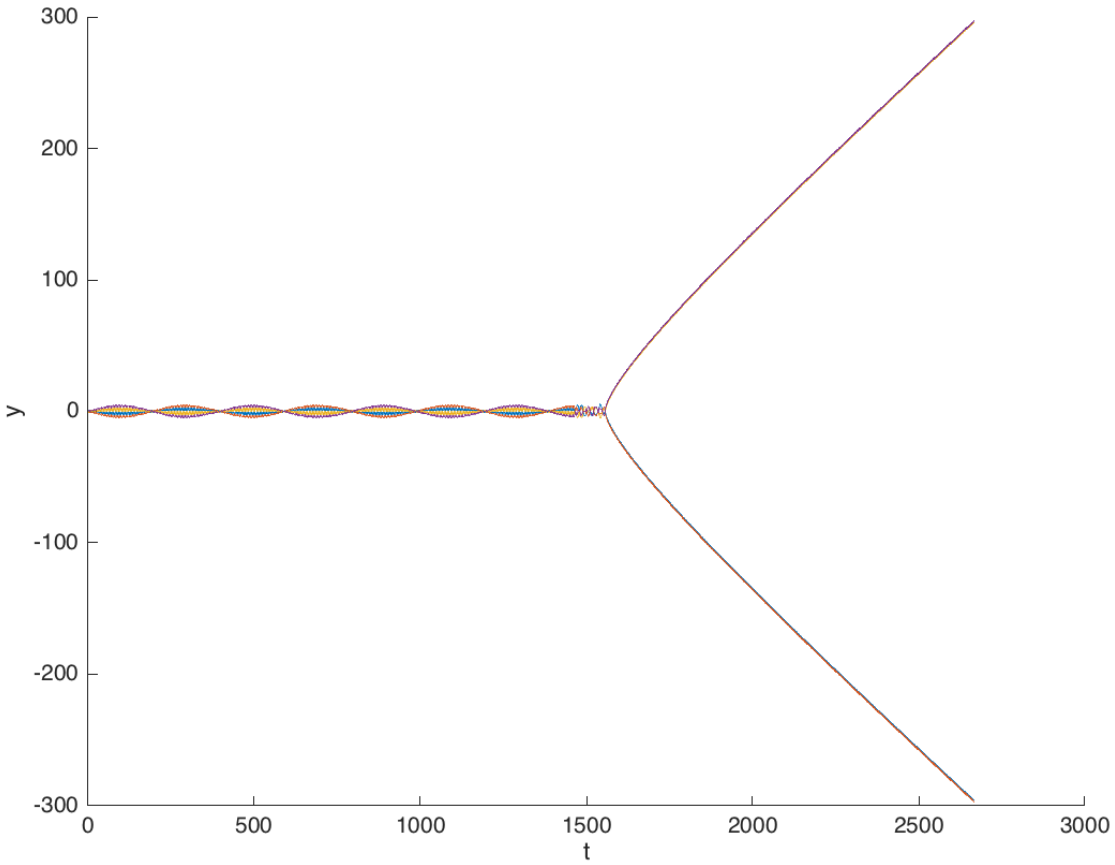

Figure 6.21: The fixed y-coordinates of four bodies against time for an unstable orbit with $A = 1.46$ (situated near orbit E). The behaviour over about 350 periods time is plotted. The system separates into two binaries after about 300 periods of direct integration.

Chapter 7

Extending the family to unequal masses

7.1 Unequal-mass collinear Schubart-like orbits

As we have seen in the previous chapter, the family with $m_1 = m_2 = 1$ begins and ends with the collinear Schubart orbit. It starts with $d_{12} = 0$, or the simultaneous collision of bodies 1 and 2, as well as bodies 3 and 4.The family finishes at $d_{12} = d_{12,max}$ with the collision of the inner bodies 2 and 3 at the centre of mass and with the outer bodies 1 and 4 far away from them. In order to relate the planar four-body system to the system of four collinear masses used in Sweatman [71], the two colliding masses on each side are swapped for the collinear orbits .

The collinear Schubart orbit itself belongs to the family of orbits with collinear masses, as was found and described by Sweatman [71]. He took the value of the total mass to be fixed with $2m_1 + 2m_2 = 4$, and the family is obtained by varying m_1 with $m_2 = 2 - m_1$.

Using the mutual conditions from Sweatman's study, the collinear family of Schubart orbits is generated. The family starts from a stable orbit with two negligible masses, $m_1 = 0$, and two heavy masses, $m_2 = 2$, (see a nearby orbit in Figure 7.1). The Schubart orbit with four equal masses is in the middle of the family. The final orbit is unstable with two heavy stationary

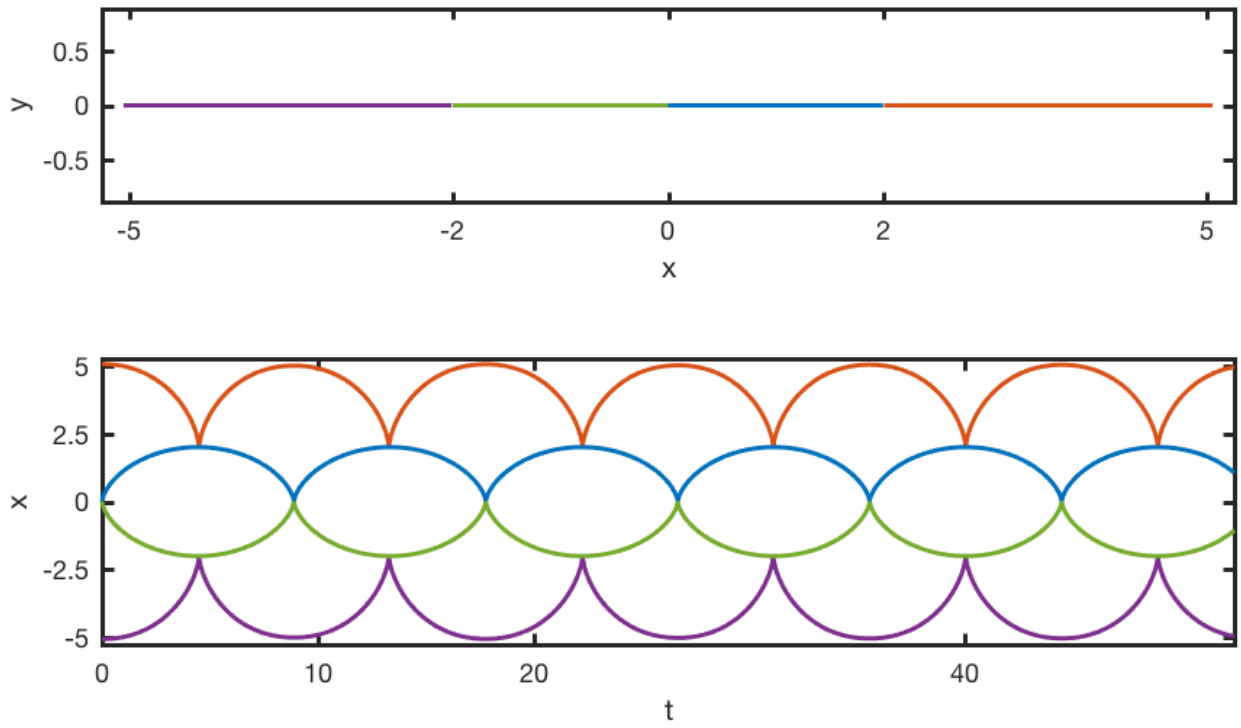

Figure 7.1: The stable Schubart orbit for $m_1 = 0.001$, $m_2 = 1.999$

masses $m_1 = 2$, and weightless m_2 masses moving very fast to prevent the outer masses from approaching each other at the centre of mass (a nearby orbit is shown in Figure 7.2).

Sweatman [71] found that there are three stable regions located in the family with $m_1 \in [0,\ 0.055],\ [0.522,\ 0.987],\ [1.276, 1.421]$. Between these regions, orbits are unstable in a symmetrical sense under collinear ($m_1 \in [0.055,\ 0.522]$) and transverse ($m_1 \in [0.987,\ 1.276]$ and $[1.421,\ 2.000]$) perturbations. Also, when increasing the mass m_1 ($m_1 > 1.400$), orbits become unstable under general transverse perturbations.

When we consider various masses m_1 and m_2 in the planar system, we expect to initially observe the same stability intervals. These intervals are now extended into the plane. We apply the same restriction on the masses of the system as for the collinear orbits, so $m_1, m_2 \in [0, 2]$. Because of the switching of the labelling of colliding bodies, the collinear stability intervals are switched too. The distance d_{12} varies from 0 to its maximum value for each mass m_1. The maximum value of d_{12} is determined by the corresponding collinear orbit for that mass m_1.

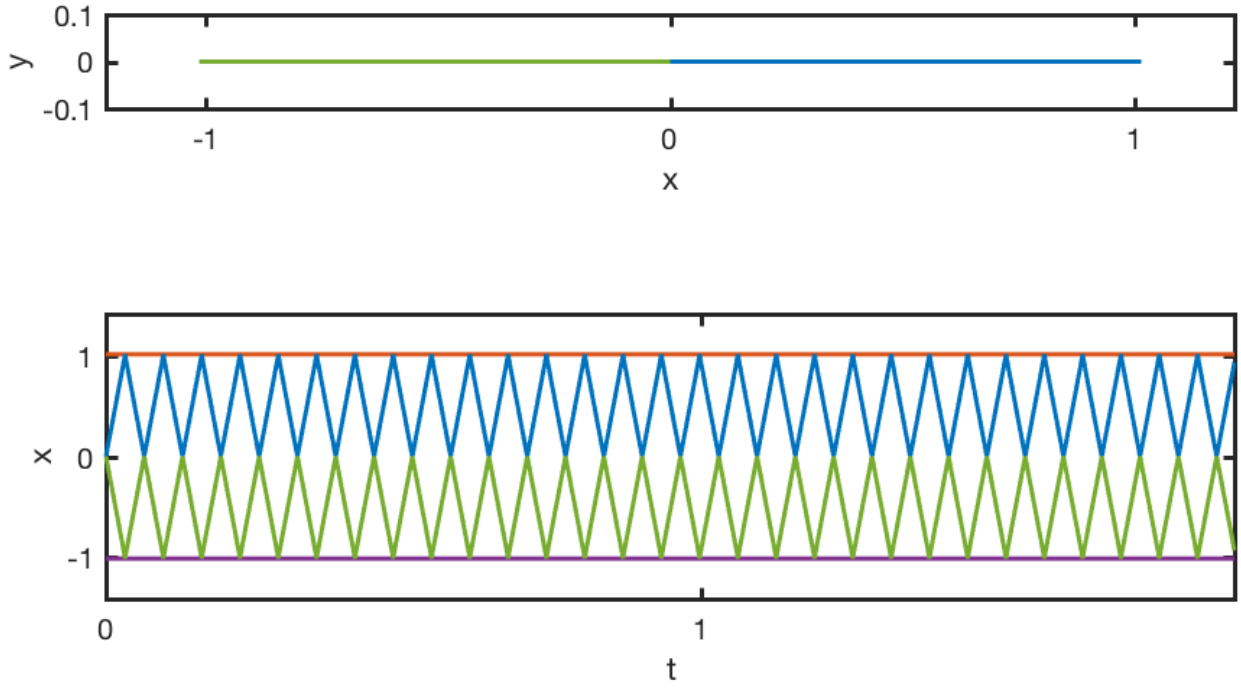

Figure 7.2: The unstable Schubart orbit for $m_1 = 1.999$, $m_2 = 0.001$

The preliminary knowledge of both ends (the collinear orbits) of the planar family allows us to construct the boundaries of the (m_1, d_{12}) region. To do that, we convert the initial coordinates that were used in Sweatman [71], to those for the Caledonian symmetric four-body problem. Sweatman uses the beginning and end of a period as times at which the ratio of the distances between inner and outer bodies is defined to be α, which is the time-independent ratio of the distances that occur in the homothetic quadruple collision orbit and is given by the sole real root of the relation [71]

$$m_1\alpha^7 + (8m_2 - 2m_1)\alpha^5 - m_2\alpha^4 + (8m_2 + 17m_1)\alpha^3 + 2m_2\alpha^2 - m_2 = 0.$$

To convert the initial conditions to those defined in our setting (see Section 3.3 for details), we need the coordinates at the times of collision between:

(A) two pairs of bodies ($d_{12} = 0$),

(B) the middle masses at the centre ($d_{12} = d_{12,\,max}(m_1)$).

Figure 7.3 shows the calculated boundaries for the unequal-mass family. These are obtained by integrating every collinear orbit until the above conditions, (A) and (B), are reached. Red and green colours indicate the unstable and stable orbits, respectively. Three stable regions in the collinear problem are now transformed into six stable regions in the near-collinear motion on the plane. The angular momentum A and the angle of rotation θ are zero on both boundaries with collinear motion.

The collinear equal-mass Schubart orbit is situated on the two ends of the blue dotted line that indicates the equal-mass family that was the subject of the previous chapter. It is shown on one of the ends in a small subplot. Orbits from Figure 7.1 and Figure 7.2 appear at the ends of the top and the bottom boundaries in small subplots: the former orbit on the stable green ends and the latter on the unstable red ends.

The double choreography, which was observed first for equal masses, remains present for every possible mass m_1. However, as we vary d_{12}, the two sets of orbits before and after the double choreography, for a distinct mass m_1, are not the same as they were for equal masses. This is illustrated in Figure 7.4 which shows two alternative sets of initial conditions (top and bottom) for an orbit with two different pairs of masses. The initial conditions differ by half a period, which is shown in the middle diagram by a schematic simulation of the motion from $t = 0$ to $t = \frac{T}{2}$. For the top image, m_1 is small and m_2 is large. On the other hand, for the bottom image, m_1 is small and m_2 is large. Thus, the same orbits appear for two related pairs of m_1 and m_2.

For example, the orbits are alike for $m_1 = 1.6$ with $m_2 = 0.4$ and for $m_1 = 0.4$ with $m_2 = 1.6$. Those orbits, that appear before the double choreography for $m_1 = 1.6$, and are in region IV, are repeated for $m_1 = 0.4$ beyond the double choreography in region I. Similarly, those orbits, that are after the double choreography for $m_1 = 1.6$, appear before that orbit for $m_1 = 0.4$. The hypothetical orbit from Figure 7.4 would exist in region II and region III. Its approximate location is shown in Figure 7.3 by blue stars.

Extending this behaviour over the whole range of orbits, we end up with four symmetric regions divided by the lines of the equal mass orbits and the double choreography orbits

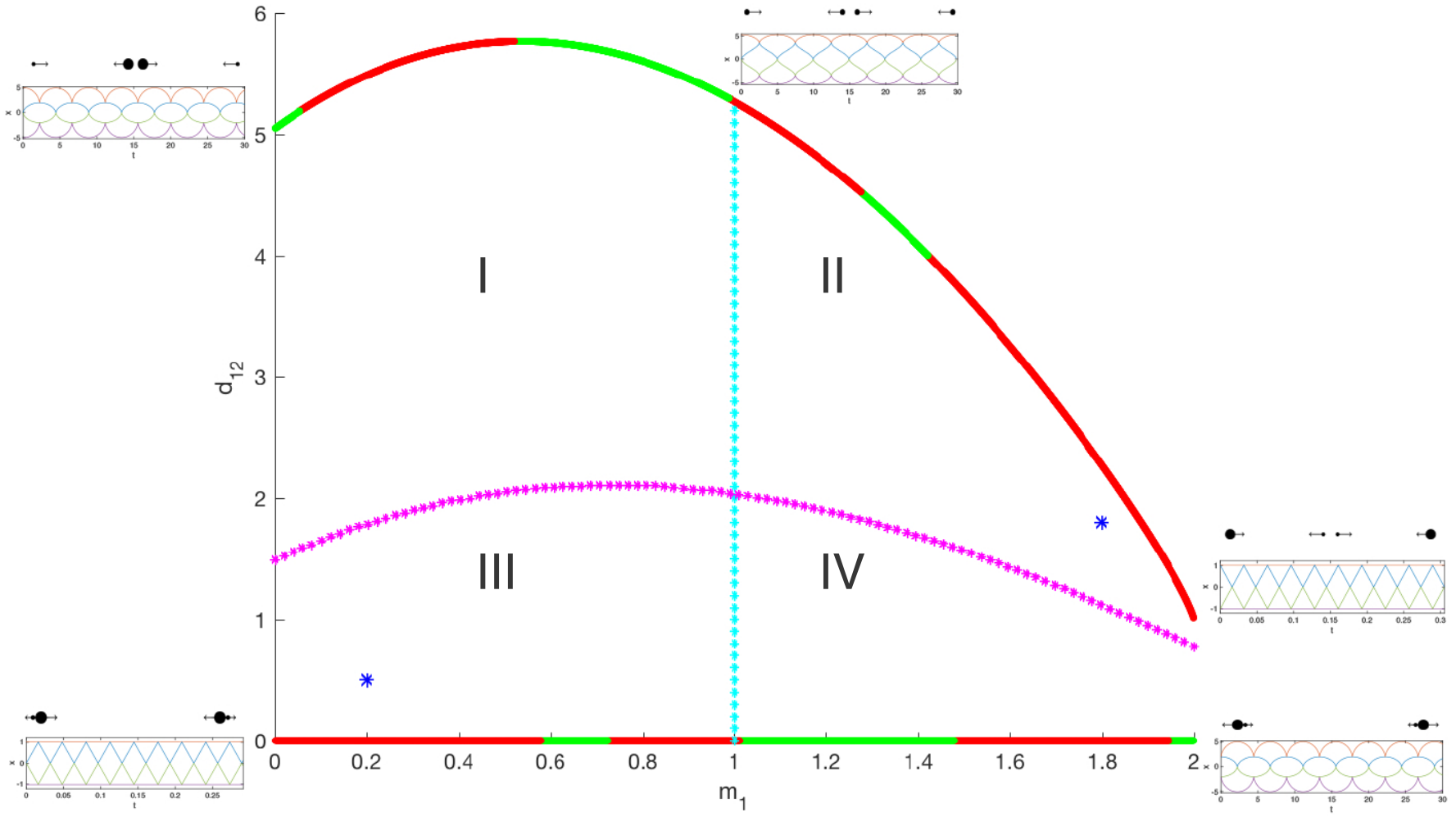

Figure 7.3: The boundaries for the unequal-mass family given by the coordinates of the unequal-mass collinear Schubart-like orbits at both possible collisions. The red and green colours correspond to the unstable and stable regions of the collinear orbits, respectively. The blue line indicates the position of the equal mass family on the surface. The magenta line accounts for the double choreography line on the surface. These lines divide the surface into four symmetric regions: region I is symmetrical with region IV, region II is symmetrical with region III.

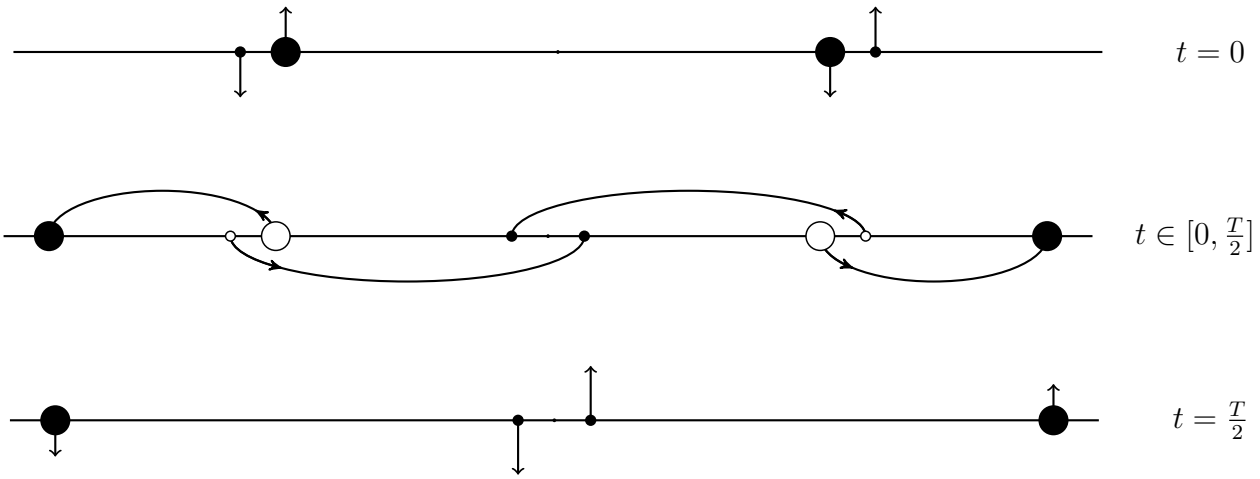

Figure 7.4: A schematic orbit simulated for a half of its period. The lighter body moves towards the centre and the heavier one shifts to the edge of the system. The top and the bottom images show the different positions and velocity vectors of the bodies at times $t = 0$ and $t = T/2$, respectively.

(Figure 7.3). Regions I and IV are corresponding regions, and so are regions II and III.

In two related regions the orbits appear in a reverse order. In this sense the equal mass line is unique because $m_1 = 2 - m_2 = 2 - m_1 = m_2 = 1$, and so it is symmetric to itself. We also notice that the collinear stability intervals on the boundaries (A) and (B) are reversed relative to each other.

So, the collinear problem study shows that when the mass m_1 and ratio between masses change, there is a significant change in the behaviour of orbits and their stability. It is now of interest to explore the behaviour of the planar orbits as the ratio between masses changes and approaches extreme values. In the next section we discuss the results accomplished for the planar family, then we inspect the stability of the newly found solutions. The last two sections are dedicated to a more detailed description of selected orbits.

7.2 The planar unequal mass family

We generate the planar symmetric family with general masses by using the algorithm described in Section 5.3. We use the same mechanism as for a single orbit search for equal masses

(Section 5.2), and enhance it so that the orbits for a single mass m_1 are all found collectively.

To make sure that we approach the orbit that belongs to the intended family, we initiate the search by progressively perturbing the mass of the outer bodies, starting from the four equal masses. The search was performed at a spacing of 0.001 until reaching the mass $m_1 = 0.730$. Then the space was increased to 0.002 for the practical reason of reducing the amount of simulations performed.

For each perturbed orbit we fix the value of energy $E = -1$, angular momentum A, initial time $t_0 = 0$ and angle $\theta(t_0) = 0$. The values of A are taken from the orbits with the closest mass m_1 that has already been processed. The other quantities are changed. Their initial values are found from the integrals of motion (4.1 - 4.3) by using Newton's method with high accuracy $(10^{-12} - 10^{-15})$. Because the step size is very small, it only requires a few Newton's method iterations to reach a solution.

After the initial values of x_1, x_2, v_1, v_2 have been found, the differential corrections take place to find the exact orbit for this initial configuration. To speed up simulations, the differential corrections are restricted to 50 iterations only, after which the process switches to a subsequent orbit. It was determined experimentally during simulations that after 50 iterations the differential corrections are not likely to converge because of either poor prediction of the initial configuration or absence of an orbit for this choice of A.

This process continues until after we have potentially found all orbits with the perturbed mass m_1 for the values of A taken from the previously analysed mass m_1. We then interpolate values of A, x_1 and x_2, of the newly-obtained orbits, for this specific mass, and get a prediction of x_1, x_2 and A for a particular d_{12}, with chosen step Δd_{12}. The idea is to fill out gaps in a mesh of possible d_{12}.

We use polynomial interpolation with degree up to $n = 5$ and apply that on the closest $n+1$ orbits to the one to be predicted. Then the search resumes for an orbit with a prediction on the initial conditions using strategies from above. The flowchart of the overall algorithm is presented in Figure 5.2 in Section 5.3.

During the search procedure we only perform computations in one direction for m_1 at a time. While processing a certain mass m_1, we actually search for orbits for that m_1 and also for $2 - m_1$ because of the symmetry for regions I - IV in the family, described in the previous section. The orbits for both masses m_1 and $2 - m_1$ are the same although the latter orbits appear in a reversed order with reversed motion. This means that the angular momentum A and angle of rotation θ will change to their opposite values but the period T will stay the same as well as the stability properties of orbits for both values of mass m_1.

Initially it does not make any difference whether the search is performed in decreasing or increasing mass m_1. When the search proceeds for masses that are distinctly different, it is easier, faster and more accurate to use the regions I and III with $m_1 < 1$. The bigger the mass m_1 becomes, the more energy and angular momentum it carries and the more effect its perturbation has on the system. The risk of applying a big perturbation lies in that the algorithm might capture the orbit from a different nearby family.

Figure 7.5 features some orbits that were discovered but belong to other families. The top and the middle orbits do not qualify because the system hierarchically consists of two binaries that form another binary, rather than the interplay of all four bodies. Some orbits of this type are featured in other studies [52, 53, 82]. For the bottom orbit two small masses rotate around the massive ones which is a different type of motion.

Sweatman observed similar behaviour for some collinear orbits in the unstable region near $m_1 = 0.056$. After several periods the orbits underwent a period-doubling bifurcation. This was an indication of a nearby stable orbit that does not belong to the family of the Schubart orbits [71].

The results of the study of the planar orbits are shown below. From the discovered orbits we have generated contour plots of the angular momentum A across the family of orbits with symmetric unequal masses (Figure 7.6), angle of rotation θ of orbits (Figure 7.8) and their period T (Figure 7.9). To better illustrate the surface of angular momentum along the family we include the slice plot of the angular momentum surface for a range of masses m_1 in Figure 7.7.

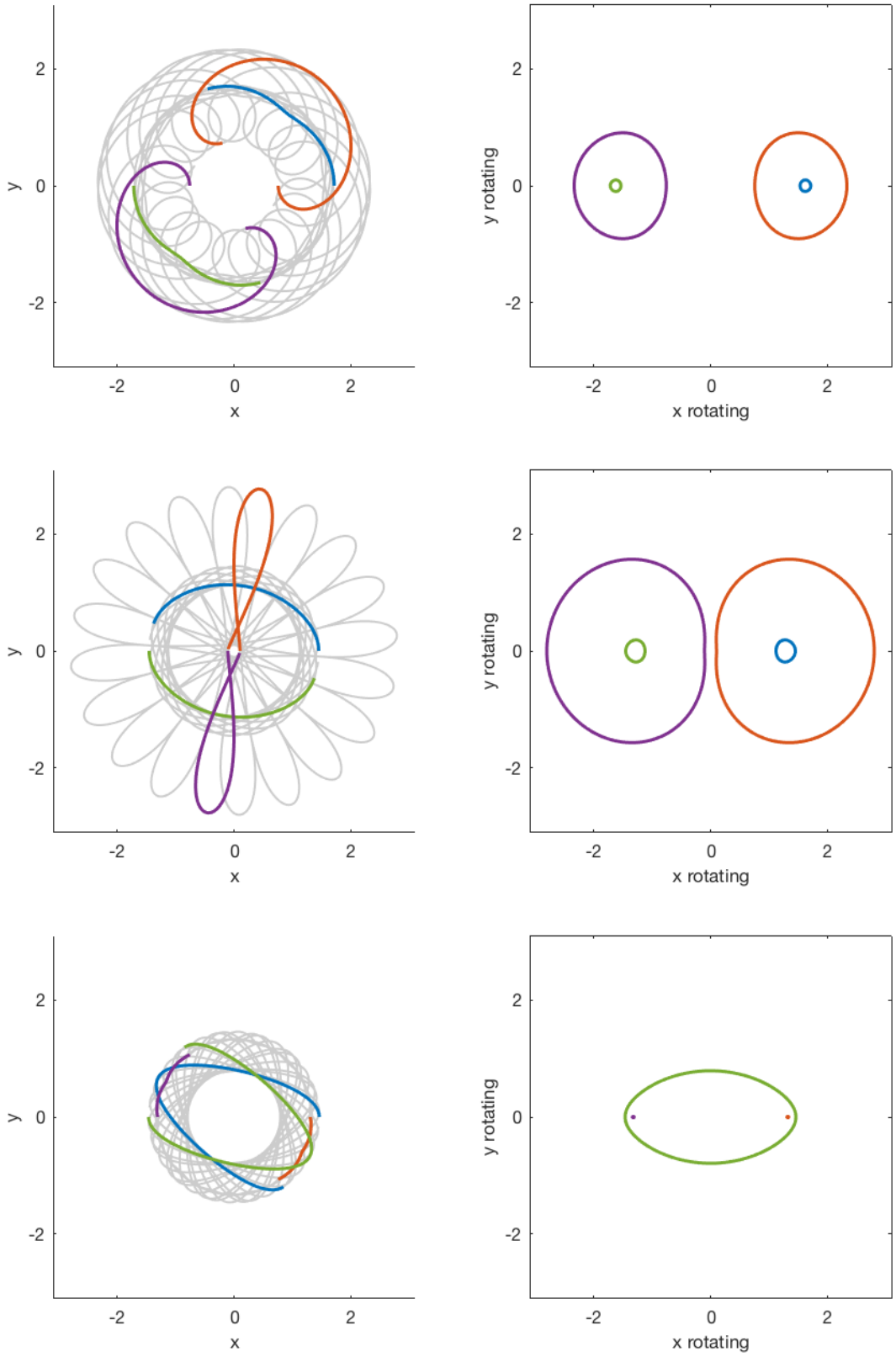

Figure 7.5: Some of the orbits captured during the search that do not belong to the family of orbits. The mass $m_1 = 1.800$ for the first two plots. For the bottom plot $m_1 = 0.072$.

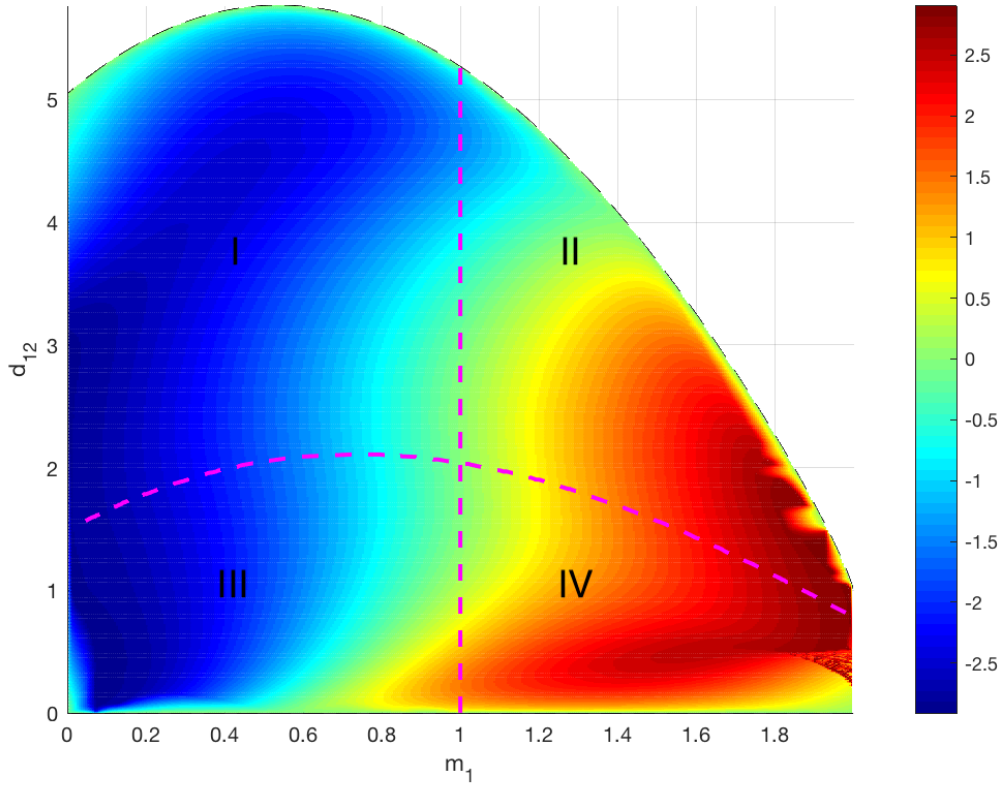

Figure 7.6: The contour plot of the values of angular momentum across the family of orbits. Magenta dashed lines indicate the location of the boundaries between regions I - IV.

As long as the mass m_1 increases, the angular momentum also increases and at some point ($m_1 = 1.421$) the angular momentum is always positive. Similarly, when mass m_1 decreases, the angular momentum also decreases. This is to be expected from the way the positions at the start of integration are chosen.

According to the initial setting of the system, the outer masses always start with a positive orientation of velocity. If the outer mass is relatively big, then it carries most of the system's angular momentum, provided that the small inner body is not too fast. When the outer mass is small, angular momentum tends to be mostly associated with the big inner mass that moves with negative velocity; so, angular momentum is negative too.

As a consequence of this, the maximum of angular momentum, that was observed for equal masses, increases for each mass in region IV until it transforms into a cusp starting from $m_1 \approx 1.75$. The cusp persists until the end of the family, however, after $m_1 \approx 1.80$ we observe

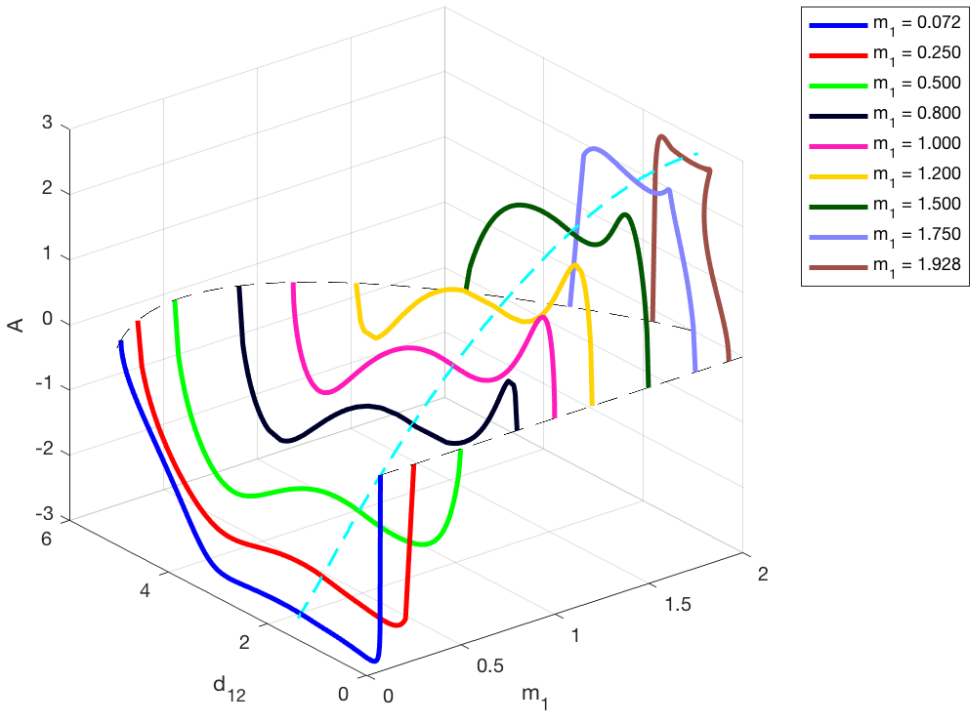

Figure 7.7: Angular momentum curves for particular values of mass m_1. The blue dashed line indicates the angular momentum values for the double choreography orbits. The black dashed lines show the location of the boundaries for the family.

that the curve of angular momentum folds back before reaching the maximum.

As a result, there is more than one orbit that exists for a particular value of d_{12}. The latter behaviour does not appear for small m_1 in region I, because the angular momentum values for the corresponding orbits change more slowly along the d_{12} axis as compared to those for the large values of m_1 in region IV.

When mass m_1 decreases in region III, the maximum of angular momentum also decreases until it fully disappears when $m_1 = 0.579$. After reaching that mass the direction of angular momentum switches to negative. Also, with decreasing m_1 in region III (or increasing m_1 in region II) the change from a collinear orbit with $A = 0$ to the one with minimal A becomes almost instantaneous.

In Figure 7.6 it can be seen that there are fluctuations on the surface of A in region II close to the collinear boundary. This is because that region features high instability, partially due

to an instantaneous change in A close to the boundary, and also due the lack of data points in this region. In principle, this could be improved by a significant reduction in size of applied perturbations in the search procedure .

Figure 7.7 also features the values of angular momentum for double choreography orbits that are shown by a cyan dashed line. The angular momentum increases for the whole range of masses from $m_1 = 0$ to $m_1 = 2$ for the double choreographies. The equal mass double choreography has a zero angular momentum. This is, again, due to symmetry between, and on the boundary of, the regions I - IV.

The angle of rotation is measured in the range between $-\pi$ to π and is shown in Figure 7.8. The jump between two extreme boundaries corresponds to the location of a double choreography. The noise in Figure 7.8 at the position of the jump is due to lack of data points. The angle of rotation is subject to the same changes for every mass ratio: it has a small local maximum before it decreases to the bottom limit ($-\pi$) of the range, then it jumps up to the upper limit (π) and decreases down through zero and reaches a local minimum.

As long as the ratio between the two pairwise symmetric masses increases, the number of orbits with close-to-collinear motion grows in region I. This can be seen in the increase of the green areas when masses move away from the equal case in Figure 7.8. The heavier masses tend to move slower and are mostly driven by the mutual attraction of each other. The light masses, in contrast, move very fast.

The relation (6.1) between angular momentum A, energy E, angle of rotation θ and period T, was checked numerically and found to agree (up to accuracy 10^{-2}) for a number of randomly chosen masses m_1 in its simplified form,

$$\frac{dT}{d\theta} = -\frac{A}{2E}. \tag{7.1}$$

The period of the orbits (shown in Figure 7.9) is greatest when d_{12} approaches its largest values, in region I, and for the corresponding orbits in region IV. The smallest values of the period are achieved on the edges in regions II and III when two heavy bodies are almost

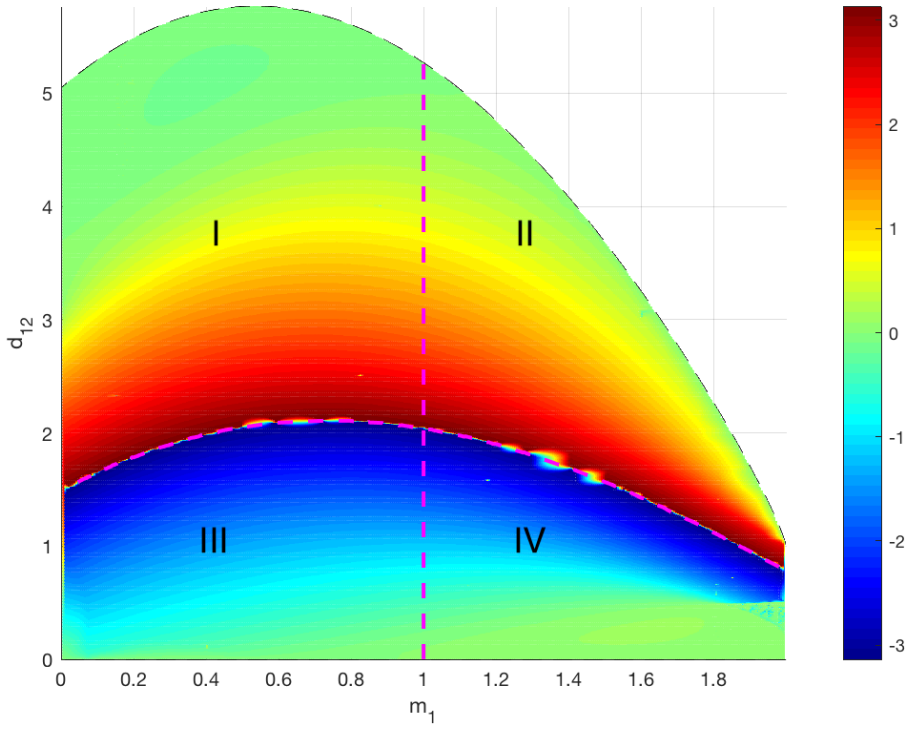

Figure 7.8: The values of angle θ (rad) across the family of orbits. Magenta dashed lines indicate the location of the boundaries between regions I - IV.

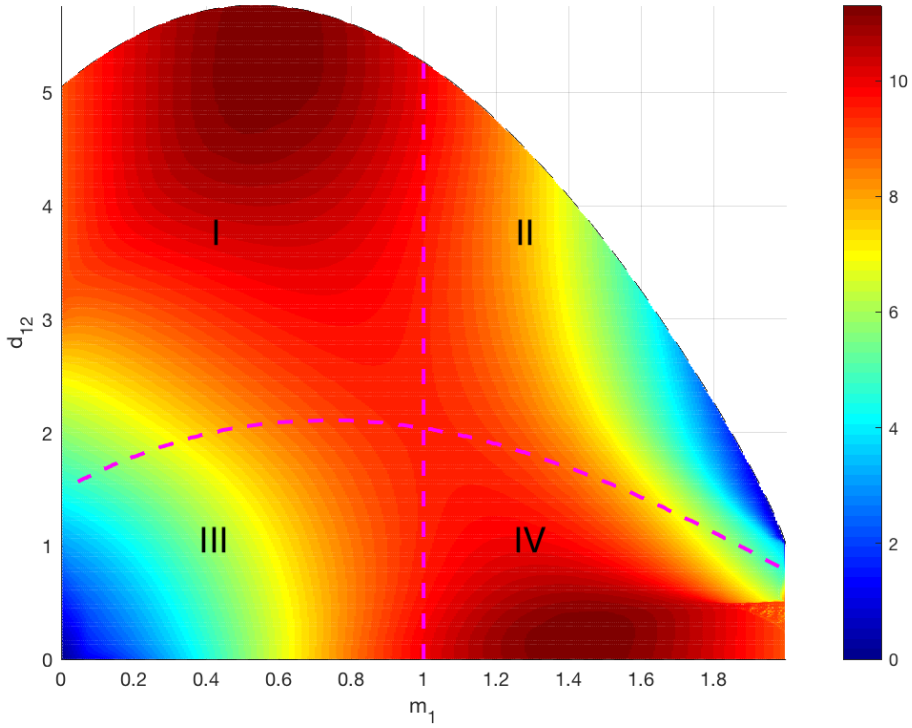

Figure 7.9: The period T across the family of orbits. Magenta dashed lines indicate the location of the boundaries between regions I - IV.

stationary and two negligible masses shift around them. In the limit $d_{12} \to 0$, $m_1 \to 0$ and the corresponding symmetric limit, the period also tends towards zero. In this limit the system is represented by two heavy inert masses, with two weightless bodies that keep the heavy masses apart.

7.3 Stability regions in the planar family

A linear stability analysis for the unequal mass family was conducted in a similar fashion to the equal mass family described in the previous chapter. It is partially performed during the search for an orbit. On each step of the iterational process we apply symmetric planar perturbations to produce a differential corrections matrix, which is essentially the monodromy matrix for the symmetric system. This includes only symmetric perturbations on the plane and generates two stability parameters out of the four associated with planar motion.

The subsequent linear stability analyses on and out of the plane have been carried out for a limited range of orbits from the family. We chose to check the stability of orbits for every fifth mass in general and for every mass when masses become extreme ($m_1 < 0.010$ and $m_1 > 1.990$). The stability test has been conducted in the regions I and III with small m_1 for the same reasons as those for prefering of these regions for the orbit search. Following the analysis, we only describe stability properties for the mass $m_1 \in [0,\ 1.000]$. This covers half of the family space (regions I and III). The other half with $m_1 \in [1.000,\ 2.000]$ features the same stability regions and properties but in reverse order.

All of the overall stable regions are shown in Figure 7.10 in green. The coloured part of the plot indicates the actual located orbits. The blank spaces conceal more orbits and in principle could be filled out by using a smaller mesh for the search. However, the stability regions and the boundaries between them are visible even with the existing coverage of the family. Figure 7.11 duplicates Figure 7.10 and shows the location of the boundaries between four regions I - IV and also shows where the angular momentum A is zero. This is shown to provide insight when interpreting the boundaries between the stability regions.

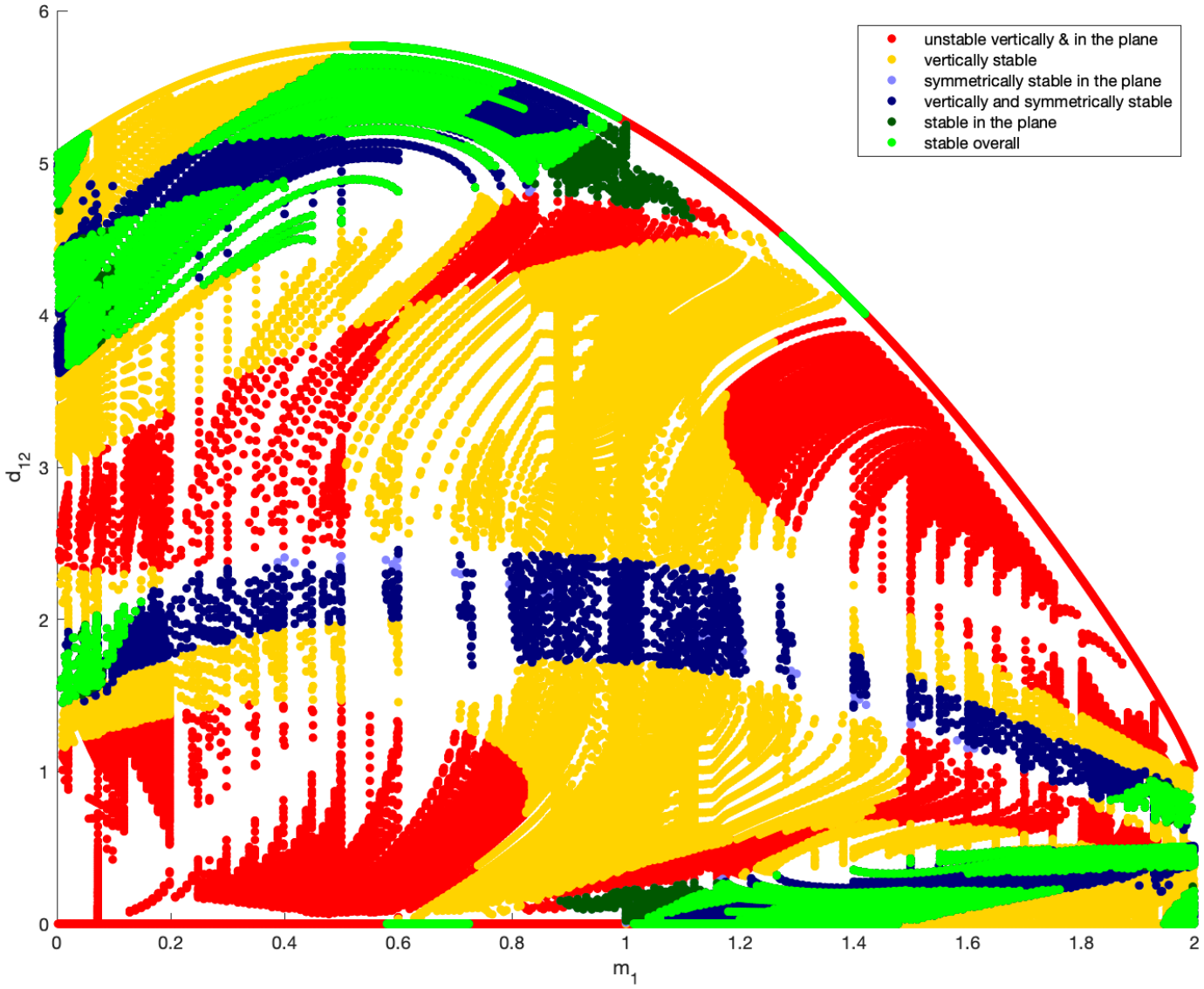

Figure 7.10: Stability regions in the planar unequal mass family.

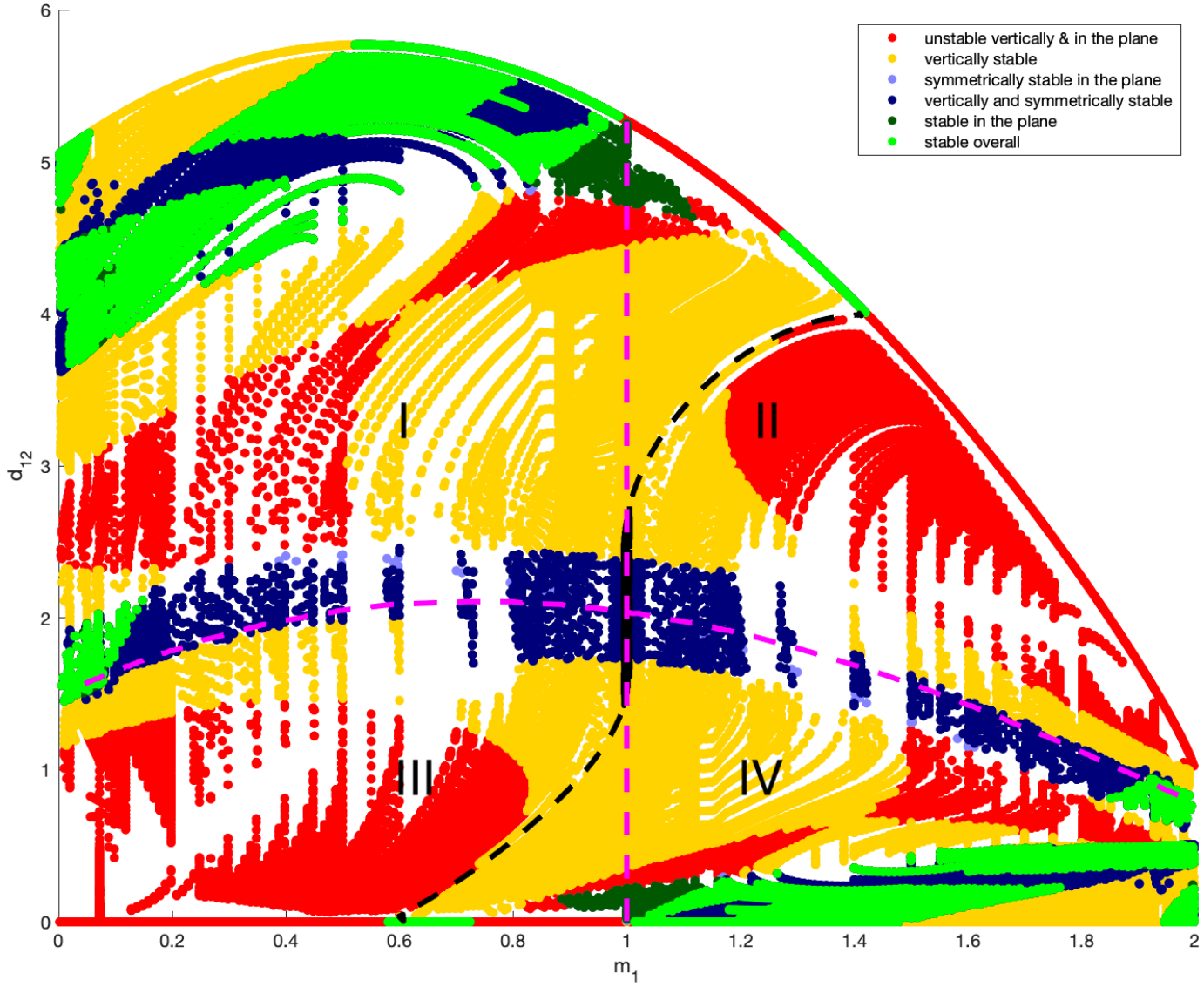

Figure 7.11: Stability regions in the planar unequal mass family. Magenta dashed lines indicate the location of the boundaries between regions I - IV. The black dashed line illustrate where the angular momentum is zero.

The motion is mostly unstable, due to various types of perturbations. The three stable regions from the collinear motion persist in the planar family. The smallest region, close to the horizontal axis for $m_1 \in [0.579;\ 0.722]$, coincides with the decrease and disappearance of the maximum of angular momentum in region III. In terms of d_{12}, stable orbits occur from the collinear motion for $d_{12} = 0$ until the maximum of A.

The other two collinearly stable regions are for masses $m_1 \in [0.522;\ 0.987]$ and $m_1 \in [0;\ 0.055]$, at the top of Figure 7.10. Another stable region appears close to these two regions. It is believed to start from mass $m_1 \approx 0.720$ and spreads out until the end of the mass range. Another stable region appears for extreme masses from $m_1 \approx 0.150$ near the double choreography line. The double choreographies become stable after reaching masses below $m_1 \approx 0.090$. Although the boundaries of the stability regions are not shown precisely, the discovered orbits allow us to get some idea about their location.

The green overall stable region (in Figure 7.10) includes orbits that are symmetrically stable, stable in the plane and vertically stable. The individual occurrence of these stabilities are individually shown in purple, dark green and yellow colours, respectively. We also introduce the dark purple region for orbits that are both vertically and symmetrically stable, but unstable under general planar perturbations. Islands of purple regions may be observed in the green "stable" regions near equal masses or for the most extreme cases: these are found to form due to the presence of complex instability. Some noise is present in the stability plot because of the chosen precision of 10^{-2} for the calculations.

The symmetrically stable region seems to overlap with either the vertically stable or the planar stable region for most of the orbits. In the middle ranges of d_{12} the symmetrically stable region, as well as the vertically stable region, closely follows the double choreography line as can be seen in Figure 7.11. (Note: this is not the actual boundary, that corresponds to the local extremum of A as discussed later in this section.) However, when masses start to differ considerably ($m_1 < 0.7$ or $m_1 > 1.3$), the symmetrical stability is no longer observed near the double choreography in regions II and III. Another plot of the symmetrically stable and unstable regions is presented in Figure 7.12. This includes all the located orbits in the family

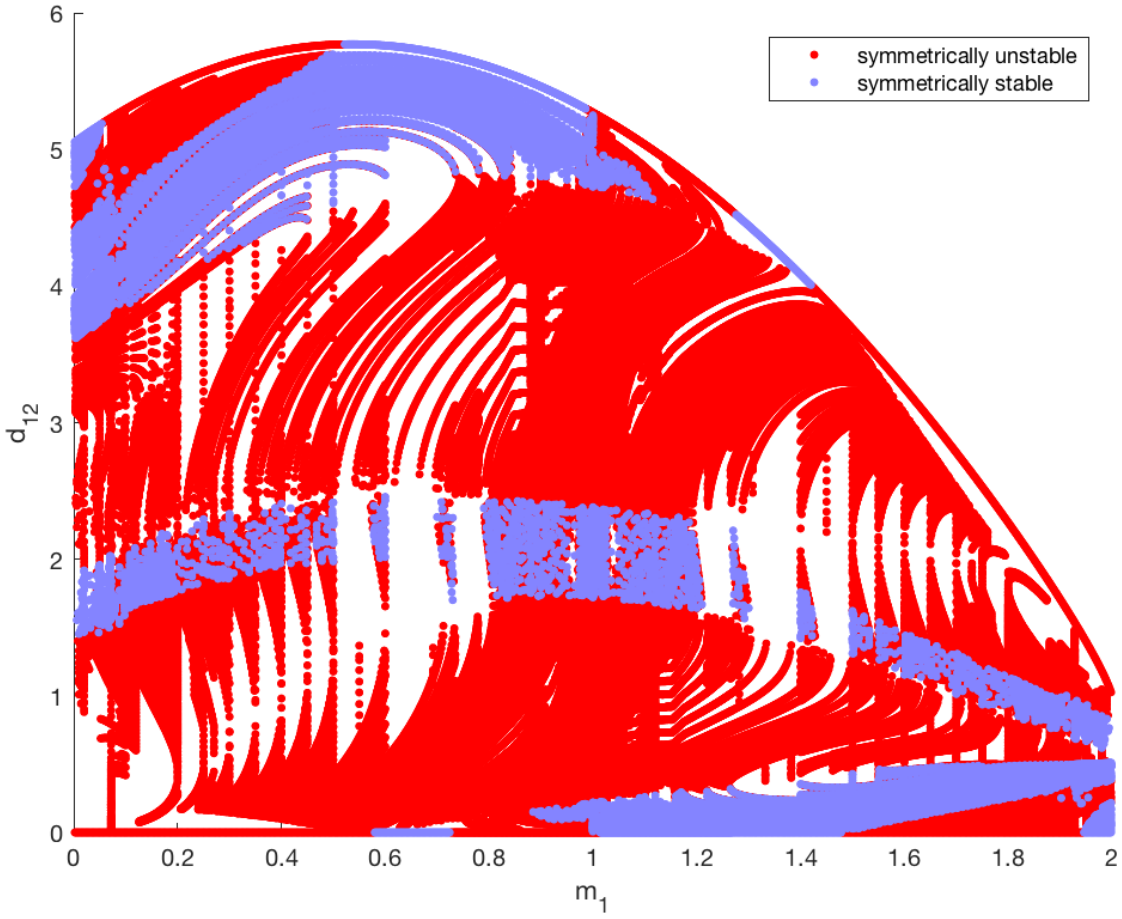

Figure 7.12: Symmetrically stable and unstable regions in the planar unequal mass family. Some of the orbits that are marked as unstable may in fact be stable: they are marked as unstable due to the low accuracy of the calculations.

since the symmetric stability analysis was performed for every single orbit as a part of the search.

As mentioned before, some orbits have errors in the calculation of the monodromy matrix. The following criterion was chosen: if the determinant of the monodromy matrix for an orbit differs from unity by more than 10^{-2}, then we consider its eigenvalues not accurate enough and mark this orbit as unstable by default. For instance, some orbits in Figure 7.12 are shown as unstable, although they are located in the stable region in the middle. Several orbits from them were checked by a nonlinear simulation for over a 1000 periods and appeared to be stable.

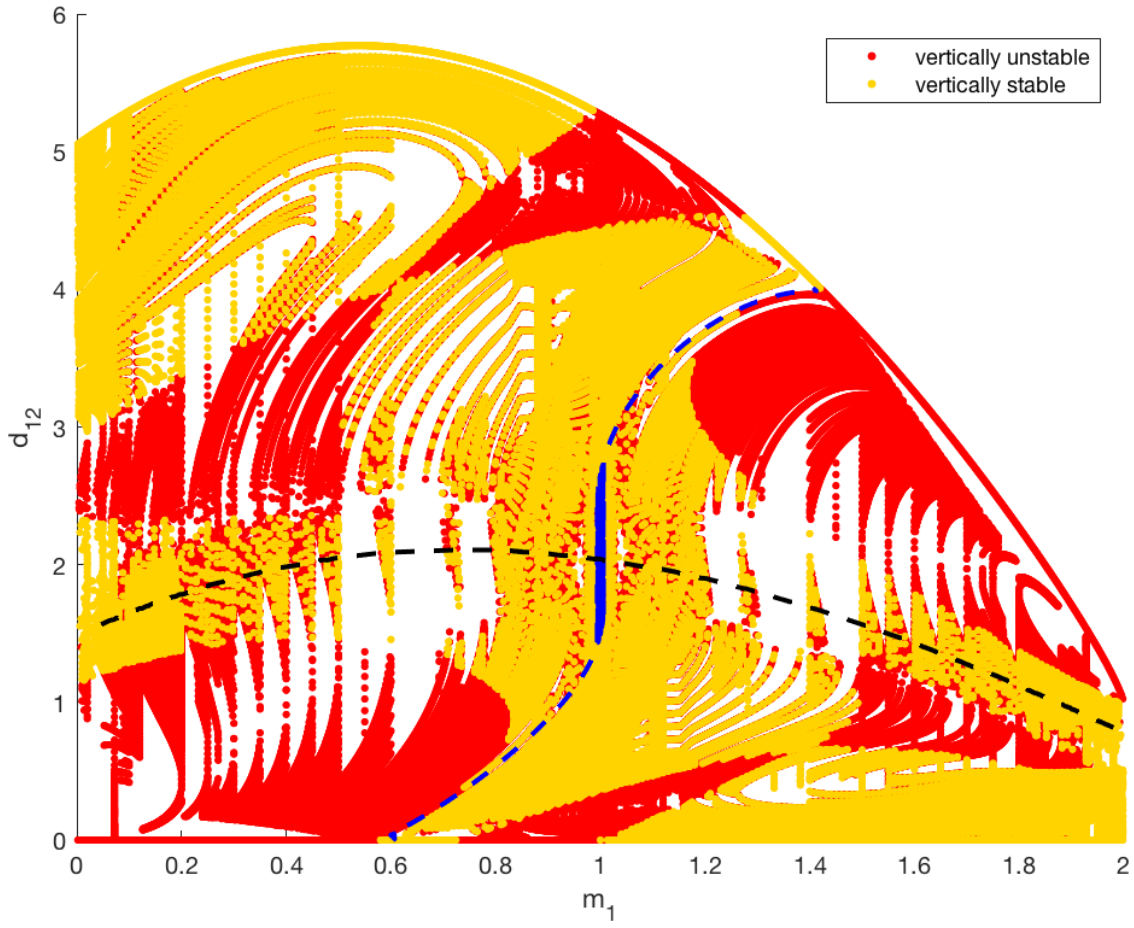

Figure 7.13: Vertically stable and unstable regions in the planar unequal mass family. The black and blue dashed lines illustrate the double choreography line and zero angular momentum line, respectively. The zero angular momentum line transforms into the small blue region in the centre since there are three crossings of zero by the angular momentum and its values do not deviate from zero by more than 0.01.

In Figure 7.10 it can be seen that there are only two big regions with planar stable orbits (shown in dark green) that are unstable vertically. These regions lie in the middle of the masses range and include the case of equal masses. The yellow, vertically stable, region in the middle includes, and is situated around, the double choreography line and the line of zero angular momentum. This is shown in Figure 7.11 and Figure 7.13 for vertically stable and unstable orbits.

The region at the beginning of the family for $m_1 \to 0$ and $d_{12} \to 0$ is highly unstable with orbits disintegrating after a couple of periods. The stability parameters in this region are of order $10^3 - 10^4$. Also, as shown in Figure 7.6 in the previous section, the rapid change from

$A = 0$ for collinear orbits to nearby planar orbits happens almost instantaneously. So, it is very hard to search for orbits in this region and the results are mostly achieved by interpolation.

Another interesting question appeared prior to the stability analysis. This concerns the connection between the angular momentum A and the symmetric stability parameter k_1. During the study of the equal mass orbits it was noticed that every time when A was at an extremum, the parameter k_1 crossed the boundary between stable and unstable orbits.

Similar behaviour was observed in the planar three-body problem by Hénon [32]. He called the orbits corresponding to the boundaries between regions "critical orbits" and made the connection between such orbits and extrema of A. He deduced that this property is valid because the perturbation of the orbit for an extremum of A corresponds to an eigenvector of the monodromy matrix which is associated with an eigenvalue 1. Thus, one of the stability parameters should be 2 since the eigenvalues of the Hamiltonian monodromy matrix occur in reciprocal pairs; and so, an extremum of A corresponds to a critical orbit.

In the planar four-body family of Schubart-like orbits for equal masses there are four extrema of A: one maximum at the beginning of the family, one local minimum in the middle before reaching the equal mass double choreography orbit and the other two symmetrically related to them. All these four extrema correspond to a critical orbit associated with a change in the stability of the symmetric stability parameter k_1.

A similar behaviour persists for the other choices of pairwise symmetric masses. As long as the maximum of angular momentum exists, it corresponds to the change from general symmetric linear stability to solely vertical stability. However, for $m_1 > 1.8$ (Figure 7.14b) when the maximum of A transforms into a cusp, we notice the following peculiarity.

In the middle of the d_{12} range for $m_1 \approx 1.872$ another two regions start forming: the yellow vertically stable region and the green overall stable region. This seems to coincide with the formation of the cusp. At the same time, the stable region at the peak of angular momentum slides down, and the cusp then corresponds to the change in vertical stability to instability. This is shown in Figure 7.14b as curves of A for particular masses m_1 that are bigger than

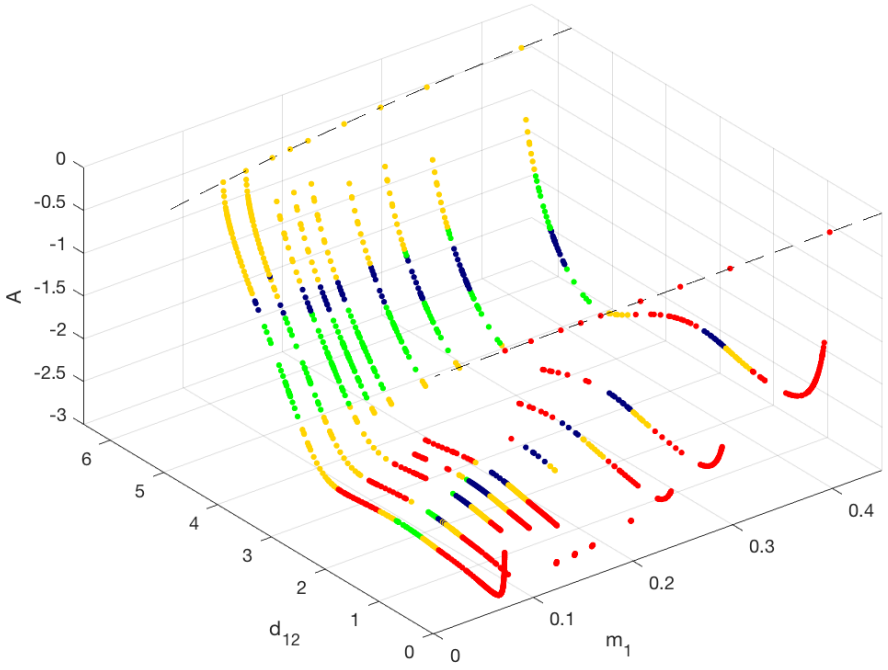

(a) Angular momentum curves for several $m_1 < 0.25$

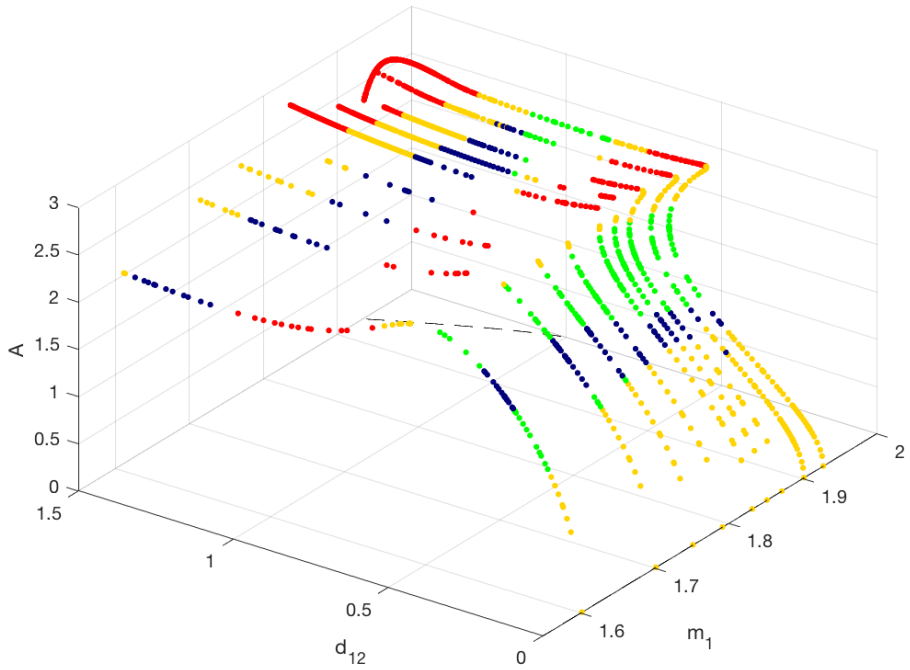

(b) Angular momentum curves for several $m_1 > 1.75$

Figure 7.14: Stability zones plotted for the values of angular momentum for extreme masses in regions I and IV. This shows the forming of the "cusp" when the third stable region appears for large values of m_1. The colours used in Figures 7.14a and 7.14b are consistent with those defined in Figure 7.10.

1.800. The stability zones are shown on top of the values of A using the same colour code as for Figure 7.10. The corresponding regions for related small values of mass m_1 are shown in Figure 7.14a.

The local maxima and minima of A near the double choreography line merge when $m_1 \approx 0.7$ and become one local minimum (or local maximum at $m_1 \approx 1.3$). For the whole range of masses m_1 this change happens between the symmetric and vertically stable orbits to the solely vertically stable orbits.

It is still of interest why no change in stability was found when angular momentum becomes purely negative for highly unstable orbits in region III (similarly when it becomes purely positive in region II). One explanation could be that initially the change is from symmetrically stable to vertically stable zones. However, in the highly unstable zone the change from $A = 0$ on the boundary to the one with A_{min} happens instantaneously, and there is no change in the stability. This requires further investigation.

7.4 Absolute periodic orbits and double choreographies

In general, the orbits that belong to the planar family of interplay orbits are relative periodic orbits [12]: they are not periodic in the fixed coordinate system, but periodic relative to a rotating coordinate frame (see Section 3.3 for details). There are, however, orbits that are periodic with respect to both fixed and rotating frame: these are called absolute periodic orbits.

One of the examples of such orbits in the family are the collinear boundaries, discussed in Section 7.1. These boundaries are constructed from the collinear Schubart orbits [71]. Since there is no rotation present, the orbits look the same in all coordinate frames. Figure 7.15 shows the location of some other absolute periodic solutions in the initial-value space of the family.

In the family there are absolute planar periodic orbits with zero angle of rotation. One

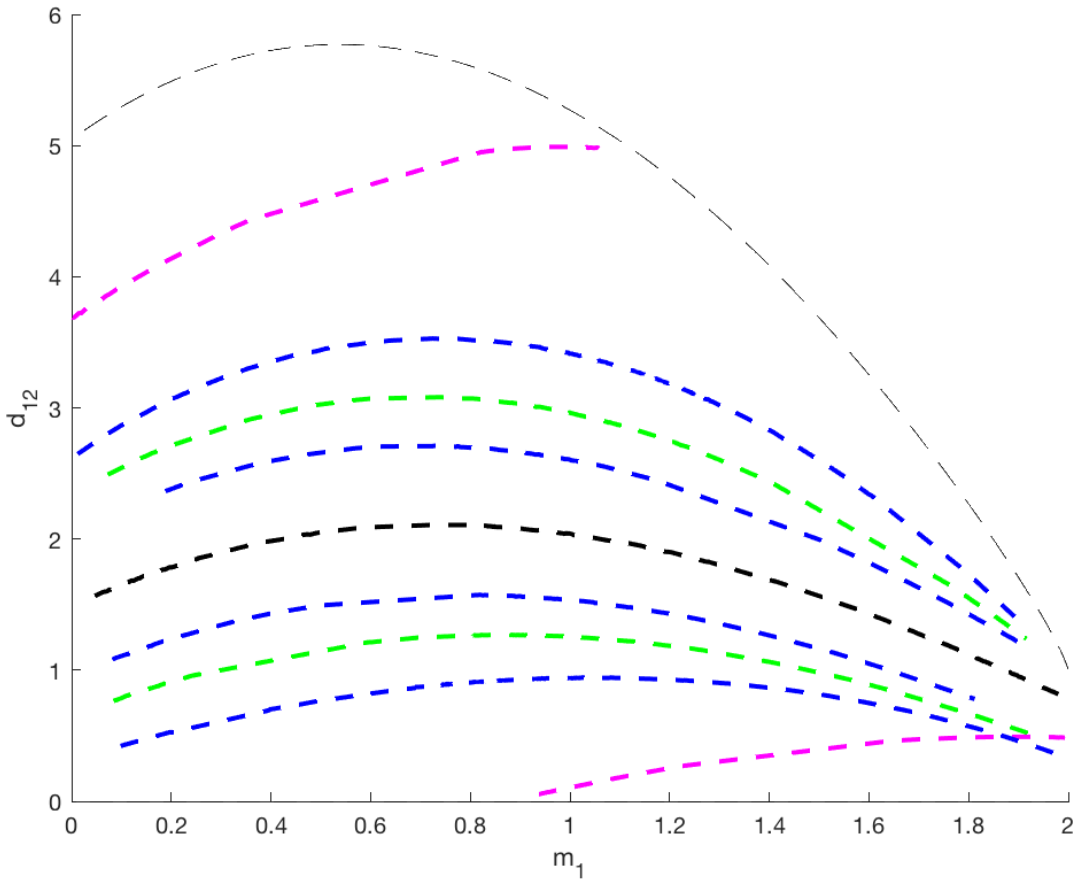

Figure 7.15: Absolute periodic orbits in the family with the angle of rotation $\theta = 0$ (magenta dashed lines), $\theta = \pi = -\pi$ (black dashed line), $\theta = \pm\, \pi/2$ (green dashed lines), $\theta = \pm 2\pi/3$ and $\theta = \pm\, \pi/3$ (blue dashed lines).

example of such orbits is provided in the previous chapter for equal masses and presented in Figures 6.3 - 6.5 as orbit D. This orbit generates a planar sub-family of the present family, with zero rotation. The zero rotation orbits are shown in Figure 7.15 by two magenta dashed lines. Interestingly, this orbit exists only for cases when the bodies are near-equal, or the big masses are in the middle and small masses are outside for most of the time.

In order to qualify for absolute periodicity, the orbit must satisfy the following criteria: the bodies must return to their initial positions and have the same initial momenta at $t = 0$ (in real non-rotating space) after one revolution about the centre of mass. In other settings of the system that means that when the absolute periodic orbit is followed for one period T, the angle of rotation is either 0 or 2π.

However, if θ is a rational multiple of 2π then at some point, possibly after performing several periods, the orbit closes up and starts to repeat. If θ is an irrational multiple of 2π then the orbit never closes up and "fills" an entire circle in space with its infinite path. If we restrict the orbit to only one full revolution about the centre of mass, then, in order to have an orbit with a closed path, the angle of rotation must be of the form $\theta = \frac{2\pi}{k}$ where $k \in \mathbb{Z} \setminus \{0\}$. The case $k = 1$ coincides with the previously discussed zero rotation orbits.

The case $k = 2$ is the double choreography orbit with $\theta = \pm\pi$. It was first discovered, and its existence was proved, by Chen [20] for the case of equal masses. It is also known as the criss-cross orbit, and its description can be found in Section 6.1 and shown in Figure 6.7.

This orbit does not have any collisions and is situated in the middle of the family (for both equal masses and unequal masses). Also, one of its features is that the masses change their configuration from collinear at times $t = 0,\ \frac{T}{2},\ T,$ etc. to a square at times $t = \frac{T}{4},\ \frac{3T}{4},$ etc., and the configuration remains a parallelogram for all times. If followed for one period, the outer bodies, as well as the inner bodies, are swapped. Following the orbit for two periods will close up the orbit. Thus, we say that the criss-cross orbit is absolute periodic with period $\hat{T} = 2T$.

There are other double choreographies in the family that exist for the case of pairwise symmetric unequal masses. As discussed in Section 7.1, the line of double choreographies

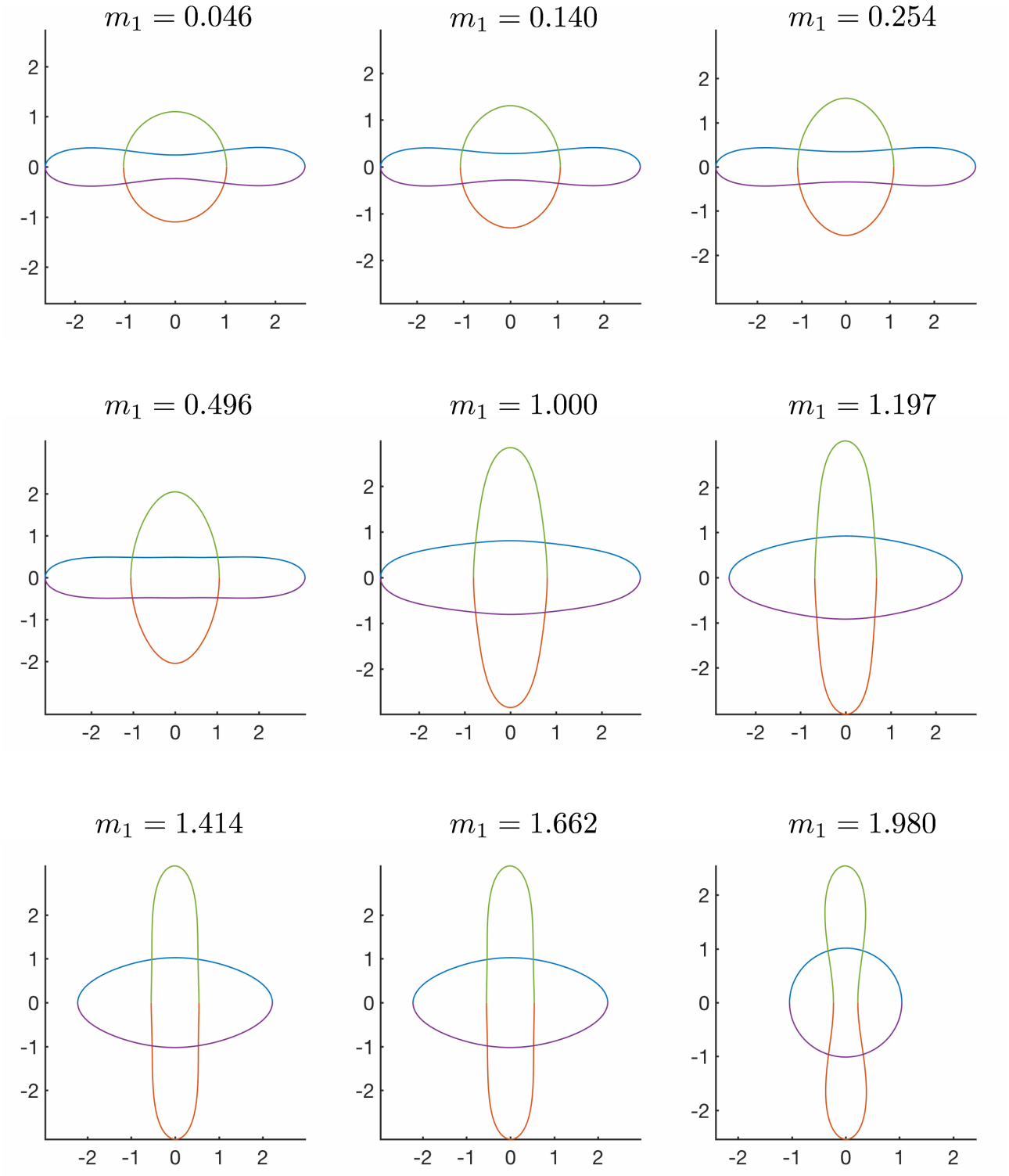

Figure 7.16: Selected double choreography orbits for particular values of m_1.

together with the equal mass line divides the family of orbits into four regions of corresponding orbits. This line is shown in Figure 7.15 in a black dashed line. Figure 7.16 shows some of the selected double choreographies in order of increasing m_1.

As mentioned in Section 7.2, the angular momentum is constantly growing with mass m_1 for double choreographies and is symmetric across the equal mass solution. From the plots in Figure 7.16 it can be noted that the lighter the body, the more elongated is its orbit. For the heavy mass, the orbit transforms into a circle.

Starting from equal masses, the double choreography orbit lies near the boundary of the symmetric linear stability but remains in the symmetrically stable region. As the ratio between pairwise symmetric masses grows, the orbits switch from being linearly stable in a symmetric and vertical sense to being linearly stable under all types of perturbations (for $m_1 \lesssim 0.150$ and $m_1 \gtrsim 0.850$).

In the case $k = 3$, the angle of rotation is $\theta = \pm\frac{2\pi}{3}$. So, in order to complete the orbit in the fixed frame, the orbit must be followed for 3 periods. Similarly, for $k = 4$, the orbit is absolute periodic and makes one full revolution about the centre of mass in 4 periods. The solution curves for $k = 3$, $k = 4$, $k = 6$ are shown in Figure 7.15.

For $k = 4$, it is interesting to note that the configuration of the bodies at $t = 2T$ is the same as at $t = 0$, but with switched outer bodies and switched inner bodies. Thus, the outer bodies are on one path and so are the inner bodies, and the orbit for $k = 4$ is another double choreography. The same was observed with the criss-cross orbit ($k = 2$) and also applies to orbits with $k = 6,\ 8,\ 10$, etc.

Overall, there is an infinite number of absolute periodic solutions in the family. The orbits with even values of k (except for $k = 0$) are also double choreographies. The number k indicates the number of periods the orbit has to complete in order to close up. Examples of the orbits for some of the values of k can be found in Appendix C.

7.5 The extreme masses

Another special case for the planar family of orbits occurs as the mass of two bodies decreases to zero. The symmetric four-body system for these solutions can be further reduced,to a restricted model such as of the three-body system.

As Steves and Roy [67] discuss, there are known equilibrium four-body solutions for particular initial configurations. One of them is a collinear configuration in a rotating system, that is analytically shown to converge to the Lagrange points of the Copenhagen problem, or the circular restricted three-body problem, when two pairwise symmetric masses go to zero. The connection between the restricted and general problems has been used by Hadjidemetriou [24, 25] in his numerical investigation of the similar family in three-body systems.

In our setting, when two of the masses become infinitesimal, the system can be considered as the restricted three-body problem. Depending on the form of the orbit, it is either the elliptic or circular (i.e. special case of elliptic) restricted problem. This has two equal masses moving on an elliptic orbit and another massless particle orbiting them. The fourth massless body will repeat the motion by symmetry. The massless particles have minimal influence on the motion of the heavy bodies, except they may restrict the heavy bodies from moving towards each other.

Table 7.1 shows a selection of orbits for a mass $m_1 = 0.072$ and $m_2 = 1.928$. This value of the mass was chosen because, at the time this analysis was carried out, it was the smallest mass for which orbits were found. Nevertheless, the difference in the masses is so dramatic that some conclusions can be drawn about the motion in the limit $m_1 \to 0$.

Also, to have a more careful look at the orbits we depict them in several rotating systems. In general, we use the rotating coordinates in terms of an angle θ which is measured between $-\pi$ and π. Another two rotating coordinate systems show θ measured in regions $[0,\ 2\pi]$ and $[-2\pi,\ 0]$.

Table 7.1: Selected orbits for mass $m_1 = 0.072$. Some of the properties of the orbits are shown, e.g. distance d_{12}, angular momentum A, and angle of rotation θ.

#	d_{12}	A	θ	orbits in different rotating systems
1	0.095	-2.889	-0.611	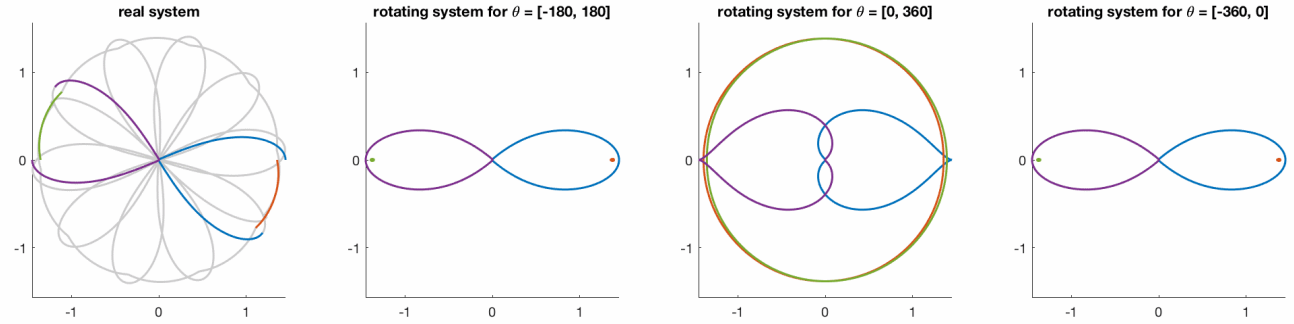
2	0.410	-2.889	-1.069	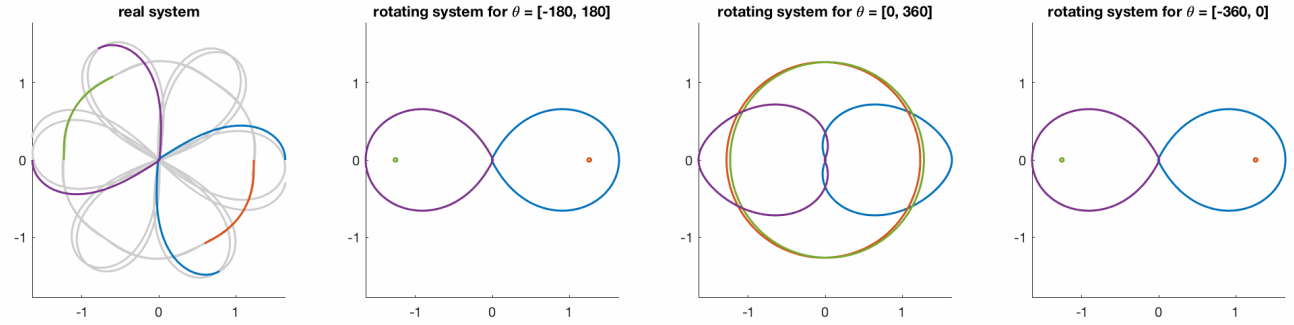
3	0.726	-2.843	-1.532	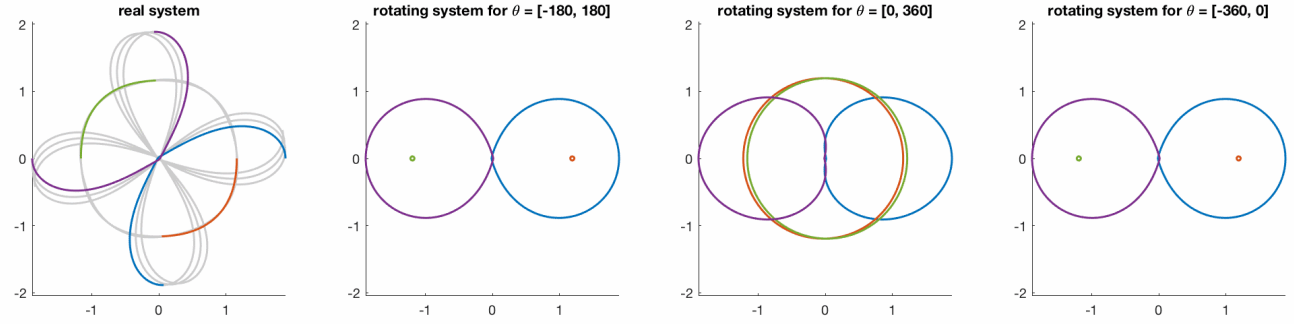

#	d_{12}	A	θ	orbits in different rotating systems
4	1.284	-2.791	-2.498	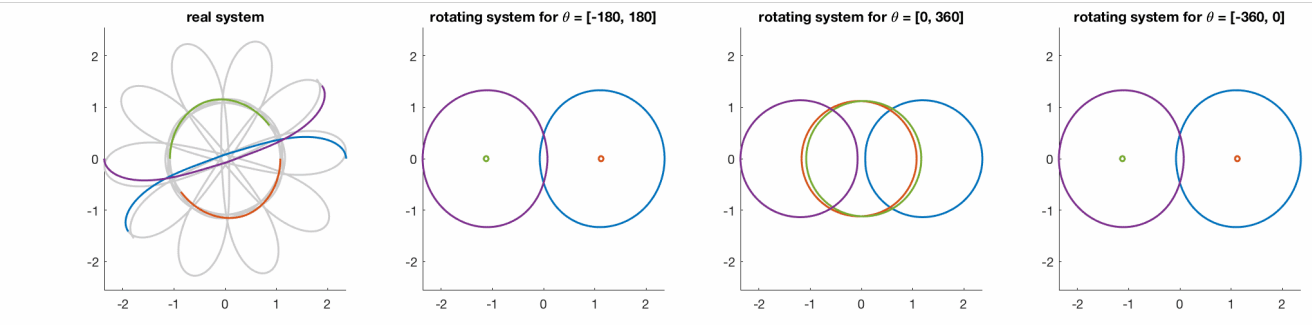
5	1.491	-2.772	-2.908	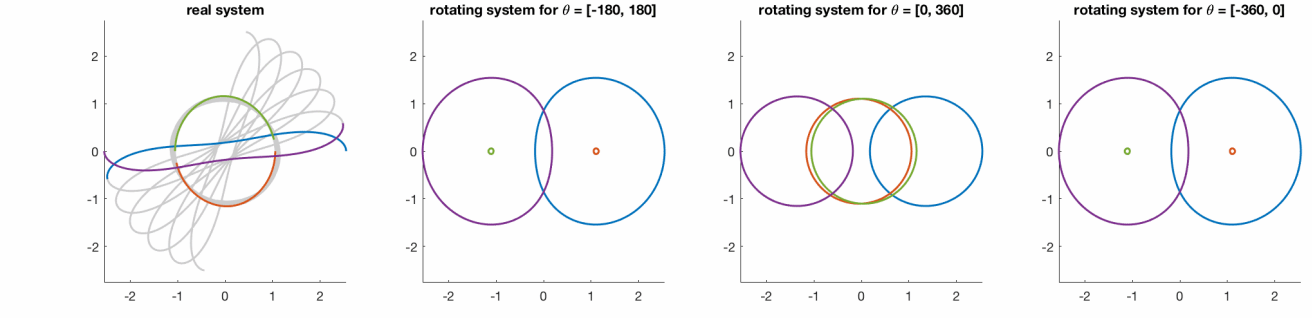
6	1.602	-2.763	-3.126	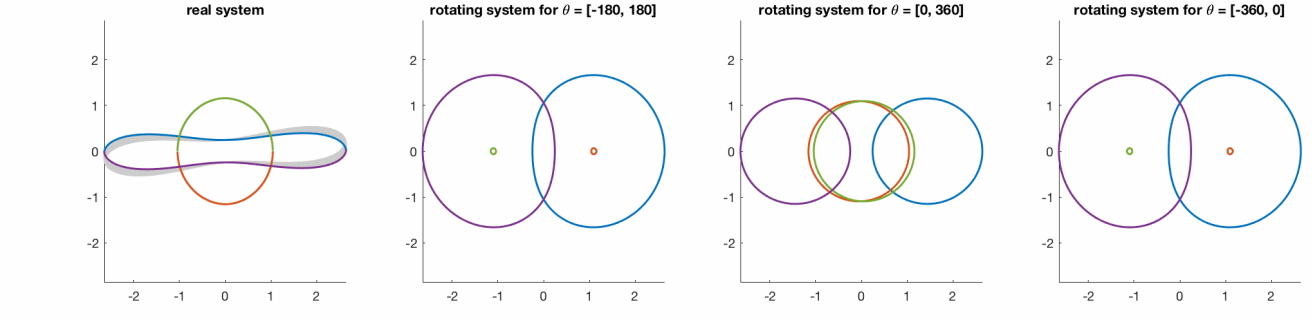

Table 7.1: Selected orbits for mass $m_1 = 0.072$. Some of the properties of the orbits are shown, e.g. distance d_{12}, angular momentum A, and angle of rotation θ, continued

#	d_{12}	A	θ	orbits in different rotating systems
7	1.805	-2.752	2.773	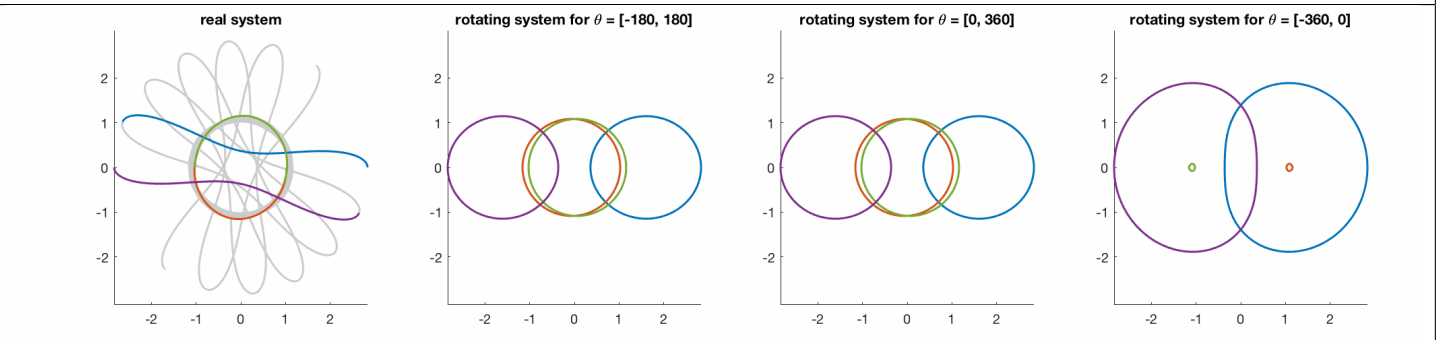
8	2.313	-2.754	1.876	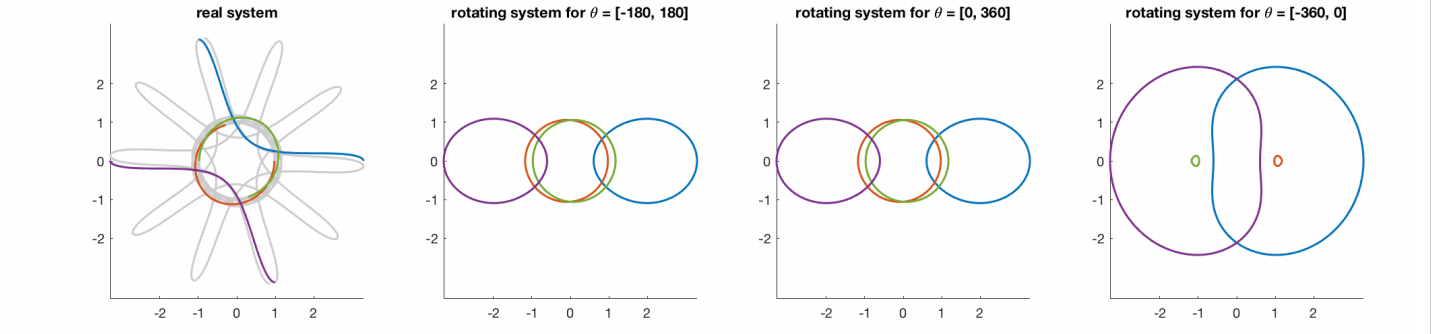
9	2.815	-2.782	1.019	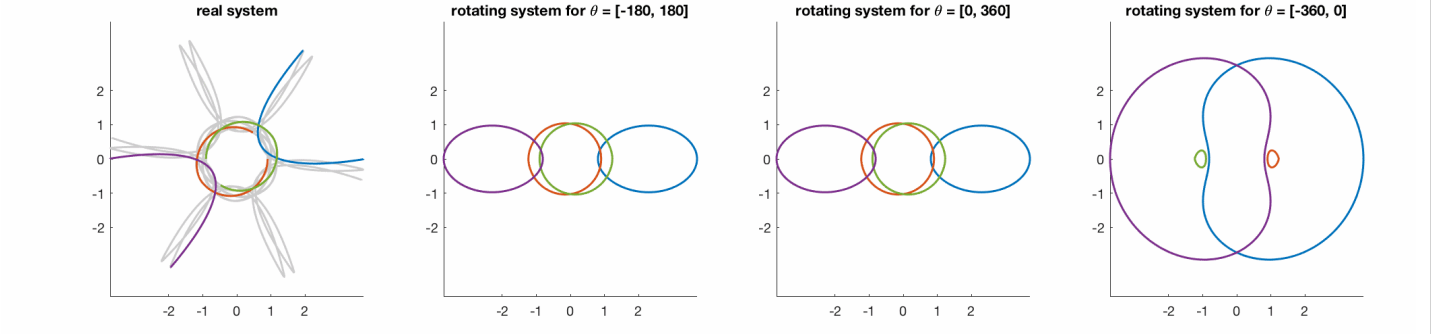

Table 7.1: Selected orbits for mass $m_1 = 0.072$. Some of the properties of the orbits are shown, e.g. distance d_{12}, angular momentum A, and angle of rotation θ, continued

#	d_{12}	A	θ	orbits in different rotating systems
10	3.125	-2.784	0.522	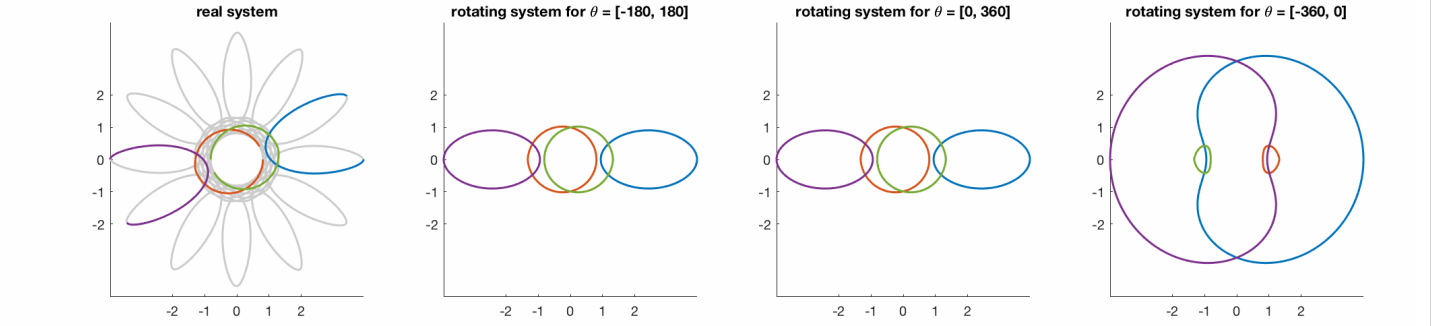
11	3.385	-2.708	0.214	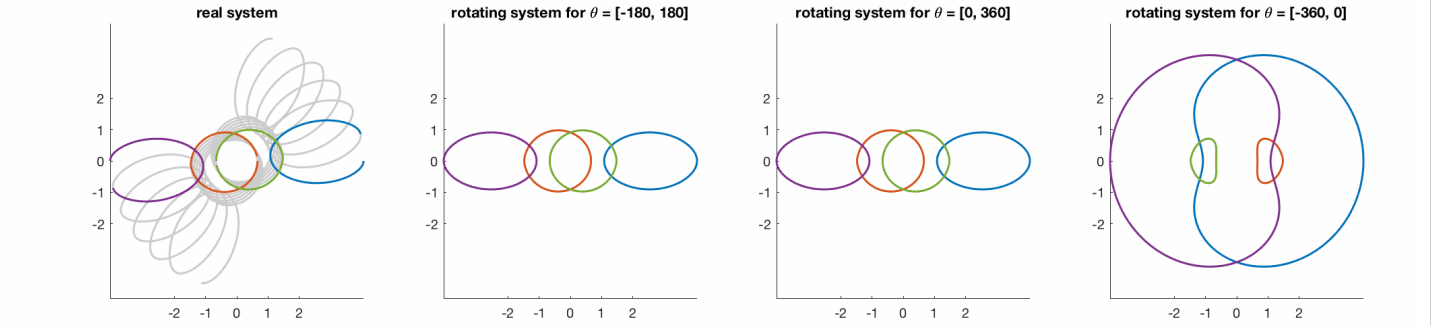
12	3.815	-2.270	0.009	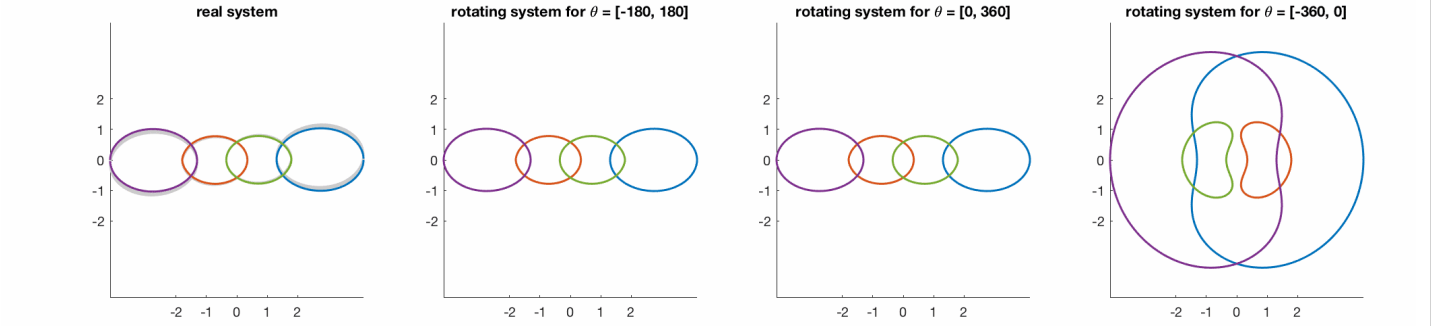

Table 7.1: Selected orbits for mass $m_1 = 0.072$. Some of the properties of the orbits are shown, e.g. distance d_{12}, angular momentum A, and angle of rotation θ, continued

#	d_{12}	A	θ	orbits in different rotating systems
13	4.465	-1.400	-0.042	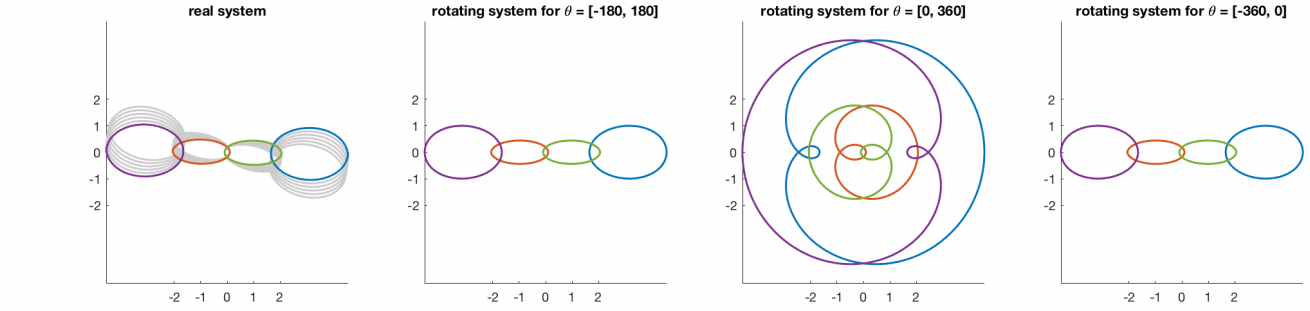
14	5.226	-0.101	-0.005	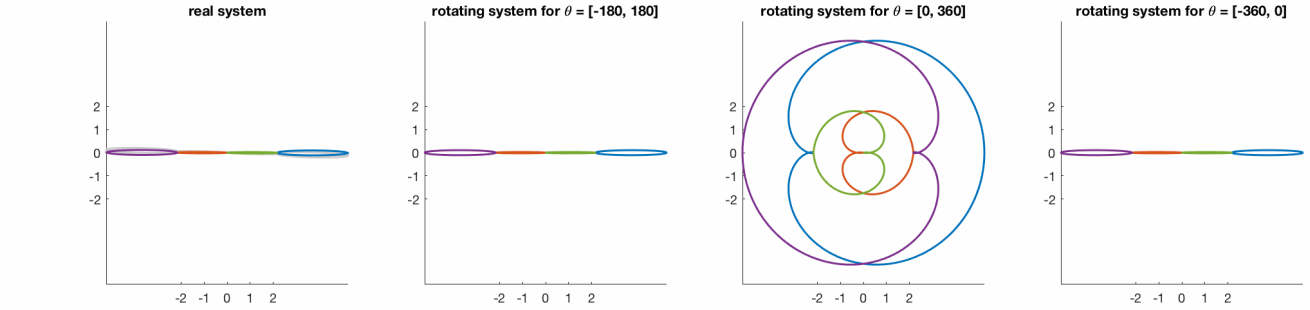

Table 7.1: Selected orbits for mass $m_1 = 0.072$. Some of the properties of the orbits are shown, e.g. distance d_{12}, angular momentum A, and angle of rotation θ, continued

Thus, the system that we use as a default coincides with one or another of these new rotating systems. In fact, when the angle θ changes from positive to negative values (or from negative to positive values), it appears as if the system "jumps" from one rotating frame to another.

The first orbits from Table 7.1 (orbits 1 - 4) belong to the highly unstable region discussed in Section 7.3. They survive roughly a dozen periods and disintegrate into two binaries that move away from each other. With increasing angular velocity, the motion of the small particles (shown in purple and blue colours in Table 7.1) becomes more circular, as seen in the default rotating systems' plots.

The heavier bodies (shown in green and red colours) are almost stationary; they are merely perturbing. However, this can be interpreted as the big masses being situated on two opposite sides of a circle and slowly moving along that circle. The light bodies, although almost massless, play an important role in the system. They move at very high speeds compared to the heavy bodies, and so the kinetic energy of the system is mostly associated with their motion. They also carry a significant part of the momenta of the system and affect the heavy bodies in the way that they are not permitted to move towards the centre.

While this type of motion persists, the orbits move from the unstable region to a vertically stable region (orbit 5) and then reach overall linear stability (orbits 6 and 7). The stable region contains the double choreography with angle $\theta = \pi = -\pi$. Because such angles are located on the boundaries of the rotating system used by default, for this orbit we observe switching from one boundary to the other one, or between the two other rotating systems. This is shown in the rotating coordinate plots for orbits 6 and 7: the former system coincides with the rotating system for $\theta \in [-2\pi,\ 0]$ and the latter coincides with the system for $\theta \in [0,\ 2\pi]$.

Soon after reaching the double choreography a change in the motion of the heavy bodies becomes conspicuous (orbits 8 and further). In the plots for the real system and the default rotating system we observe a collapse of the single circular orbit for the massive bodies into two different orbits. The four-body system motion then transforms into a recognisable chain-like interplay similar to the equal-mass orbits from Chapter 6.

Continuing along the family, the circular orbits of the heavy bodies reduce to more eccentric ellipses. In the extreme limit $d_{12} \to d_{12,\,max}(m_1)$, they eventually become rectilinear Schubart orbits. Closer to the end of the family, the small bodies also restrict their motion towards the line with angular momentum reaching near-zero values (orbit 14). They no more meet at the centre; on the contrary, they are staying as the outer bodies and only interact with the closest heavy bodies. The heavy bodies are situated in the middle and bounce off each other at the centre. We notice another switch between the two different rotating coordinates between orbits 12 and 13, when the angle of rotation becomes negative. Between these two orbits lies another absolute periodic orbit with zero angle of rotation.

In principle, for extreme masses we recognise four different types of motion. The first type (not shown in Table 7.1) is represented by a single orbit for $d_{12} = 0$. The heavy masses are not moving, and the motion of the small masses is purely collinear. The motion instantaneously transforms from collinear to planar and thus switches to the second type with heavy masses moving on a slightly perturbed circle. The third type occurs as soon as the circle falls apart into two ellipses, which become progressively more extended and eccentric. The fourth recognised type is again collinear with two central heavy masses moving on a line and bouncing off each other at the centre of mass.

As was pointed out earlier in this section, eventually when $m_1 = 0$ (or $m_1 = 2$), the system mostly depends on the motion of the heavy bodies. The other two bodies, although being massless, play an important part in the system. Because they shift in the middle of the system at very high speeds, they carry a part of the system's momenta and prevent the big bodies from moving towards the origin. This changes while the heavy bodies move close together, with the small bodies on the sides of the system. When this happens, the system is mostly dominated by the motion of the heavy masses which are almost independent of the massless bodies.

Since the origin is the centre of mass of the two heavy bodies, we can always choose the rotating x-axis so that the heavy bodies are not moving in the rotating frame. So, the problem becomes the elliptic restricted problem with two equal heavy bodies and two zero masses (with initially highly eccentric orbits; later, near-circular).

Chapter 8

Summary and conclusions

In this study we have investigated a new family of orbits that exists in the framework of the Caledonian symmetric four-body problem (CS4BP) [66, 58]. This planar family is generated from the Schubart orbits that are collinear interplay orbits, discovered and studied by Sweatman [70, 71, 73]. We have parametrised the family by two physical variables of the system: the mass of the outer body m_1 and the distance d_{12} between the two bodies 1 and 2.

The orbits - members of the family - are not periodic in the sense that each time the system performs a period, it repeats itself in the real physical space. They are rather periodic relative to a rotating frame in which the bodies return to their initial configuration and scale [22]. In the real frame the configuration after one period is rotated by an angle θ, which is associated with the angular velocity of the system about the centre of mass. This type of orbit is often called a relative periodic solution [12, 13].

The orbits from the discovered family have a very important characteristic: during the period of their integration there are two different close encounters of the masses in the system. One of them is a simultaneous close approach by two pairs of masses on two sides of the system's centre of mass. This is followed by a flyby of the two masses near the centre of mass. As long as the system is planar, there are no collisions. However, the closer it is to collinear motion, the closer the encounters are to a collision.

All four bodies gravitationally interact with each other. The system can be considered as follows. Two masses rotate about their common centre of mass and never meet each other. Each mass has another mass nearby and forms a close binary with it. The other two masses are attracted by each other and encounter each other near the centre of mass. As a result of the motion, the four-body orbit is illustrated by a chain of single orbits.

The CS4BP, that was used, is the simplified problem that studies the four-body systems with special symmetries: about the centre of mass and in time. The central symmetry fixes the centre of mass of the system at the origin. The time symmetry is applied in the form of the Mirror theorem [57, 58, 66], which defines the initial state of the system. Using these two kinds of symmetries allowed us to significantly reduce the initial number of variables.

We have closely followed the approaches by Hénon [31, 32, 33, 34], who studied the original Schubart orbit for three bodies, and Sweatman [70, 71], who did a similar study for the collinear Schubart orbit in the four-body system. Some alterations have been introduced in the algorithm. For example, the definition of the system's period has been modified in order to increase the algorithm's efficiency. A different regularisation has been used for a search: we have used the Levi-Civita coordinates with the relation for rescaled time, similar to that proposed by Heggie [27].

In studying the planar systems of four bodies, we have considered and applied two different versions of the problem: the CS4BP with symmetries and the general problem of four bodies. The latter has been used for studying the orbital stability and the orbit's survival under various types of introduced perturbations.

In Chapter 2 we have reviewed the literature dedicated to three and four-body problems, especially that closely-connected with the study of the Schubart orbits, for both three and four-body systems. The numerical and analytical investigations in different aspects of the problem have been discussed. We have also given an overview of the regularisation methods and the history of their development.

In Chapters 3, 4 and 5 we have provided a mathematical model of the problem and the

methods that have been used for solving it. In Chapter 3 we introduced the CS4BP in the way it was originally formulated by Steves and Roy [66, 67], also Roy [58].

We have developed the framework for integrating the equations of motion, with the chosen initial configuration of the system provided. In doing so, we have followed the approach by Sivasankaran, Steves and Sweatman [63, 64]. We have introduced and defined a rotating frame for a system and the criterion that is used for indicating the time at which the bodies have completed one period within both the rotating and real coordinate frames.

In Chapter 4 we have formulated the general problem of four bodies and the general equations of motion. The different, unrestricted by symmetries or simplifications, version of the system has been considered and applied. For dealing with close encounters and collisions, we have used a different regularisation method which uses Mikkola's [40] implementation of the Heggie [27] global regularisation with time transformation in the form of an inverse of the system's Lagrangian. Following the generalisation of the problem, we have introduced the rotating coordinate frame that deals with the orbits perturbed in the three-dimensional space.

One of the major outputs of this work has been presented in Chapter 5 which explains the program developed for the search and analysis of the orbits. The program is based on an algorithm that is applicable to any solution of the CS4BP when provided with the existence of this solution and an initial guess of the configuration of the bodies.

We have provided a flowchart of the overall program and the differential corrections algorithm used for a single orbit search. We have generated the family of the orbits by varying two parameters, the mass m_1 and the angular momentum of the system A. The parameter A is implicitly connected to the distance d_{12}: by following the trend of A we aim to constantly increase d_{12}.

The search procedure is performed by introducing linear differential corrections to the dataset of orbits, which is updated with a newly discovered orbit on every successful iteration of the algorithm. The initial dataset is represented by the orbits previously discovered by Sweatman [70, 71, 73].

Before each round of differential corrections, polynomial interpolation has been used to achieve a prediction of the initial configuration that corresponds to the chosen values of m_1 and d_{12}. We have also introduced criteria for a resetting of the search, when the solution is not achievable with satisfactory accuracy within the chosen time frame.

The successful passage through the differential corrections step is followed by the analysis of the orbital stability. For an orbit, we have developed three different versions of the formal stability analysis which all introduce perturbations of a chosen kind to the orbit. The symmetrical planar linear stability analysis is performed immediately after the orbit has been found. The subsequent planar linear stability analysis and vertical linear stability analysis have been applied to selected orbits (members of the family).

We have also developed a non-linear stability check in the form suggested by Mikkola and Hietarinta [44]. This check has been used for a selection of orbits in order to have a quick interpretation whether each orbit is stable or unstable overall, without performing the full linear stability analysis.

We have presented the results of the current work, the planar four-body family of the interplay orbits, in Chapters 6 and 7. In Chapter 6 we have considered the special case of the family with four equal masses. The results presented in this chapter have been presented in the published paper [22].

The relation between the planar orbit from Sweatman [73] and the Schubart orbit [70, 71] has been confirmed. It has been found that the equal-mass family starts and ends with the Schubart orbit, at different points in the orbit. In the middle of the family we have discovered and located the double choreography solution, also known as the criss-cross orbit [17, 20, 48, 49, 50].

We have analysed and followed the changes occuring in the physical variables of the system along the equal-mass family, such as the angular momentum A, angle of rotation θ, period T and the initial position and momentum coordinates of the system. The linear stability analysis showed the existence of symmetrically stable, planar and vertically stable regions in the family.

The results have been confirmed by the non-linear stability check. The family was found to be overall unstable as was the ancestral Schubart four-body orbit.

In Chapter 7 we have presented the family of orbits that arose by varying the ratio between masses in the family from Chapter 6. By varying the mass m_1 we have generated and observed the family from the cases of heavy outer bodies with massless inner bodies to the cases of relatively small outer masses with heavy inner masses.

We have used the results from Sweatman [70, 71] to construct the boundaries within which the planar family exists. The symmetries of the family have been discussed by introducing four regions I - IV, separated by the equal-mass line and the double choreography line. Based on this discussion, the analysis of the family has been conducted.

Similarly to the equal-mass case, as considered in Chapter 6, we have followed the physical quantities of the system and have drawn a connection between them and changes in the orbits. The stabilities of the orbits have been analysed. Because of the abundance of data (164,215 orbits overall), we have performed a full stability analysis only on the orbits for every 5th value of the mass m_1.

We have found that there are five overall stable regions: three of them originate from the collinear motion. Another stable region is situated nearby and exists for about a half of the values of the mass m_1 (if two corresponding symmetric regions are considered). The fifth stable region forms when the masses m_1 and m_2 differ significantly. The relation between the angular momentum of the system and some of the stability regions has been discussed.

Some of the special orbits that belong to the planar family have been considered. The double choreography solutions have been generated for many mass ratios. It has been found that, although the equal-mass double choreography is unstable, the double choreographies become stable when reaching the cases of extreme masses.

We have also classified the absolute periodic orbits, i.e. the orbits that are periodic in both real and rotating coordinate frames, that exist in the family. An orbit is absolute periodic if the angle θ is an integer multiple of 2π (a rational multiple if several revolutions about the

centre of mass are considered). If, for absolute periodic orbits, the angle θ is an even multiple of 2π, an orbit is a double choreography.

The behaviour of the orbits has been considered when the outer mass becomes extremely small or big. The orbits close to limits in mass have been shown with the use of three different rotating coordinate frames. Using different perspectives of the orbits we have deduced the motion in the limits. A conclusion has been drawn about the four types of final motion and the relation with the elliptic restricted three-body problem.

Some of the questions that arose in this work still remain unanswered. It is still unclear how the formation of the "cusp" in the angular momentum affects the motion in the region of extremely heavy masses m_1. We have observed and commented on the dependence between the angular momentum and the stability parameter k_1. This has been shown valid in the three-body system [32], and the four-body system for most of the masses m_1 except for the highly-unstable zone in Regions II and III.

The algorithm developed and presented in Chapter 5, could be improved both in terms of precision and performance. Some suggestions are presented. In the future we plan to achieve better accuracy for the results presented in this work. The planar and vertical linear stability analysis will be applied for the whole range of orbits. This will produce more accurate boundaries of the stability regions.

Another aspect of the problem which would be interesting to explore is an investigation of the family with an introduced central mass (The Caledonian Symmetric Five-Body Problem). This system can be studied in terms of the four equal masses or the pairwise symmetric masses. It is maybe more practical to think of a system rotating about the centre of mass that has its own mass, especially for the cases of the heavy central body and the four comparatively near-massless orbiting bodies. Two examples of such systems are presented in Figures 8.1 and 8.2. These five-body orbits are extended from the criss-cross orbit (discussed in Section 6.1 and presented in Figure 6.7) by introducing the stationary mass m_0 at the origin with the condition on the total mass $M = 2m_1 + 2m_2 + m_0 = 4$ and four equal masses ($m_1 = m_2$).

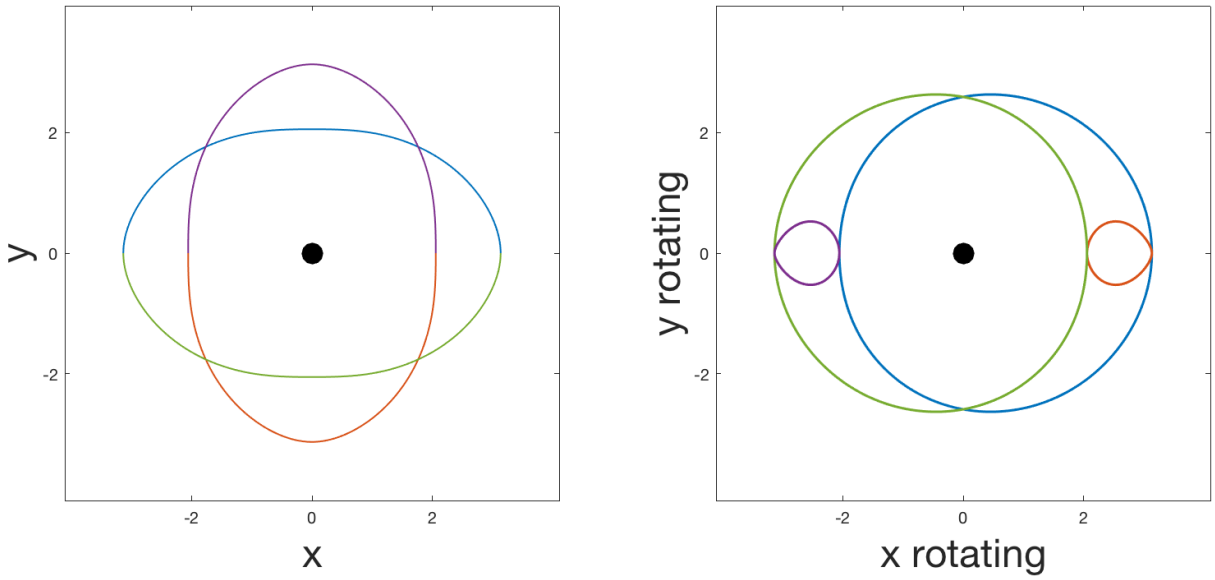

Figure 8.1: The criss-cross orbit for the system of five bodies. The central mass m_0 is four times larger than the other four equal masses.

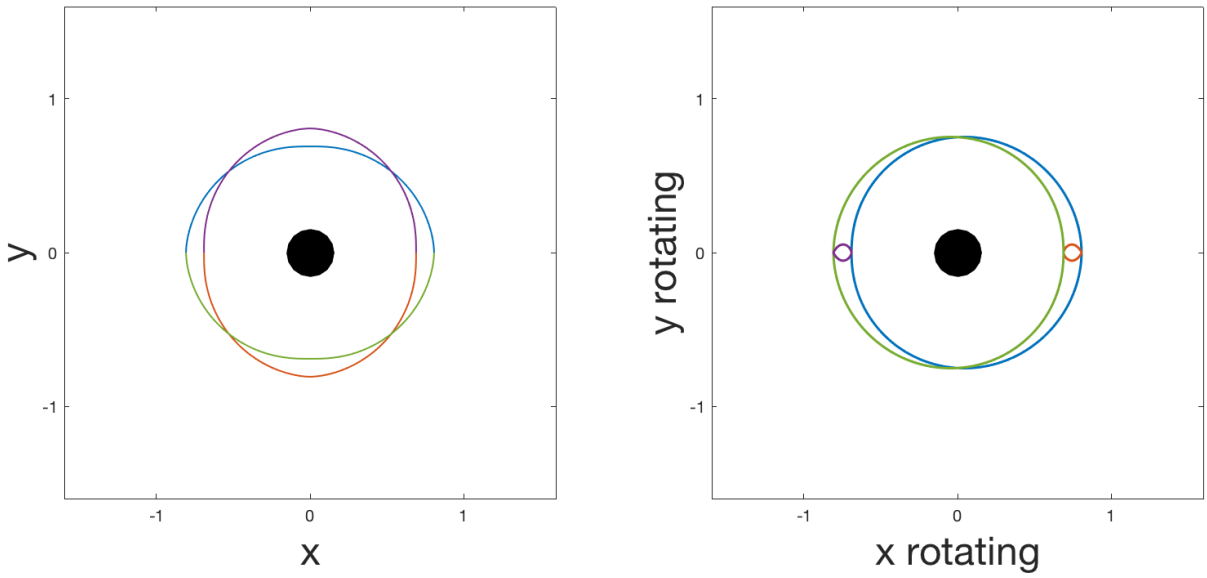

Figure 8.2: The criss-cross orbit for the system of five bodies. The central mass $m_0 = 3.6$ dominates the system with the four masses $m_1 = m_2 = 0.1$.

Bibliography

[1] Aarseth, S. J. (2003) *Gravitational N-body simulations.* Cambridge Monographs on Mathematical Physics. Cambridge: Cambridge University Press.

[2] Aarseth, S. J., & Zare, K. (1974) *A regularization of the three-body problem.* Celestial Mechanics, 10(2), 185-205. doi:10.1007/bf01227619

[3] Alexander, M. E. (1986) *Simulation of binary-single star and binary-binary scattering.* Journal of Computational Physics, 64(1), 195-219. doi:10.1016/0021-9991(86)90025-2

[4] Bakker, L. F., Ouyang, T., Yan, D., Simmons, S., & Roberts, G. E. (2010) *Linear stability for some symmetric periodic simultaneous binary collision orbits in the four-body problem.* Celestial Mechanics and Dynamical Astronomy, 108(2), 147-164. doi:10.1007/s10569-010-9298-y

[5] Bakker, L. F., Ouyang, T., Yan, D., & Simmons, S. (2011) *Existence and stability of symmetric periodic simultaneous binary collision orbits in the planar pairwise symmetric four-body problem.* Celestial Mechanics and Dynamical Astronomy, 110(3), 271-290. doi:10.1007/s10569-011-9358-y

[6] Barrabes, E. & Mikkola, S. (2005) *Families of periodic horseshoe orbits in the restricted three-body problem.* Astronomy & Astrophysics, 432, 1115-1129. doi: 10.1051/0004-6361:20041483

[7] Barutello, V., & Terracini, S. (2006) *Double choreographical solutions for N-body type problems.* Celestial Mechanics and Dynamical Astronomy, 95, 67-80.

[8] Bettis, D. G., & Szebehely, V. (1971) *Treatment of close approaches in the numerical integration of the gravitational problem of N bodies.* Astrophysics and Space Science, 14, 133-150.

[9] Boyd, P.T., & McMillan, S. T. W. (1992) *Initial-value space structure in irregular gravitational scattering.* Physical Review A, 46(10), 6277-6287.

[10] Broucke, R. (1969) *Stability of periodic orbits in the elliptic, restricted three-body problem.* AIAA Journal, 7(6), 1003-1009. doi:10.2514/3.5267

[11] Broucke, R. (1971) *Periodic collision orbits in the elliptic restricted three-body problem.* Celestial Mechanics, 3, 461-477. doi:10.1007/BF01227792

[12] Broucke, R. (1975) *On relative periodic solutions of the planar general three-body problem.* Celestial Mechanics, 12(4), 439-462. doi:10.1007/bf01595390

[13] Broucke, R., Boggs, D. (1975) *Periodic orbits in the planar general three-body problem.* Celestial Mechanics, 11(1), 13-38. doi: 10.1007/bf01228732

[14] Broucke, R. A. (2001) *Stable orbits of planets of a binary star system in the three-dimensional restricted problem.* Celestial Mechanics and Dynamical Astronomy, 81(4), 321-341. doi:10.1023/a:1013238413100

[15] Broucke, R. (2004) *Classification of periodic orbits in the four- and five-body problems.* Annals of the New York Academy of Sciences, 1017(1), 408-421. doi:10.1196/annals.1311.023

[16] Celletti, A. (2010) *Regularization theory.* In: Stability and Chaos in Celestial Mechanics (pp. 207-226). Berlin, Heidelberg: Springer Berlin Heidelberg.

[17] Chang, X., Ouyang, T., & Duokui Yan (2016) *Linear stability of the criss-cross orbit in the equal-mass three-body problem.* Discrete and Continuous Dynamical Systems, 36(11), 5971-5991. doi:10.3934/dcds.2016062

[18] Chenciner, A., & Montgomery, R. (2000) *A remarkable periodic solution of the three-body problem in the case of equal masses.* Annals of Mathematics, 152, 881901.

[19] Chenciner, A., & Venturelli, A. (2000) *Minima de L'intégrale D'action du Problème Newtonien de 4 Corps de Masses Égales Dans* $\mathbb{R}3$*: Orbites 'Hip-Hop'.* Celestial Mechanics & Dynamical Astronomy, 77(2), 139-151. doi:10.1023/A:1008381001328

[20] Chen, K. (2001) *Action-minimizing orbits in the parallelogram four-body problem with equal masses.* Archive for Rational Mechanics and Analysis, 158(4), 293-318.

[21] Chen, K. (2003) *Variational methods on periodic and quasi-periodic solutions for the N-body problem.* Ergodic Theory and Dynamical Systems, 23(6), 1691-1715

[22] Chopovda, V., & Sweatman, W. L. (2018) *The family of planar periodic orbits generated by the equal-mass four-body Schubart interplay orbit.* Celestial Mechanics and Dynamical Astronomy, 130(5), 1-15. doi:10.1007/s10569-018-9831-y

[23] Dormand, D.J., & Prince, P.J. (1980) *A family of embedded Runge-Kutta formulae.* Journal of Computational and Applied Mathematics, 6(1), 19-26.

[24] Hadjedemetriou, J. D., & Christides, T. (1974) *Families of periodic orbits in the planar three-body problem.* Celestial mechanics, 12(2), 175-187. doi:10.1007/10.1007/BF01230210

[25] Hadjedemetriou, J. D. (1975) *The stability of periodic orbits in the three-body problem.* Celestial mechanics, 12(3), 255276. doi:10.1007/BF01228563

[26] Hadjedemetriou, J. D. (2003) *Periodic orbits in gravitational systems.* In: Steves, B. A., Maciejewski, A. J., Hendry, M. (Eds.), Chaotic Worlds: From Order to Disorder in Gravitational N-Body Dynamical Systems (pp. 43 - 79). NATO Science Series II: Springer Netherlands.

[27] Heggie, D. C. (1974) *A global regularisation of the gravitational N-body problem.* Celestial mechanics, 10(2), 217-241. doi:10.1007/bf01227621

[28] Heggie, D., Hut, P. (2003) *The Gravitational Million-Body Problem. A Multidisciplinary Approach to Star Cluster Dynamics.* Cambridge: Cambridge University Press.

[29] Hénon, M. (1971) *The Monte Carlo method.* Astrophysics and Space Science, 14(1), 151-167. doi:10.1007/bf00649201

[30] Hénon, M. (1973) *Vertical stability of periodic orbits in the restricted problem. I. Equal masses.* Astronomy and Astrophysics, 28, 415-426.

[31] Hénon, M. (1974) *Families of periodic orbits in the three-body problem.* Celestial Mechanics, 10(3), 375-388. doi:10.1007/bf01586865

[32] Hénon, M. (1976) *A family of periodic solutions of the planar three-body problem, and their stability.* Celestial mechanics, 13(3), 267-285. doi:10.1007/bf01228647

[33] Hénon, M. (1977) *A relation in families of periodic solutions.* Celestial mechanics, 15(1), 99-105. doi:10.1007/bf01229050

[34] Hénon, M. (1977) *Stability of interplay motions.* Celestial mechanics, 15(2), 243-261. doi:10.1007/bf01228465

[35] Hietarinta, J., & Mikkola, S. (1993) *Chaos in the one-dimensional gravitational three-body problem.* Chaos, 3(2), 183-203. doi:10.1063/1.165984

[36] Martínez, R. (2012) *On the existence of doubly symmetric "Schubart-like" periodic orbits.* Discrete and Continuous Dynamical Systems, 17(3), 943-975. doi:10.3934/dcdsb.2012.17.943

[37] Martínez, R. (2013) *Families of double symmetric "Schubart-like" periodic orbits.* Celestial Mechanics and Dynamical Astronomy, 117(3), 217-243.

[38] McGehee, R. (1974) *Triple collision in the collinear three-body problem.* Inventiones mathematicae, 27(3), 191-227. doi:10.1007/BF01390175

[39] Mikkola, S. (1983) *Encounters of binaries. I - Equal energies.* Monthly Notices of the Royal Astronomical Society, 203(4), 1107-1121. doi:10.1093/mnras/203.4.1107

[40] Mikkola, S. (1985) *A practical and regular formulation of the N-body equations.* Monthly Notices of the Royal Astronomical Society, 215(2), 171-177. doi:10.1093/mnras/215.2.171

[41] Mikkola, S., & Aarseth, S. J. (1989) *A chain regularization method for the few-body problem.* Celestial Mechanics and Dynamical Astronomy, 47(4), 375-390. doi:10.1007/bf00051012

[42] Mikkola, S., & Hietarinta, J. (1989) *A numerical investigation of the one-dimensional Newtonian three-body problem.* Celestial Mechanics and Dynamical Astronomy, 46(1), 1-18. doi:10.1007/bf02426707

[43] Mikkola, S., & Hietarinta, J. (1989) *A numerical investigation of the one-dimensional Newtonian three-body problem II. Positive energies.* Celestial Mechanics and Dynamical Astronomy, 47(4), 321-331. doi:10.1007/bf00051009

[44] Mikkola, S., & Hietarinta, J. (1991) *A numerical investigation of the one-dimensional Newtonian three-body problem. III. Mass dependence in the stability of motion.* Celestial Mechanics and Dynamical Astronomy, 51(4), 379-394. doi:10.1007/bf00052929

[45] Mikkola, S., & Aarseth, S. J. (1993) *An implementation of N-body chain regularisation.* Celestial Mechanics and Dynamical Astronomy, 57(3), 439-459. doi:10.1007/BF00695714

[46] Mikkola, S. *Brief history of Regularisation.* Dynamical Evolution of Dense Stellar Systems, Proceedings of the International Astronomical Union, IAU Symposium, 246, 218-227. doi:10.1017/S1743921308015639

[47] Moeckel, R. (2008) *A topological existence proof for the Schubart orbits in the collinear three-body problem.* Discrete and Continuous Dynamical Systems, 10(2-3), 609-620. doi:10.3934/dcdsb.2008.10.609

[48] Moore, C. (1993) *Braids in classical dynamics* Physical Review Letters, 70(24), 3675-3679.

[49] Nauenberg, M. (2001) *Periodic orbits for three particles with finite angular momentum.* Physics Letters A, 292(1-2), 93-99.

[50] Nauenberg, M. (2006) *New periodic orbits for the N-body problem.* Journal of Computational and Nonlinear Dynamics, 1(4), 307-311. doi:10.1115/1.2338323

[51] Ouyang, T., & Yan, D. (2011) *Periodic solutions with alternating singularities in the collinear four-body problem.* Celestial Mechanics and Dynamical Astronomy, 109(3), 229-239. doi:10.1007/s10569-010-9325-z

[52] Ouyang, T., & Xie, Z. (2018) *A continuum of periodic solutions to the planar four-body problem with two pairs of equal masses.* Journal of Differential Equations, 264(7), 4425-4455. doi:10.1016/j.jde.2017.12.016

[53] Peng, H., Yan, D., Xu, S., & Ouyang, T. (2016) *Linear stability of double-double orbits in the parallelogram four-body problem.* Journal of Mathematical Analysis and Applications, 433(2), 785802. doi:10.1016/j.jmaa.2015.08.014

[54] Poincaré, H. (1982) *Les méthodes nouvelles de la méchanique céleste*, Volume 1, Gauthier-Villars, Paris

[55] Roberts, G. E. (2007) *Linear stability analysis of the figure-eight orbit in the three-body problem.* Ergodic Theory and Dynamical Systems, 27(06), 1947-1963. doi:10.1017/S0143385707000284

[56] Roberts, G. E. (2002) *Linear stability of the elliptic Lagrangian triangle solutions in the three-Body Problem.* Journal of Differential Equations, 182(1), 191-218. doi:10.1006/jdeq.2001.4089

[57] Roy, A.E. & Ovenden, M.W. (1955) *On the occurrence of commensurable mean motions in the solar system II: The mirror theorem.* Monthly Notices of the Royal Astronomical Society, 115(3), 296-309.

[58] Roy, A.E. (2005) *Orbital motion* (4th ed.). Bristol, UK: IOP Publishing.

[59] Schubart, J. (1956) *Numerische Aufsuchung periodischer Lösungen im Dreikörperproblem.* Astronomische Nachrichten, 283(1), 17-22. doi:10.1002/asna.19562830105

[60] Sekiguchi, M. & Tanikawa, K. (2003) *On the symmetric collinear four-body problem.* Publications of the Astronomical Society of Japan, 56(1), 235-251.

[61] Sessions, L. (2017) *Castor is 6 stars in one.* Retrieved from `http://earthsky.org/brightest-stars/best-castor-brightest-second-magnitude-star` on 01 May 2016.

[62] Siegel, C.L., Moser, J.K. (1995) *Lectures on celestial mechanics. Reprint of the* 1971 *Edition.* Berlin, Germany: Springer-Verlag Berlin Heidelberg (Original work published 1971).

[63] Sivasankaran, A., Steves, B. A., & Sweatman, W. L. (2009) *Close encounters in the Caledonian symmetric four-body problem.* In: Varvoglis, H., Knežević, Z. (Eds.), Dynamics of celestial bodies - Proceedings of the 2008 International Conference in honor of John D. Hadjidemetriou, 23 - 26 June 2008, Litohoro, Greece (pp. 177-180). Publications of the Astronomical Observatory of Belgrade.

[64] Sivasankaran, A., Steves, B. A., & Sweatman, W. L. (2010) *A global regularisation for integrating the Caledonian symmetric four-body problem.* Celestial Mechanics and Dynamical Astronomy, 107(1), 157-168. doi:10.1007/s10569-010-9270-x

[65] Skokos Ch. (2003) *Stability of periodic orbits of multidimensional Hamiltonian systems. Application to systems with four degrees of freedom.* In Bountis T. C., Ichtiaroglou S. & Pnevmatikos S., K. Sfakianaki (Eds.), Order and Chaos in Non-linear Dynamical Systems, Vol.8 (pp. 111-126), Thessaloniki, Greece.

[66] Steves, B. A., & Roy, A. E. (1998) *Some special restricted four-body problems - I. Modelling the Caledonian problem.* Planetary and Space Science, 46(1112), 1465-1474. doi:10.1016/S0032-0633(98)00077-4

[67] Steves, B. A., & Roy, A. E. (1998) *Some special restricted four-body problems - II. From Caledonia to Copenhagen.* Planetary and Space Science, 46(1112), 1475-1486. doi:10.1016/S0032-0633(98)00087-6

[68] Steves, B. A., & Roy, A. E. (2001) *Surfaces of separation in the Caledonian symmetrical double binary four body problem.* In Steves, B. A. & Maciejewski, A. J. (Eds.), The restless universe: Applications of gravitational N-body dynamics to planetary, stellar and galactic systems (pp. 301325). Bristol, Great Britain: J W Arrowsmith Ltd, Bristol.

[69] Stiefel, E.L., Scheifele, G. (1971) *Linear and regular celestial mechanics.* Berlin, Germany: Springer-Verlag Berlin Heidelberg.

[70] Sweatman, W.L. (2002) *The symmetrical one-dimensional Newtonian four-body problem: A numerical investigation.* Celestial Mechanics and Dynamical Astronomy, 82(2), 179-201. doi:10.1023/a:1014599918133

[71] Sweatman, W.L. (2006) *A family of symmetrical Schubart-like interplay orbits and their stability in the one-dimensional four-body problem.* Celestial Mechanics and Dynamical Astronomy, 94(1), 37-65. doi:10.1007/s10569-005-2289-8

[72] Sweatman, W.L. (2014) *Orbits near central configurations.* Celestial Mechanics and Dynamical Astronomy, 119(3-4): 379-395. doi:10.1007/s10569-014-9556-5

[73] Sweatman, W.L. (2014) *Symmetric four-mass Schubart-like systems.* In Z. Knežević, & A. Lemaitre (Eds.) Proceedings IAU Symposium No. 310, 2014: Complex Planetary Systems, Cambridge University Press, [Conference Paper in Published Proceedings], 106-107.

[74] Sweatman, W.L. (2015) *Symmetric four-body problems.* In G. M. Cojocaru, S. I. Kotsireas, N. R. Makarov, N. R. V. Melnik, & H. Shodiev (Eds.), Interdisciplinary Topics in Applied Mathematics, Modeling and Computational Science (pp. 439-444). Cham: Springer International Publishing.

[75] Szebehely, V.G. (1967) *Theory of orbits, the restricted problem of three bodies.* New York, NY: Academic Press.

[76] Szebehely, V., Peters, C.F. (1967) *A new periodic solution of the problem of three bodies.* Astronomical Journal, Vol. 72, p. 1187. doi: 10.1086/110398

[77] Tanikawa, K., & Mikkola, S. (2000) *Triple collisions in the one-dimensional three-body problem.* Celestial Mechanics and Dynamical Astronomy, 76(1), 23-34. doi:10.1023/a:1008397420958

[78] Tanikawa, K., & Mikkola, S. (2000) *One-dimensional three-body problem via symbolic dynamics.* Chaos, 10(3), 649-657.

[79] Waldvogel, J. (1972) *A new regularization of the planar problem of three bodies.* Celestial Mechanics, 6(2), 221-231. doi:10.1007/BF01227784

[80] Wagner, K., Apai, D. Kasper, M., Kratter, K., McClure, M., Robberto, M. & Beuzit, J. (2016) *Direct imaging discovery of a Jovian exoplanet within a triple-star system.* Science. Retrieved from `http://science.sciencemag.org` on 1 October, 2017. doi: 10.1126/science.aaf9671

[81] Whittaker, E.T. (1917) *A treatise on the analytical dynamics of particles and rigid bodies.* (2nd ed.) Cambridge: Cambridge University Press.

[82] Yan, D. (2018) *Action minimizers under topological constraints in the planar equal-mass four-body problem* Journal of Differential Equations, 264(7), 4764-4805. doi:10.1016/j.jde.2017.12.029

Appendices

Appendix A

Units of the four-body system

Following Hénon's [29] concept of choosing N-body units, we define units of mass U_m, length U_l and time U_t by the condition that the gravitational constant $\tilde{G}$ and the total energy $\tilde{E}$ of the system, expressed in these units, should be respectively:

$$G = 1, \qquad E = -1.$$

We set $\tilde{m} = U_m m$, where $\tilde{m}$ is the actual mass of the body, m is the dimensionless mass, and

$$U_m = \tilde{m}_{av} = \frac{\text{total mass of the system}}{\text{number of bodies in the system}},$$

where $\tilde{m}_{av}$ is the average mass of a body in the system.

The corresponding unit of length is

$$U_l = -\frac{\tilde{G}\tilde{m}_{av}^2}{\tilde{E}},$$

and $\tilde{x} = U_l x$, $\tilde{y} = U_l y$, $\tilde{r} = U_l r$, where $\tilde{x}, \tilde{y}$ are actual coordinates of the body, x, y are their dimensionless counterparts, and $\tilde{r}$ and r denote the interbody distance in dimensional and non-dimensional forms, respectively.

The unit of time is

$$U_t = \frac{\tilde{G}\tilde{m}_{av}^{\frac{5}{2}}}{(-\tilde{E})^{\frac{3}{2}}},$$

and time is rescaled by $\tilde{t} = U_t t$.

Similarly, the velocities $\tilde{v}$ and $\tilde{u}$, the angular momentum $\tilde{A}$, total energy $\tilde{E}$, kinetic energy $\tilde{K}$, potential energy U and the gravitational constant $\tilde{G}$ are rescaled by

$$\begin{aligned}
\tilde{v} &= \frac{U_l}{U_t} v, \\
\tilde{u} &= \frac{U_l}{U_t} u, \\
\tilde{A} &= \frac{U_l^2}{U_t} A, \\
\tilde{E} &= \frac{U_l^2}{U_t^2}\, U_m E, \\
\tilde{K} &= \frac{U_l^2}{U_t^2}\, U_m K, \\
\tilde{U} &= \frac{U_l^2}{U_t^2}\, U_m U, \\
\tilde{G} &= \frac{U_l^3}{U_t^2\, U_m} G.
\end{aligned}$$

Appendix B

The collinear four-body Schubart orbits

In this section we produce some of the collinear Schubart orbits that build the boundaries for the family. The orbits shown in Table B.1 were discovered by Sweatman [70, 71] by varying the ratio between the outer and inner masses with a fixed value of total mass. The mass m_1 in the Table B.1 indicates the mass of the outer bodies (red and purple, respectively). The green and the blue bodies have mass $m_2 = 2 - m_1$.

m_1	Orbit
0.001	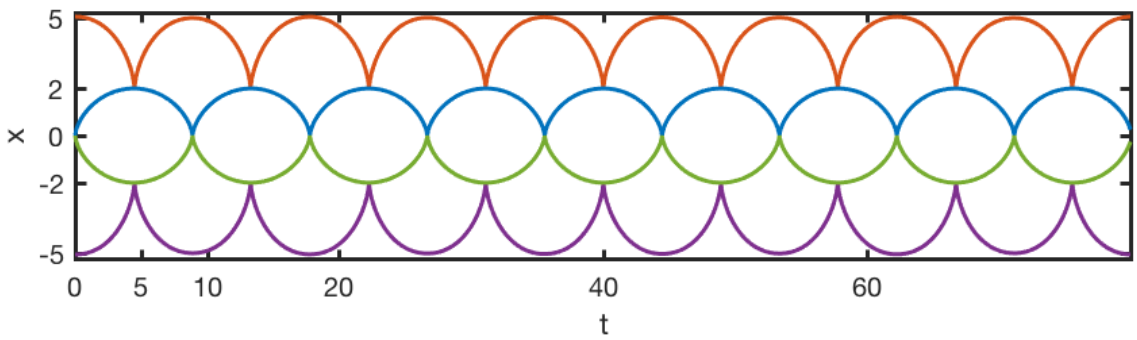

0.300	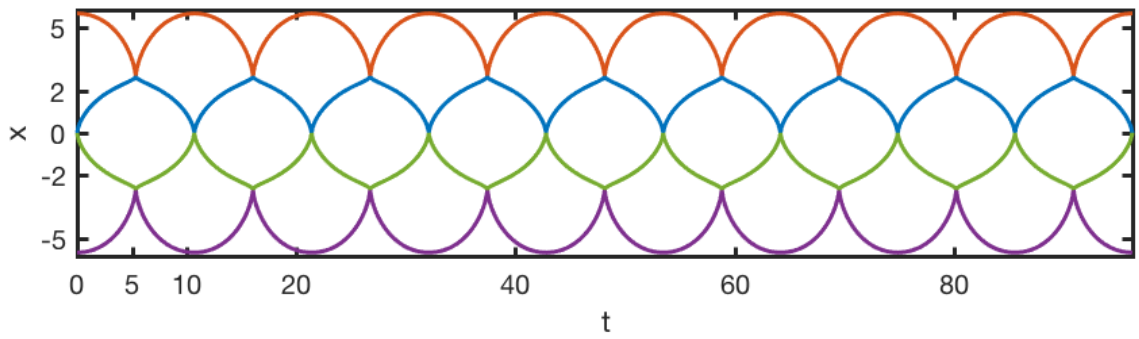
0.500	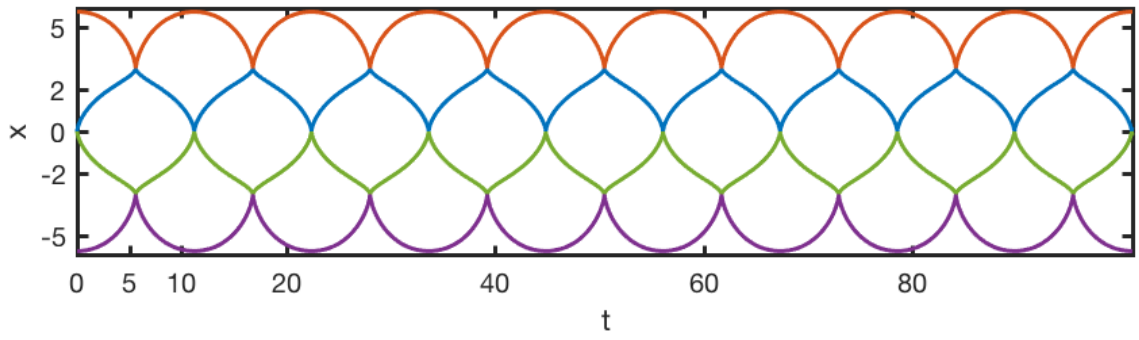
0.800	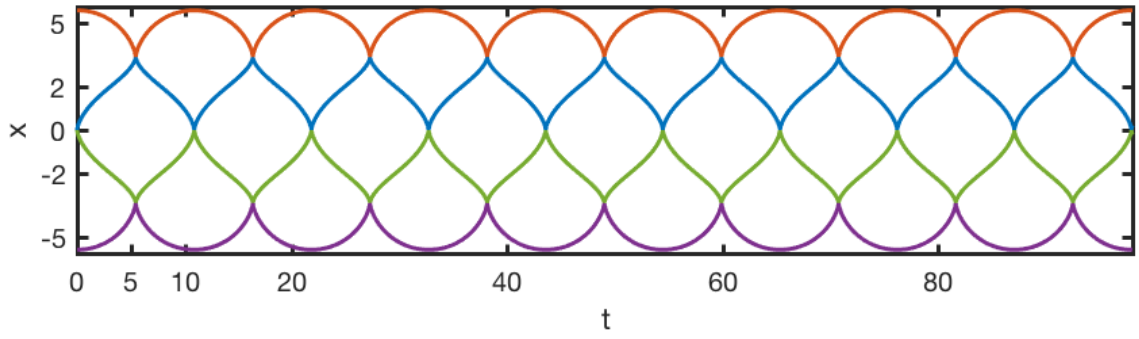
1.000	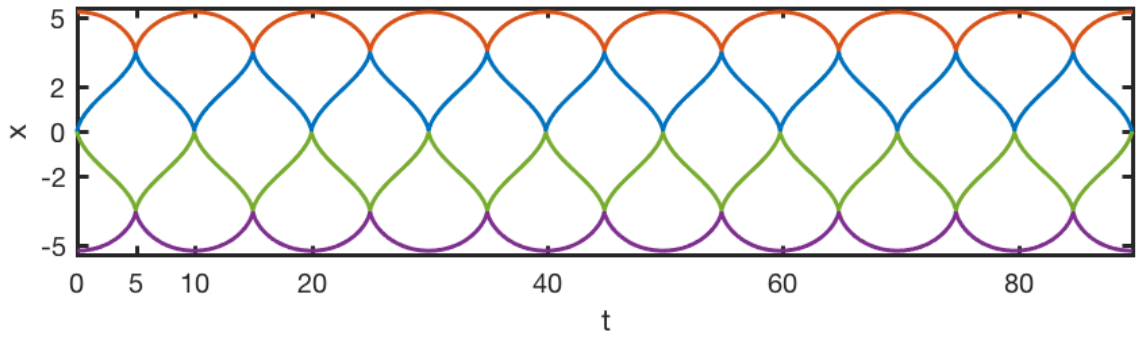

1.200	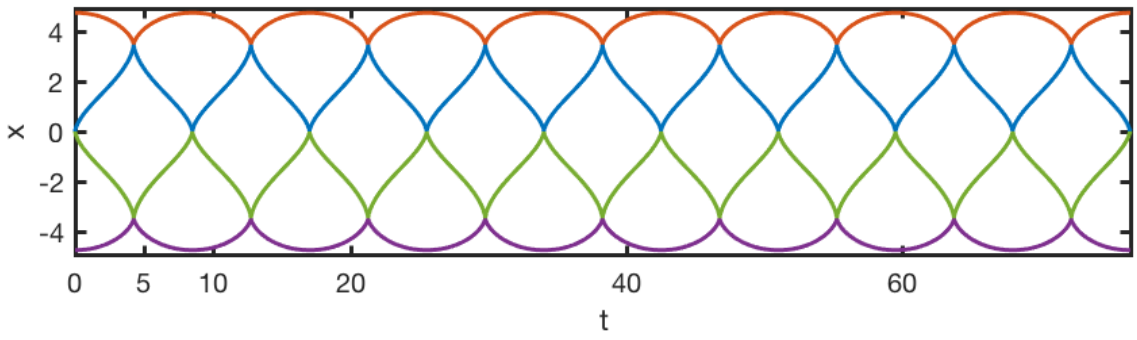
1.500	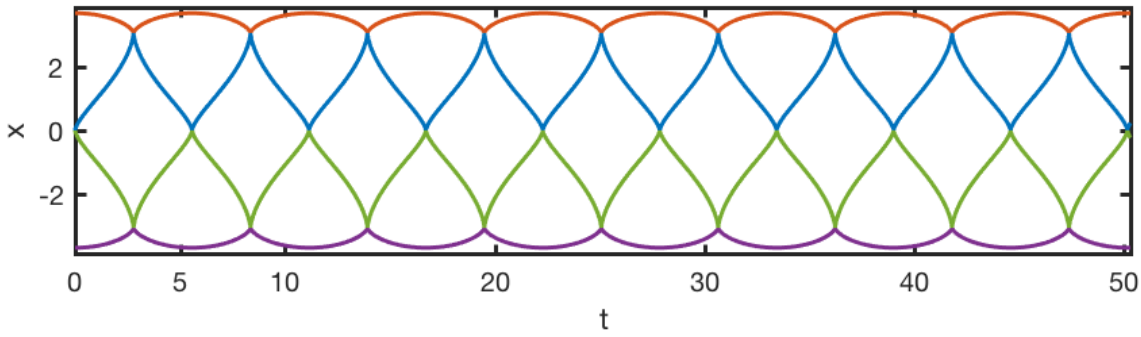
1.800	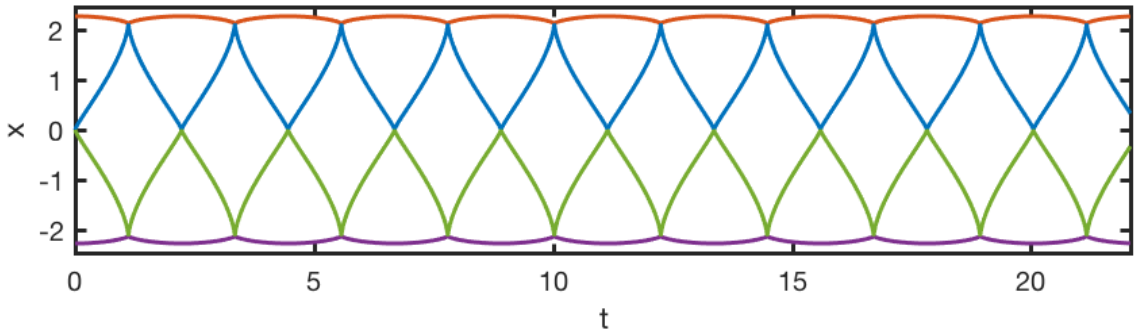
1.999	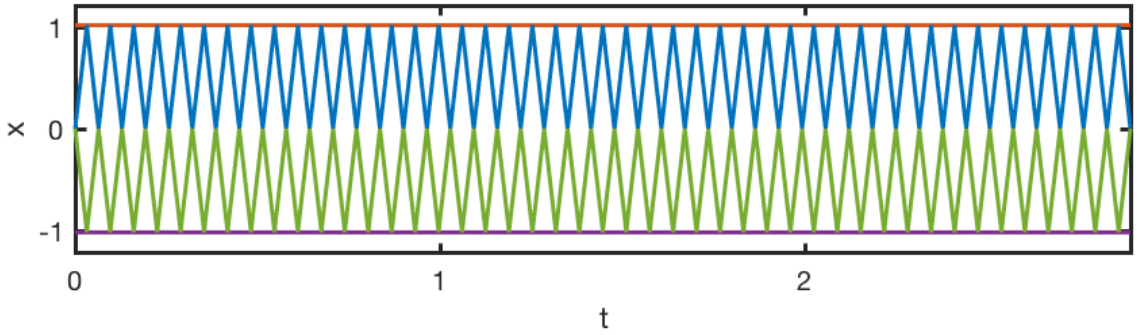

Table B.1: Some of the collinear Schubart orbits

Appendix C

Absolute periodic orbits in the planar family of interplay orbits

We present the absolute periodic orbits that appear in the planar family of interplay orbits for various masses. We showed that these orbits appear when the angle of rotation is $\theta = \frac{2\pi}{k}$ where $k \in \mathbb{Z}$. In the following sections we show some of the examples of these orbits for different values of k. We provide the value of the parameter m_1 for these orbits.

The orbits are integrated until they perform one full revolution about the centre of mass, i.e. 'close up' one orbit. For double choreographies we integrate the orbits for only half of the revolution in order to show that the symmetric bodies are on the same path.

In all of the following plots the bodies 1 and 4 have a mass m_1 and are shown with blue and purple paths, respectively. The bodies 2 and 3 have a mass $m_2 = 2 - m_1$ and are shown with red and green paths, respectively.

C.1 $k = 1$

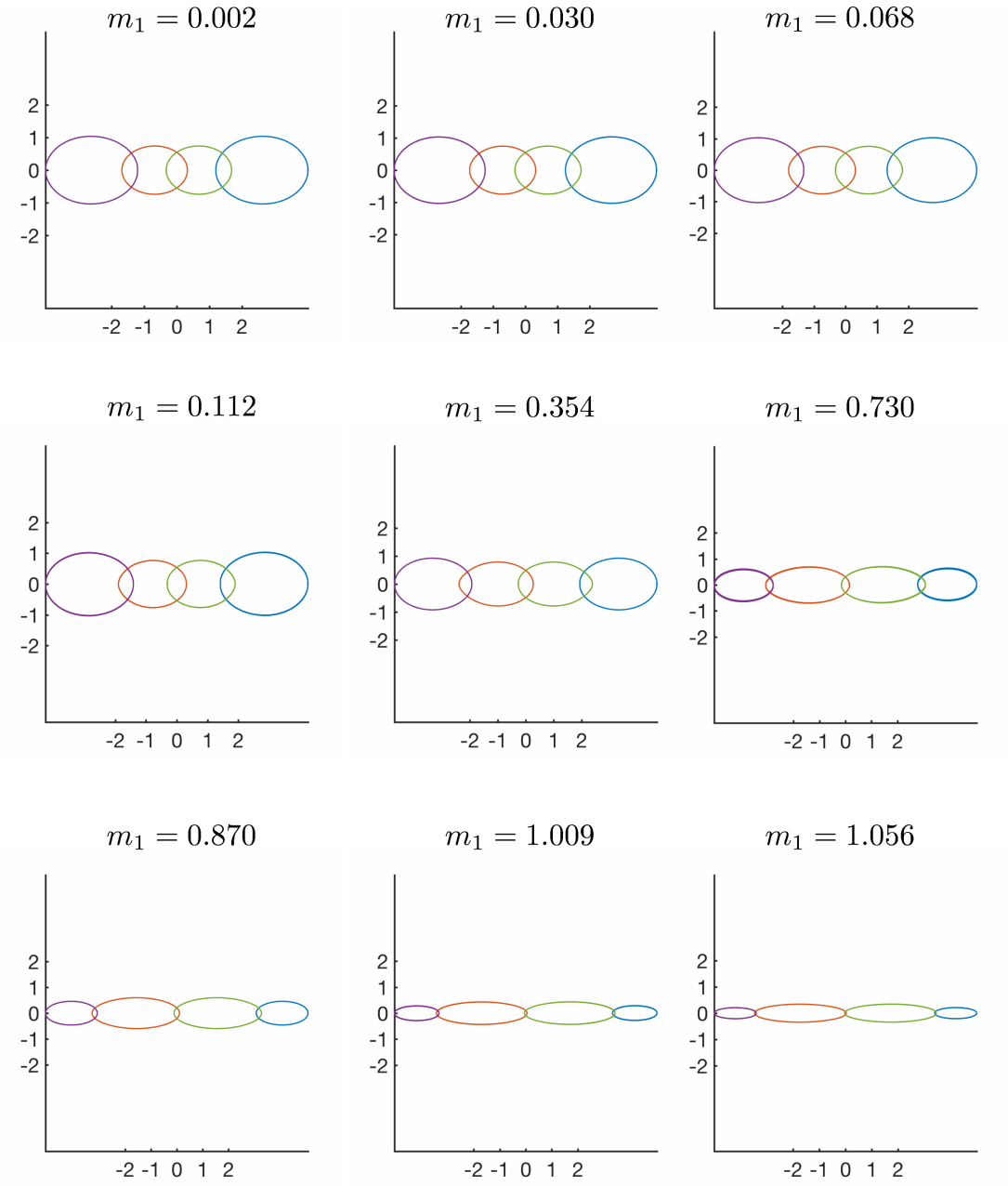

Figure C.1: Absolute periodic orbits for $\theta = 0$.

C.2 $k = 2$

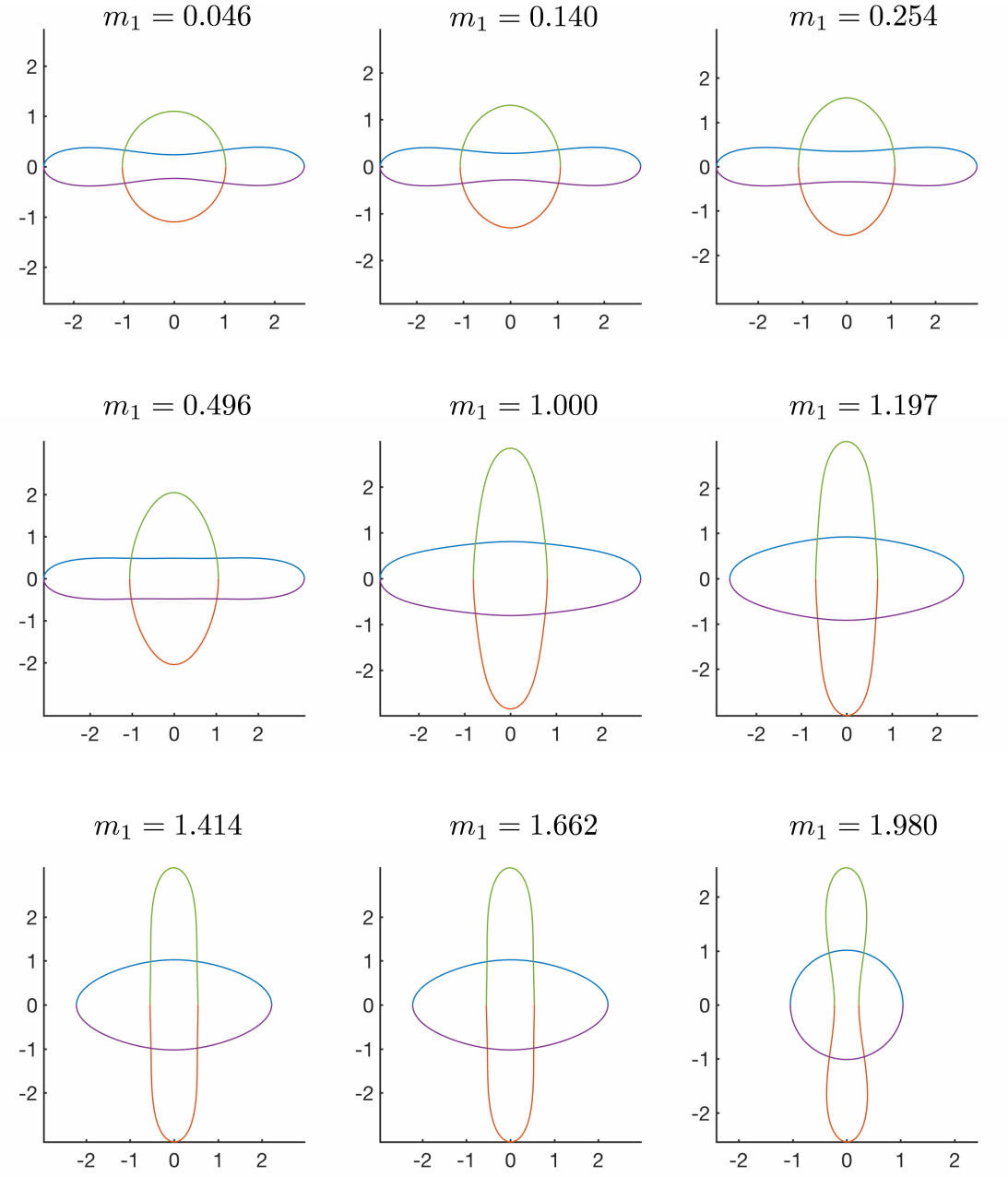

Figure C.2: Double choreographies for $\theta = \pi$. (A reproduction of Figure 7.16).

C.3 $k = 3$

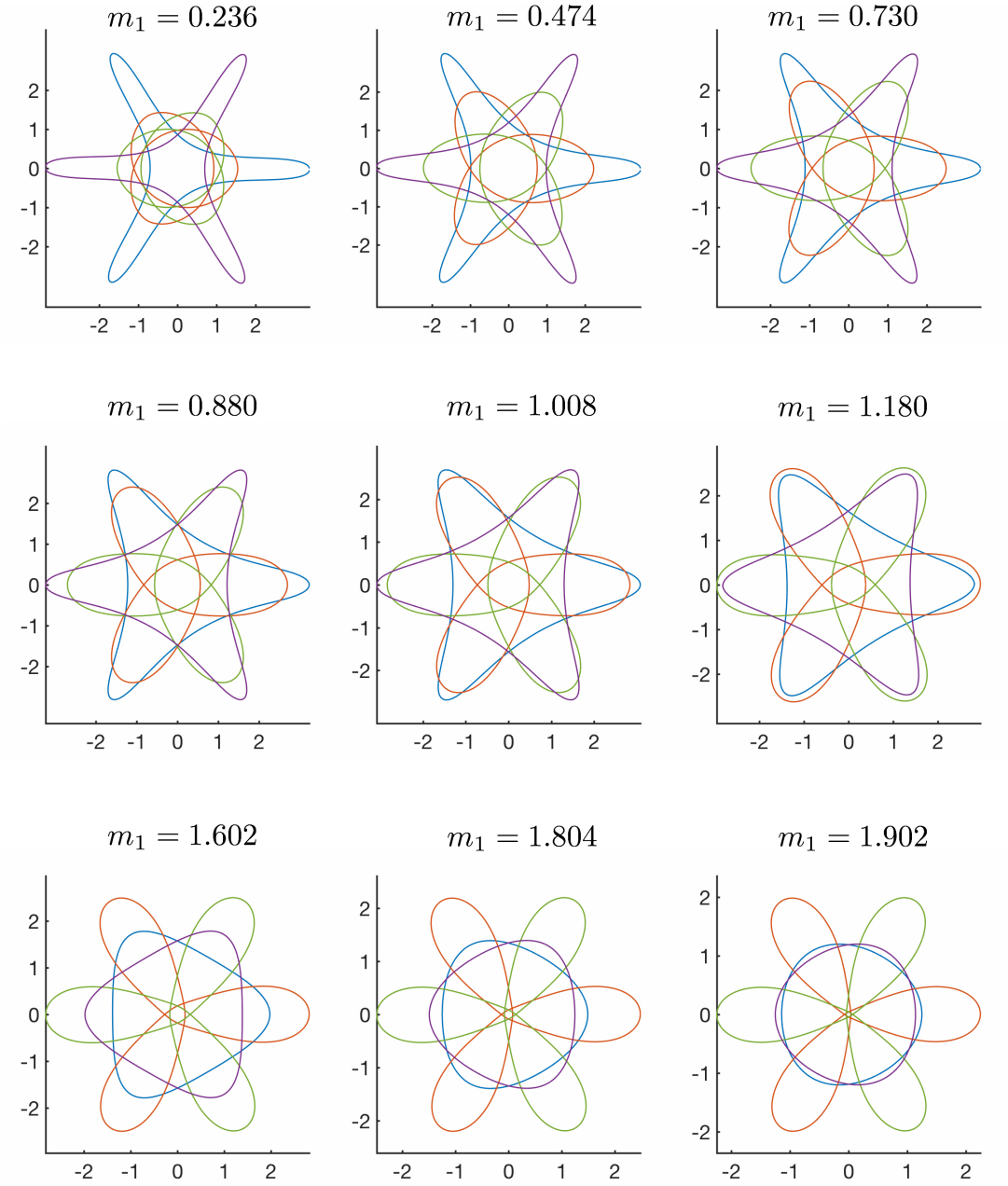

Figure C.3: Absolute periodic orbits for $\theta = 2\pi/3$.

C.4 $k = 4$

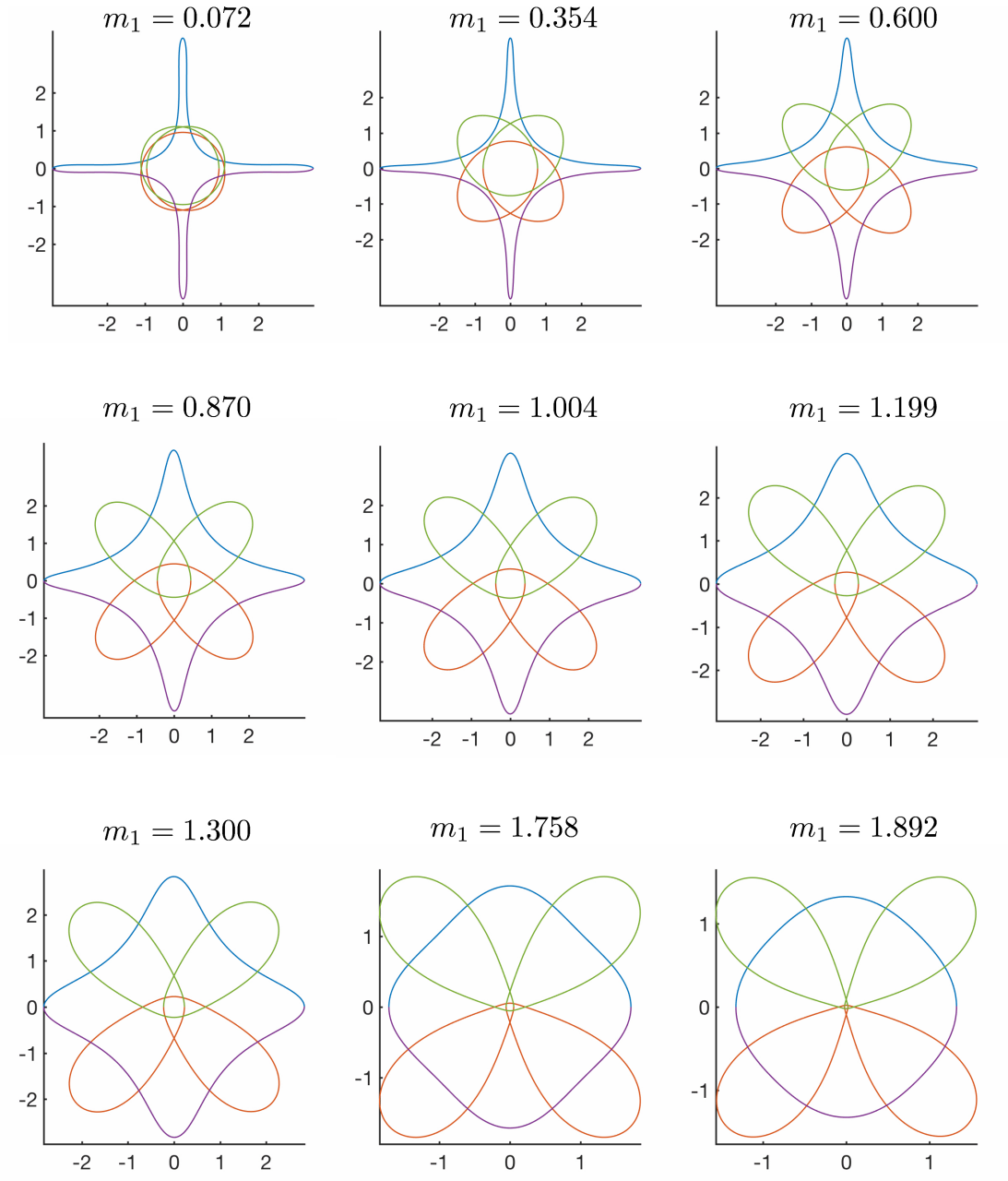

Figure C.4: Double choreographies for $\theta = 2\pi/4 = \pi/2$.

C.5 $k = 5$

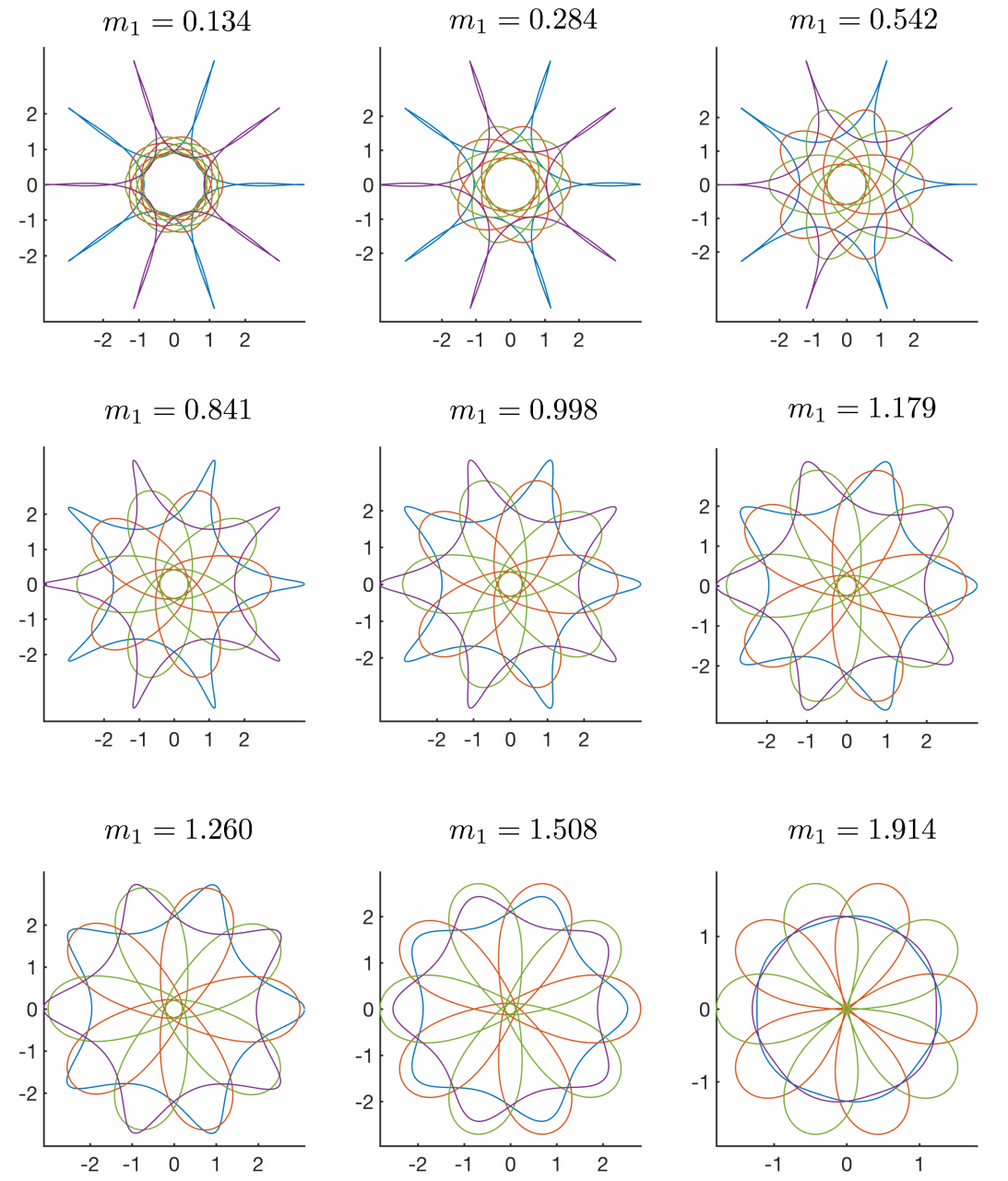

Figure C.5: Absolute periodic orbits for $\theta = 2\pi/5$.

C.6 $k = 6$

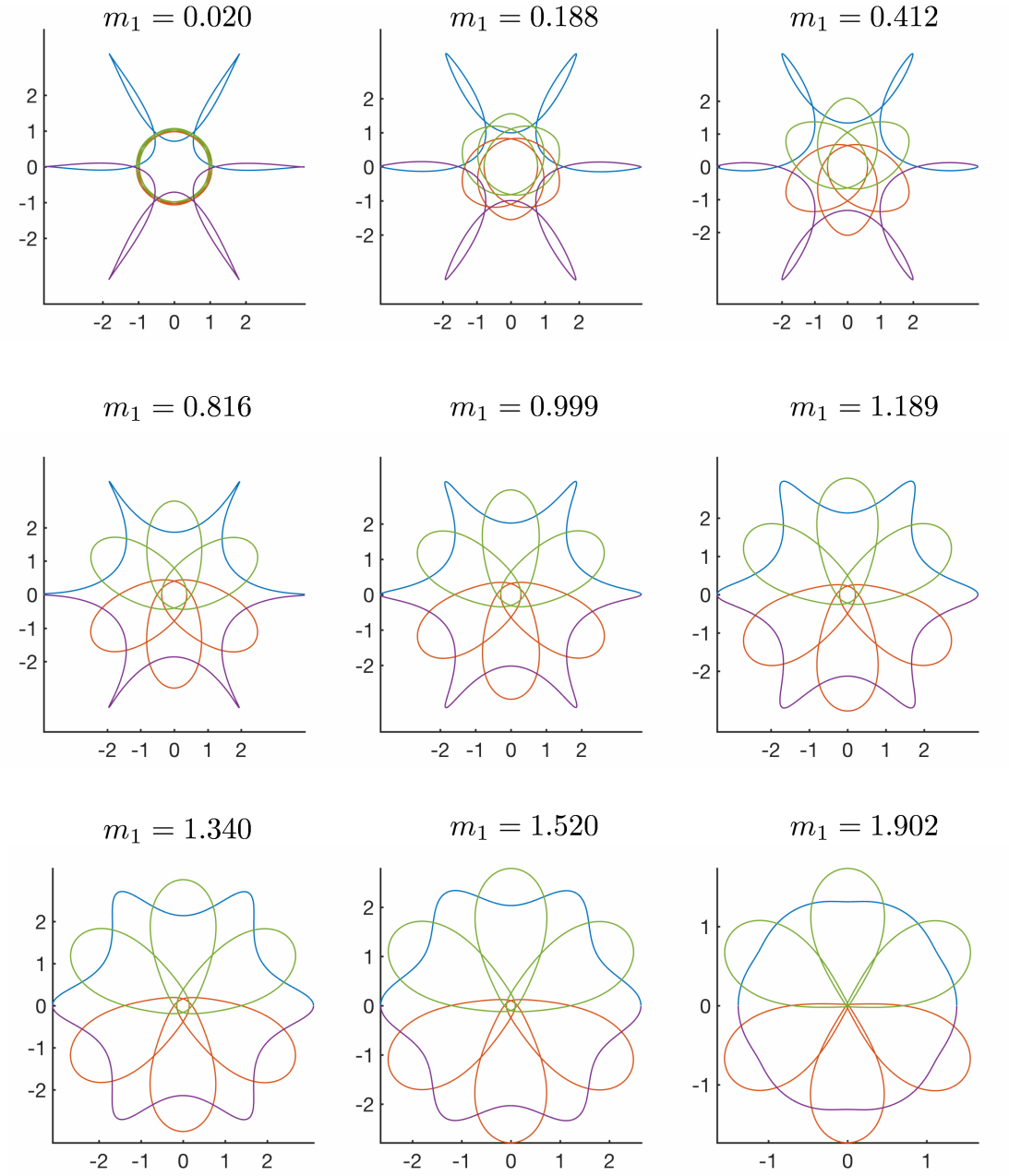

Figure C.6: Double choreographies for $\theta = 2\pi/6 = \pi/3$.

C.7 $k = 7$

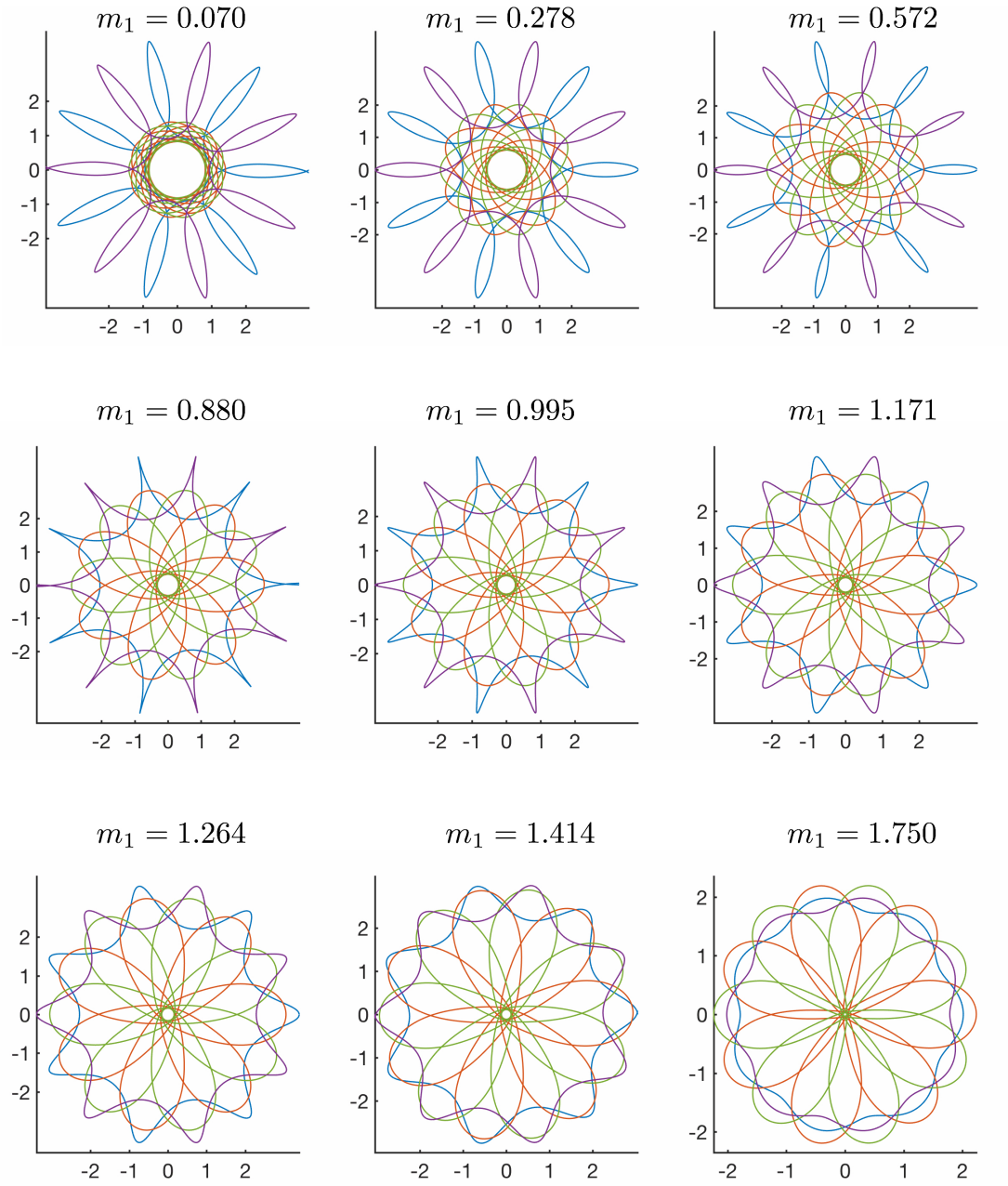

Figure C.7: Absolute periodic orbits for $\theta = 2\pi/7$.

C.8 $k = 8$

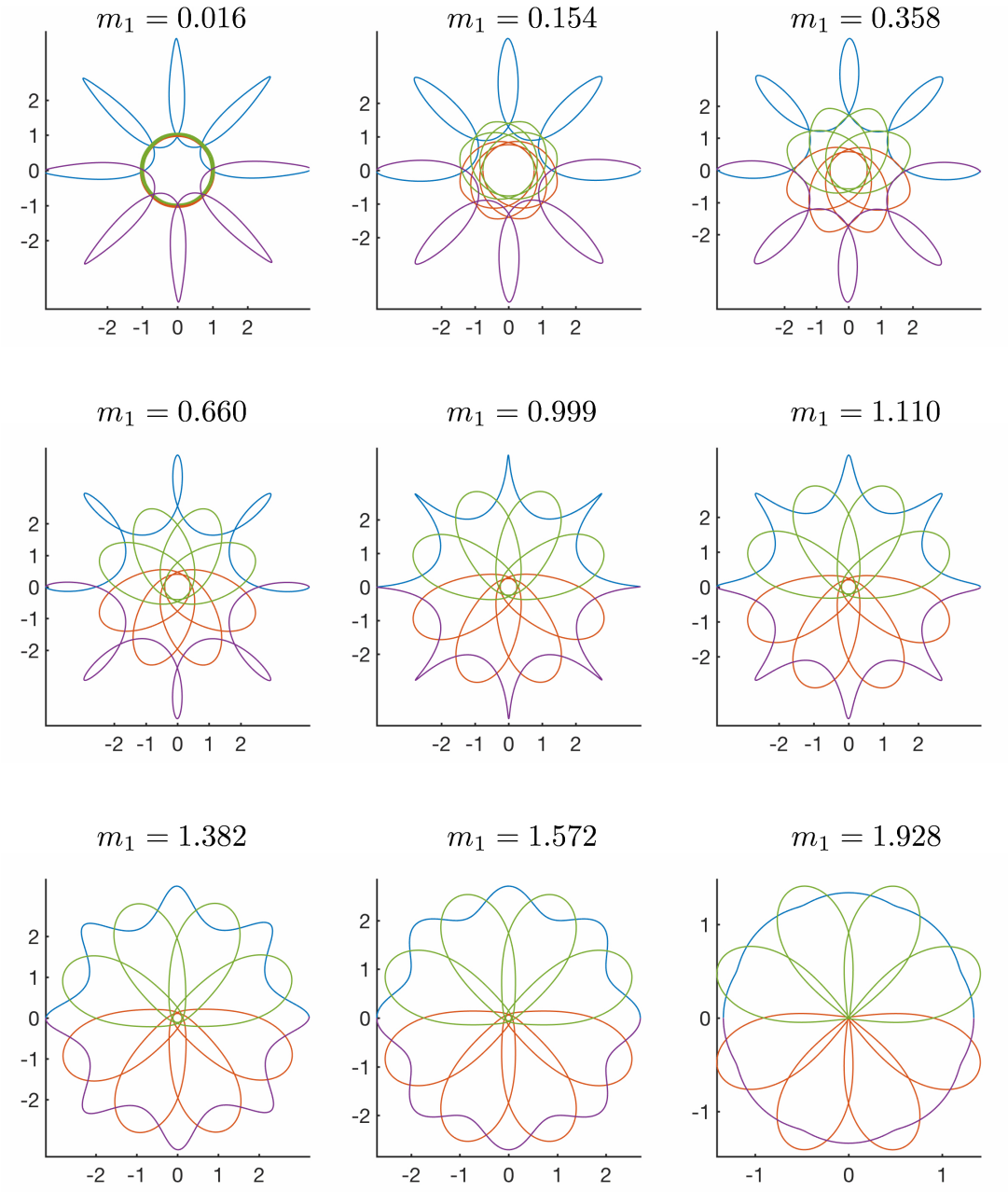

Figure C.8: Double choreographies for $\theta = 2\pi/8 = \pi/4$.

C.9 $k = 9$

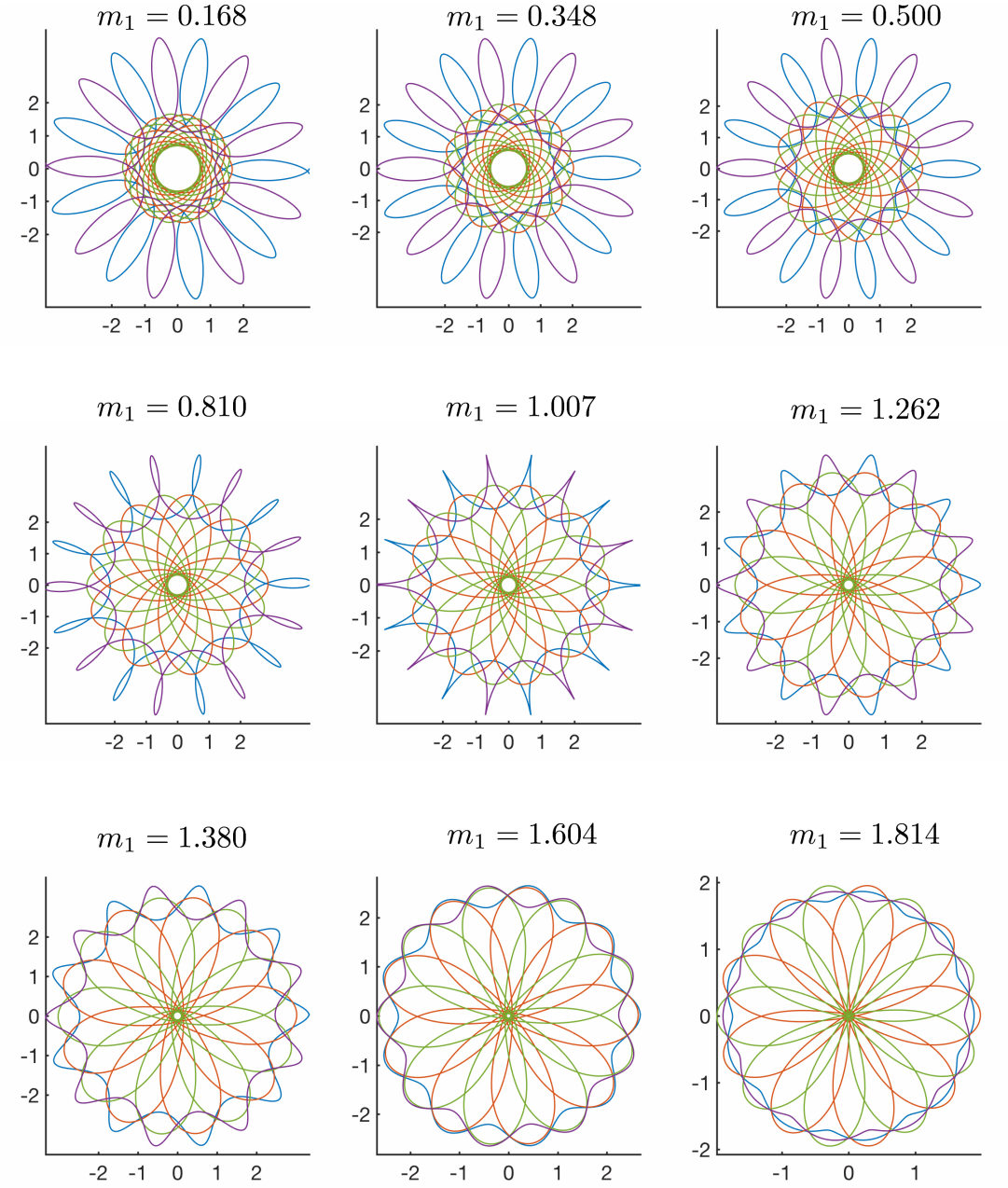

Figure C.9: Absolute periodic orbits for $\theta = 2\pi/9$.

C.10 $k = 10$

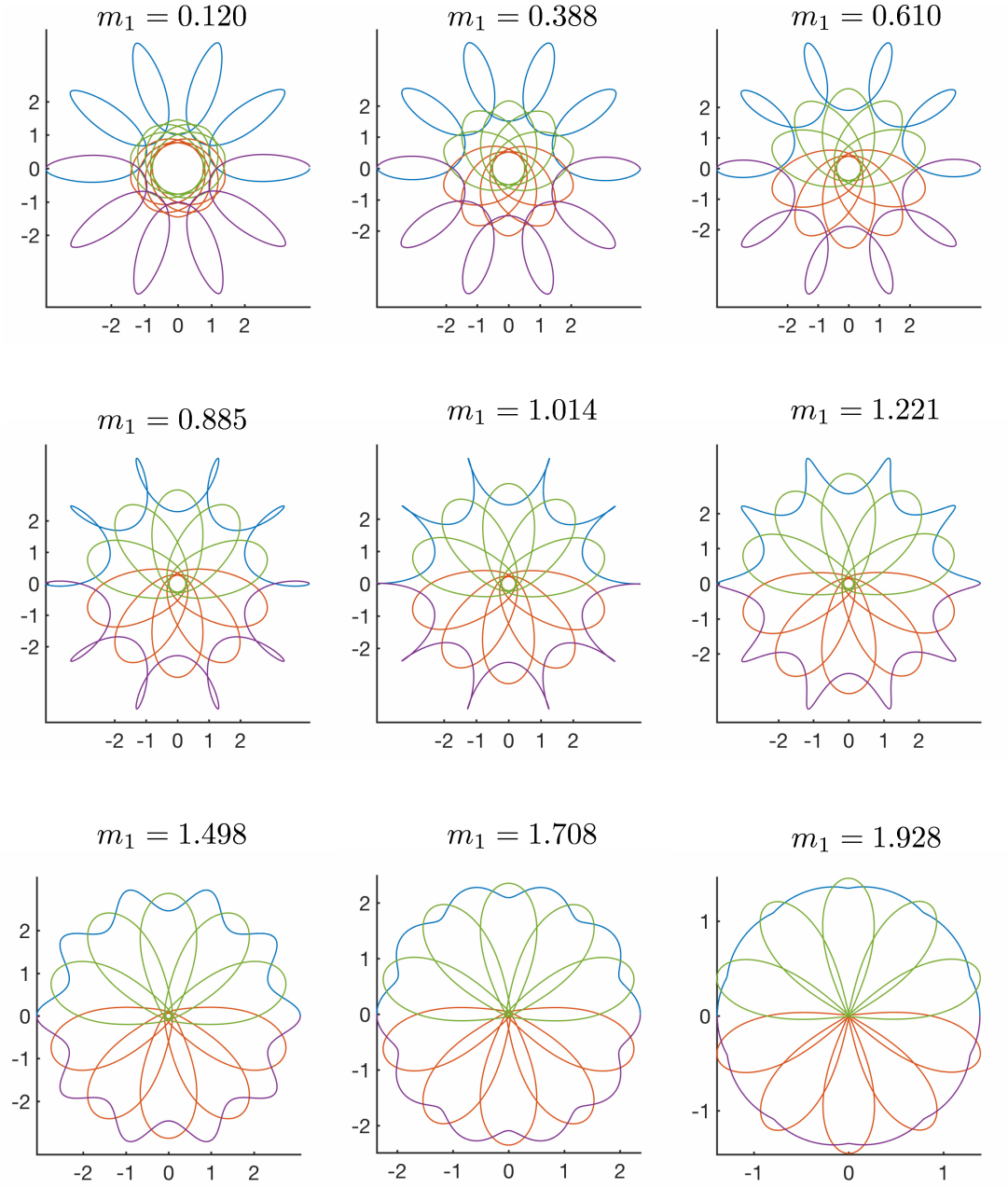

Figure C.10: Double choreographies for $\theta = 2\pi/10 = \pi/5$.

C.11 $k = 20$

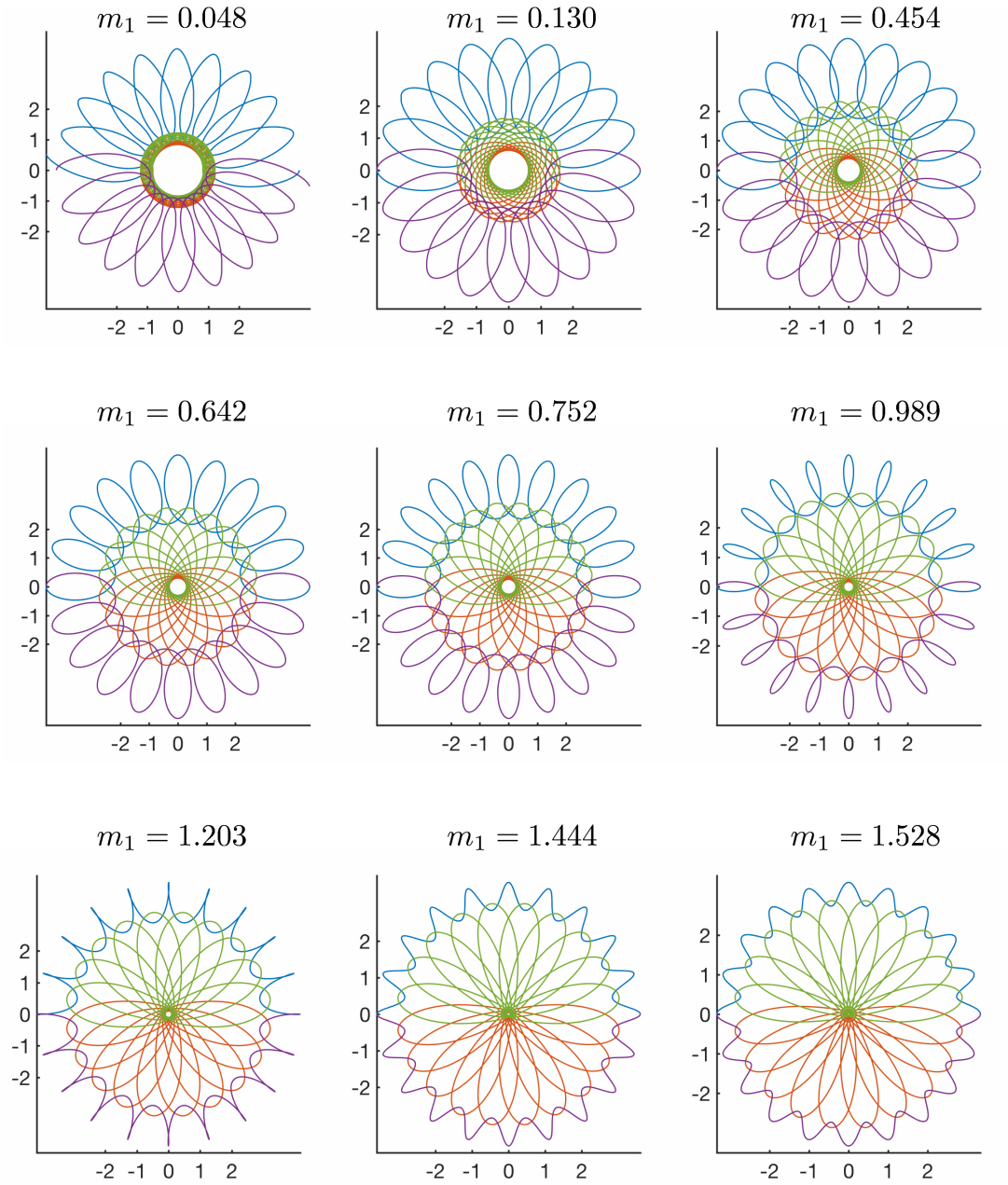

Figure C.11: Double choreographies for $\theta = 2\pi/20 = \pi/10$.